TRANSPORTATION RESEARCH RECORD **1105**

Structure Foundations

TRB
TRANSPORTATION RESEARCH BOARD
NATIONAL RESEARCH COUNCIL
WASHINGTON, D.C. 1986

Transportation Research Record 1105
Price $9.00
Editor: Edythe Traylor Crump
Compositor: Lucinda Reeder
Layout: Betty L. Hawkins

modes
1 highway transportation
3 rail transportation

subject areas
25 structures design and performance
62 soil foundations

Transportation Research Board publications are available by ordering directly from TRB. They may also be obtained on a regular basis through organizational or individual affiliation with TRB; affiliates or library subscribers are eligible for substantial discounts. For further information, write to the Transportation Research Board, National Research Council, 2101 Constitution Avenue, N.W., Washington, D.C. 20418.

Printed in the United States of America

Library of Congress Cataloging-in-Publication Data
National Research Council. Transportation Research Board.

Structure foundations.

(Transportation research record, ISSN 0361–1981 ; 1105)
1. Foundations—Congresses. 2. Piling (Civil engineering)—Congresses. 3. Bridges—Foundations and piers—Congresses. I. National Research Council (U.S.). Transportation Research Board. II. Series.
TE7.H5 no. 1105 380.5 s 87–12373
[TA775] [624.1'5]
ISBN 0–309–04451–0

Sponsorship of Transportation Research Record 1105

GROUP 2—DESIGN AND CONSTRUCTION OF TRANSPORTATION FACILITIES
David S. Gedney, Harland Bartholomew & Associates, chairman

Soil Mechanics Section
Raymond A. Forsyth, California Department of Transportation, chairman

Committee on Foundations of Bridges and Other Structures
Bernard E. Butler, New York State Department of Transportation, chairman
Arnold Aronowitz, Jean-Louis Briaud, W. Dale Carney, Richard S. Cheney, Murty S. Devata, Albert F. Dimillio, Bengt H. Fellenius, George G. Goble, Richard J. Goettle III, James S. Graham, Larry K. Heinig, Hal W. Hunt, Gay D. Jones, Jr., Philip Keene, Hugh S. Lacy, Clyde N. Laughter, Robert M. Leary, John F. Ledbetter, Jr., Richard P. Long, Lyle K. Moulton, Michael Wayne O'Neill, Arthur J. Peters, Austars R. Schnore, Harvey E. Wahls

Committee on Subsurface Soil-Structure Interaction
Michael G. Katona, TRW Ballistic Missiles Division, chairman
George Abdel-Sayed, Baidar Bakht, Sangchul Bang, C. S. Desai, J. M. Duncan, Delon Hampton, An-Bin Huang, J. Neil Kay, Raymond J. Krizek, Richard W. Lautensleger, G. A. Leonards, Donald Ray McNeal, Michael C. McVay, A. P. Moser, William Thomas Nearn II, Richard A. Parmelee, Russell B. Preuit, Jr., Ernest T. Selig, Corwin L. Tracy

Neil F. Hawks, Transportation Research Board staff

Sponsorship is indicated by a footnote at the end of each paper. The organizational units, officers, and members are as of December 31, 1985.

Transportation Research Record 1105

The **Transportation Research Record** series consists of collections of papers on a given subject. Most of the papers in a Transportation Research Record were originally prepared for presentation at a TRB Annual Meeting. All papers (both Annual Meeting papers and those submitted solely for publication) have been reviewed and accepted for publication by TRB's peer review process according to procedures approved by a Report Review Committee consisting of members of the National Academy of Sciences, the National Academy of Engineering, and the Institute of Medicine.

The views expressed in these papers are those of the authors and do not necessarily reflect those of the sponsoring committee, the Transportation Research Board, the National Research Council, or the sponsors of TRB activities.

Transportation Research Records are issued irregularly; approximately 50 are released each year. Each is classified according to the modes and subject areas dealt with in the individual papers it contains. TRB publications are available on direct order from TRB, or they may be obtained on a regular basis through organizational or individual affiliation with TRB. Affiliates or library subscribers are eligible for substantial discounts. For further information, write to the Transportation Research Board, National Research Council, 2101 Constitution Avenue, N.W., Washington, D.C. 20418.

Contents

Pressuremeter and Shallow Foundations on Stiff Clay

JEAN-LOUIS BRIAUD, KENNETH E. TAND, AND ERIK G. FUNEGARD

The bearing capacity and settlement rules for the design of shallow foundations on stiff clays using the results of pressuremeter tests are reviewed. The results of 17 footing tests on 8 stiff clays are used, together with pressuremeter test results to evaluate the existing rules. New simplified bearing capacity rules are proposed. Menard's equation for settlement is proven reasonably accurate. An elasticity approach to settlement calculations using the pressuremeter modulus is proposed.

The pressuremeter can be used for the design of shallow foundations on stiff clays. Rules of design were developed in the early 1960s by Menard and his coworkers. These rules were adjusted in the mid-1970s by the Laboratoire des Ponts et Chaussées. In this paper the rules of design using pressuremeter test results for shallow foundations on stiff clays are examined in light of recent footing tests. Both bearing capacity and settlement considerations are addressed; adjusted bearing capacity rules are proposed, as well as an alternative settlement approach.

PRESSUREMETER TEST AND PARAMETERS

Several different types of pressuremeters exist. The preboring pressuremeter, the selfboring pressuremeter, and more recently the sampler and cone pressuremeters. This paper deals only with the preboring pressuremeter whereby the probe is inserted in an open borehole. Once inserted, the probe is inflated and pushes radially against the borehole wall. The plot of the radial stress at the cavity wall versus the relative increase in probe radius is the typical result of a pressuremeter test (PMT) after proper account of membrane stiffness and volume corrections. Standard procedures for preparing the borehole, performing the test, and reducing the data have been proposed *(1–3)*. It is recommended that any pressuremeter curve be plotted as shown in Figure 1 because this type of curve allows any pressuremeter data to be compared and the pressuremeter parameters to be calculated without any additional information on the probe dimensions.

From the pressuremeter curve, two main parameters are calculated: the pressuremeter modulus E_o and the net limit pressure p_L^*. The modulus E_o is obtained from the straight part of the curve (AB in Figure 1) using the equation based on the expansion of a cylindrical cavity in an isotropic homogeneous elastic space:

$$E_o = (1 + \nu)\,(p_2 - p_1)\,\{[1 + (\Delta R/R_o)_1]^2 + [1 + (\Delta R/R_o)_2]^2\}/[1 + (\Delta R/R_0)_1]^2 - [1 + (\Delta R/R_o)_2]^2 \quad (1)$$

where

- ν = Poisson's ratio, usually taken equal to 0.33;
- R_o = deflated radius of the probe;
- p_1, $(\Delta R/R_o)_1$ = coordinates of the point at the beginning of the straight line on the curve (A in Figure 1); and
- p_2, $(\Delta R/R_o)_2$ = coordinates of the point at the end of the straight line on the curve (B in Figure 1).

The limit pressure p_L is defined as the pressure reached when the initial volume of the cavity has been doubled. This corresponds to a value of $\Delta R/R_o$ equal to $0.41 + 1.41\,(\Delta R/R_o)_1$. The net limit pressure p_L^* is

$$p_L^* = p_L - p_{OH} \quad (2)$$

where p_{OH} is the total horizontal pressure at rest (Figure 1).

In addition, a reload modulus E_R is often obtained from the slope of the unload reload loop (CD in Figure 1). The value of E_R is calculated by using Equation 1 applied to points C and D instead of A and B in Figure 1.

It must be emphasized that the preparation of a quality pressuremeter borehole is the single most important step in the use of the pressuremeter in design. The error in foundation behavior predictions induced by the design rules themselves is much less than the error that can be induced by using the results of poor quality pressuremeter tests; this is especially true for settlement predictions because the modulus E_o is more sensitive to borehole disturbance than the limit pressure. Therefore it is essential that pressuremeter tests be performed only by experienced personnel. A suggested practice for the preparation of a pressuremeter borehole has been proposed *(1)*.

CORRELATIONS BETWEEN PRESSUREMETER, STANDARD PENETRATION, AND CONE PENETROMETER TESTS

A data base of pressuremeter test data and other test data was formed. The pressuremeter data were collected over the last 10

J. L. Briaud, Civil Engineering Department, Texas A&M University, College Station, Tex. 77843. K. E. Tand, Kenneth E. Tand and Associates, Inc., 1408 E. North Belt Drive, Suite 150, Houston, Tex. 77032. E. G. Funegard, Amoco Research Center, Amoco Corporation, P.O. Box 400, Naperville, Ill. 60566.

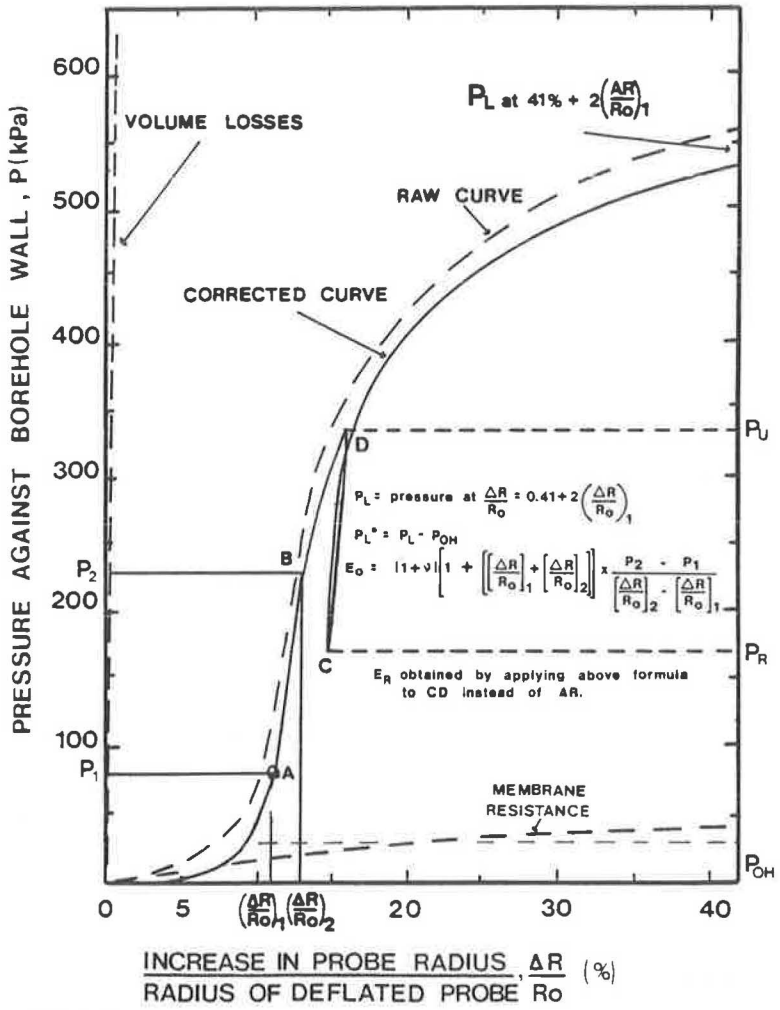

FIGURE 1 Typical preboring pressuremeter test curve.

years on various research and consulting projects. The pressuremeters used were the Menard, the TEXAM, and the pavement pressuremeters. The 82 pressuremeter borings were located in the south, southwest, west, and central United States with 36 sand, 44 clay, and 2 silt sites. Other borings were performed next to the PMT borings, leading to data on undrained shear strength s_u, effective stress friction angle ϕ, standard penetration test (SPT) blow count N, and cone point and friction resistance qc and fs. A record was created at each depth in a boring, which consisted of E_o, E_R, p_L, s_u, Φ, qc, and fs. A total of 463 records were accumulated. The data are described in detail by Briaud et al. *(4)*. Best fit linear regressions were performed for combinations of any two parameters. Of interest are the following equations for clays:

$$p_L = 7.5\ S_U \quad (3)$$

$$E_o = 100\ S_U \quad (4)$$

$$E_R = 300\ S_U \quad (5)$$

$$p_L = 0.2\ qc \quad (6)$$

$$E_o = 2.5\ qc \quad (7)$$

$$E_R = 13\ qc \quad (8)$$

The scatter involved in the preceding correlations is large as shown by the example in Figure 2. These correlations must not be used in design; they are presented only to give an idea of the order of magnitude of the pressuremeter parameters compared with other soil parameters.

BEARING CAPACITY: ORIGINAL RULES

The approach proposed by Menard *(5)* is to relate the ultimate capacity of a footing, q_L, to the net limit pressure obtained from the pressuremeter

$$q_L = k\ p^*_{Le} + q_o \quad (9)$$

where p^*_{Le} is the equivalent net limit pressure within the zone of influence of the footing, k is the bearing capacity factor, and q_o is the total stress overburden pressure at the footing depth. The value of p^*_{Le} is to be obtained by

$$p^*_{Le} = (p^*_{L1} \times p^*_{L2})^{1/2} \quad (10)$$

where p_{L1} is the average net limit pressure within $\pm$ 0.5B above

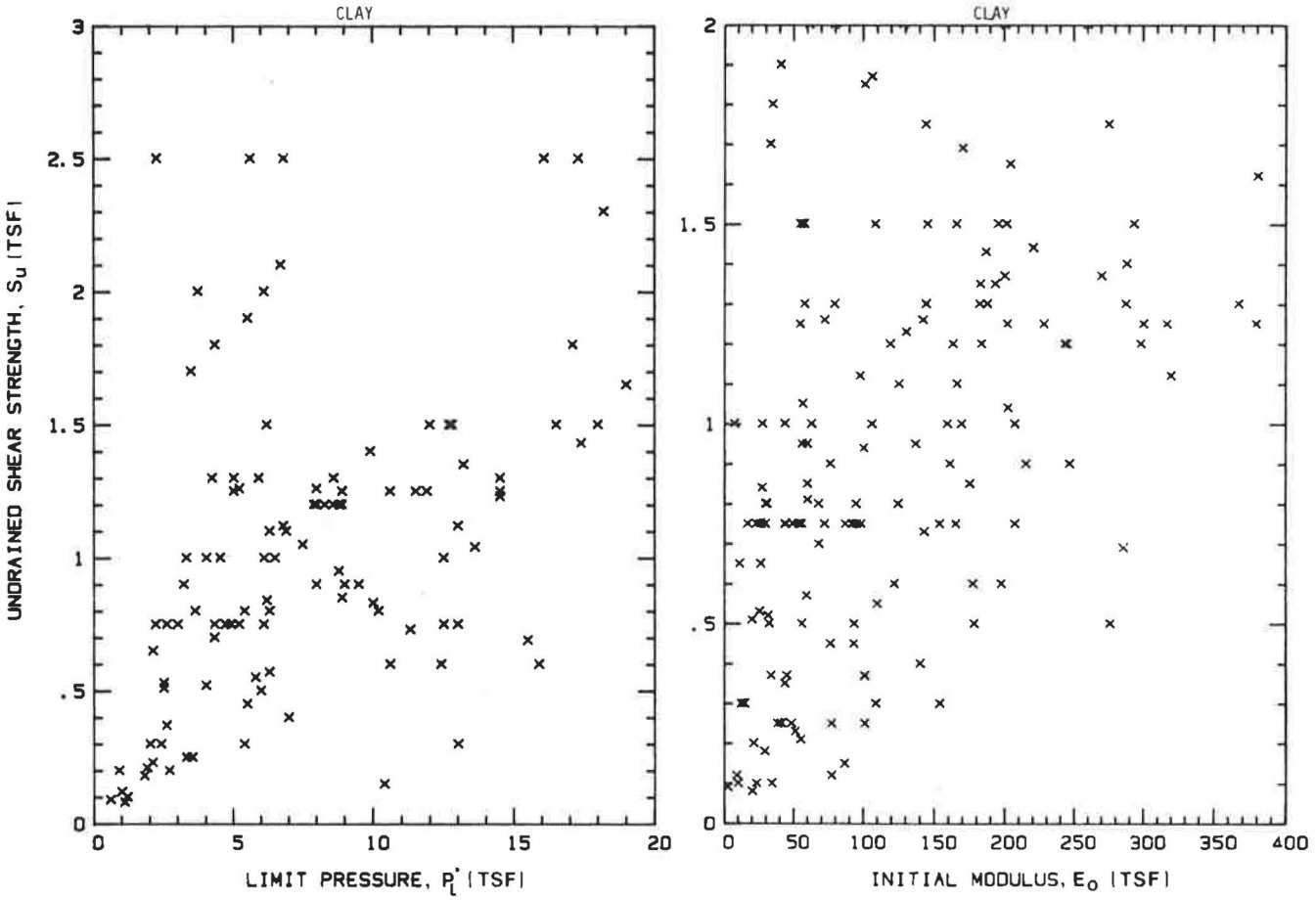

FIGURE 2 Example of correlations from the data base.

and below the footing depth and p_{L2} is the average net limit pressure within 0.5B to 1.5B below the footing level where B is the footing width. Menard *(5)* originally proposed a chart giving k as a function of relative embedment H_e (Figure 3), where H_e is the effective embedment depth calculated as

$$H_e = 1/p^*_{Le} \sum_{o}^{D} p^*_{Li}\,\Delta z_i \qquad (11)$$

where D is the embedment depth of the footing, and p^*_{Li} is the net limit pressure in a Δz_i thick layer within the depth of embedment. This definition of H_e allows layers within the depth of embedment to be taken into consideration; these layers are stronger or weaker than the layer on which the footing is resting.

BEARING CAPACITY: PRESSUREMETER VERSUS UNDRAINED STRENGTH APPROACH

The preceding approach is to be compared with the undrained shear strength-plasticity theory approach:

$$q_L = N_c S_U + \gamma D \qquad (12)$$

The term $N_c S_U$ in Equation 12 compares directly with the term $k^*_p Le$ in Equation 9. For surface circular footing, the factor N_c is 6.2 *(6)*, the factor k is 0.8 (Figure 3). This leads to a value of p^*_{Le} equal to 7.75 S_U, which compares very favorably with the 7.5 S_U of Equation 3 for the data base.

The factor N_c increases as the depth of embedment of the footing increases. N_c reaches a maximum of 9 at a depth of embedment to width of footing ratio D/B of 4 *(6)*. The k value

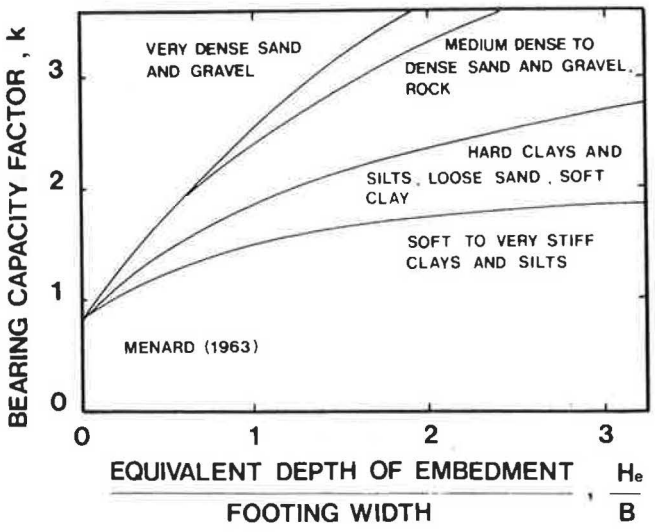

FIGURE 3 Bearing capacity factor *(5)*.

would then be expected to reach a maximum value of 9/6 × 0.8 = 1.16 at D/B of 4. Figure 3 shows a k value much larger than 1.16 for a D/B of 4.

Another factor influencing the ultimate bearing pressure, q_L, is the compressibility of the clay; an N_c factor that depends on a compressibility index, I, was proposed by Vesic *(7)*. This was done in an effort to correct for the shortcomings of the rigid-plastic solution. This important factor is incorporated directly into p_{Le} because the compressibility of the clay affects the pressuremeter limit pressure. Indeed the theoretical expression of p_L in the case of undrained behavior is

$$p_L = p_o + S_U [1 + Ln(G/S_U)] \quad (13)$$

BEARING CAPACITY: RECENT LOAD TEST RESULTS

In 1978 Baguelin et al. *(8)* updated Menard's rules (Figure 4). Since then footing tests have become available that were not included in Menard's 1963 rules nor the Laboratoire des Ponts et Chaussées (LPC) 1978 rules (Table 1).

Shields and Bauer *(9)* reported the results of two footing tests on a stiff sensitive clay. The first footing was a 0.46-m (1.5 ft) diameter rigid plate (Figure 5). The test was performed at the bottom of a 1.3-m (4.26 ft) wide, 2.6-m (8.52 ft) deep trench. The second footing was a 3.1 × 3.1-m (10.2 ft × 10.2 ft) square, 0.66-m (2.2 ft) thick concrete footing at the ground surface (Figure 6). The soil was an overconsolidated sensitive clay with the following average properties: undrained shear strength from vane tests 110 kPa (1.12 tsf), water content 43 percent, and unit weight 18 kN/m^3 (114.6 pcf). The pressuremeter test results are shown in Figures 5 and 6 together with the test configuration and the load settlement curves.

O'Neill and Sheikh *(10)* reported the results of a drilled shaft test on a stiff clay. The 0.762-m (2.5 ft) diameter shaft was 2.36 m (7.75 ft) deep with a 2.41-m (7.92 ft) diameter bell (Figure 7). The soil was a stiff clay with the following average properties: undrained shear strength from unconsolidated undrained triaxial tests 86 kPa (0.88 tsf), water content 22 percent, unit

TABLE 1 SHALLOW FOOTINGS DATA BASE

Study No.	Footing I.D. No.	Reference	Soil	Footing Width (m)	Footing Depth (m)	Footing Type
1	1	Deschenes	Medium	0.30	0	Strip
	2	Briaud	Dense	0.30	0.30	Strip
	3	*(24, 25)*	Sand	0.30	0.60	Strip
	4			0.30	0.90	Strip
2	5	Deschenes	Dense	0.30	0	Strip
	6	Briaud	Sand	0.30	0.30	Strip
	7	*(24, 25)*		0.30	0.60	Strip
3	8	Amar-Baguelin	Silt	1.0	0	Square
	9	Canepa *(18)*		1.0	0.60	Square
	10			1.0	1.0	Square
4	11	Shields-Bauer	Clay	0.46	2.6	Circular
	12	*(9)*		3.1	0.70	Square
5	13	O'Neill-Sheikh, Briaud *(10, 11)*	Clay	2.41	2.36	Circular
6	14	O'Neill-Reese,	Clay	0.76	7.0	Circular
	15	WCC *(12, 13)*		2.29	7.0	Circular
7	16	Tand-Funnegard	Clay	0.60	1.50	Circular
	17	Briaud *(14, 15)*		0.60	1.50	Circular
	18			0.60	1.50	Circular
8	19	Menard *(5)*	Sand/ Silt	0.25-0.6	0.5-1.7	Circular
9	20	Marsland-Randolph	Clay	0.865	6.1	Circular
	21	*(16)*		0.865	12.2	Circular
	22			0.865	18.3	Circular
	23			0.865	24.0	Circular
10	24	Johnson *(17)*	Clay	0.762	0.0	Circular

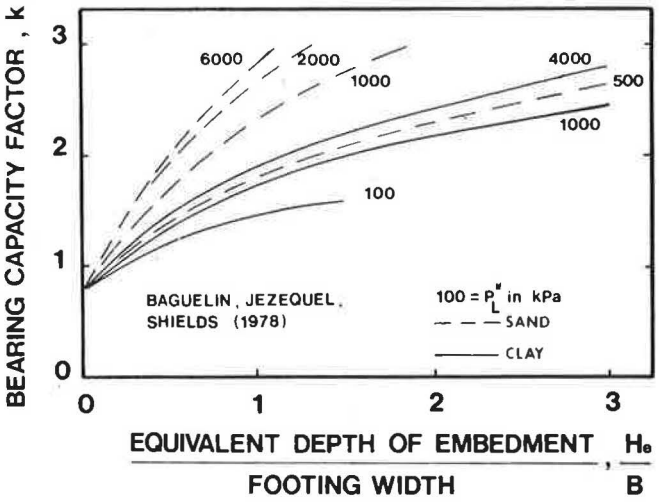

FIGURE 4 Bearing capacity factor *(8)*.

weight 19.8 kN/m^3 (126 pcf), and cone point resistance 2700 kPa (27.6 tsf). The test configuration and the load settlement curves obtained at the base of the bell are shown in Figure 7. Briaud and Riner *(11)* reported the results of pressuremeter tests at the same site; these results are shown in Figure 7.

O'Neill and Reese *(12)* reported the results of two drilled shaft tests on a stiff clay. The first drilled shaft was 7 m (23 ft) deep and 0.762 m (2.5 ft) in diameter (Figure 8). The second shaft was identical to the first shaft except for a 2.29-m (7.5 ft) diameter bell (Figure 9). The soil was a stiff clay with the following average properties within the zone of interest: undrained shear strength from unconfined compression tests 98

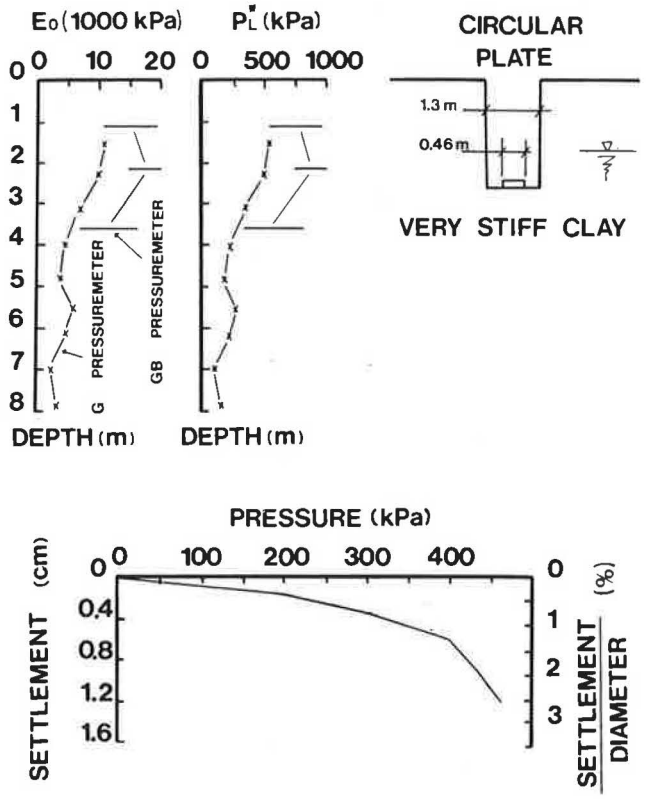

FIGURE 5 Shields-Bauer plate test *(9)*.

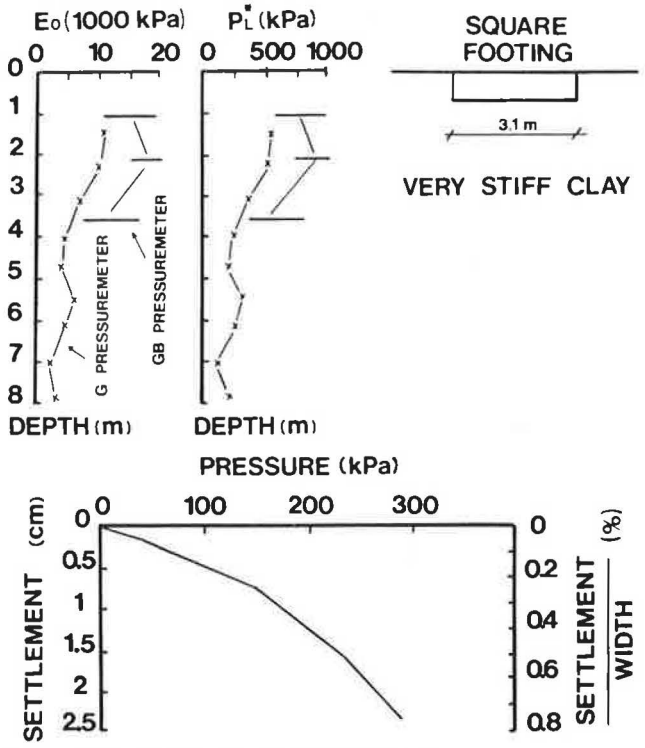

FIGURE 6 Shields-Bauer footing test *(9)*.

kPa (1 tsf), water content 24 percent, and unit weight 20.4 kN/m^3 (130 pcf). The test configuration and the load settlement curves obtained at the base of the shafts are shown in Figures 8 and 9. Woodward Clyde Consultants *(13)* performed a series of pressuremeter and cone penetrometer tests at the same site. The average cone point resistance close to the point of the shaft was

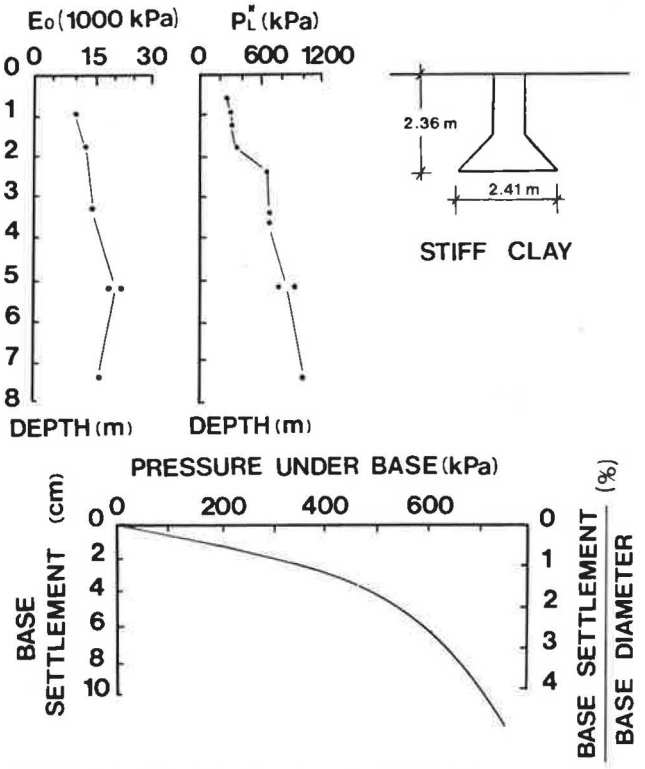

FIGURE 7 O'Neill-Sheikh-Briaud test *(10, 11)*.

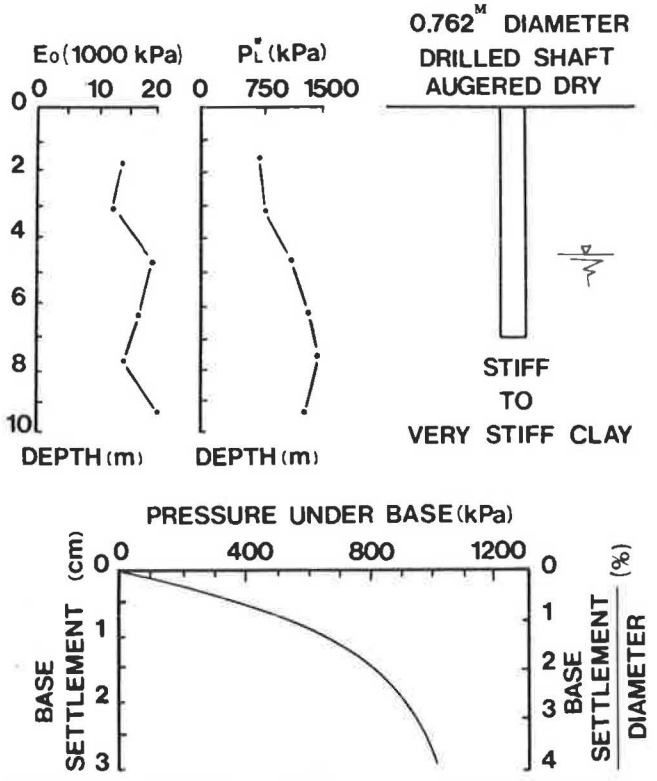

FIGURE 8 O'Neill-Reese-WCC test on straight drilled shaft *(12, 13)*.

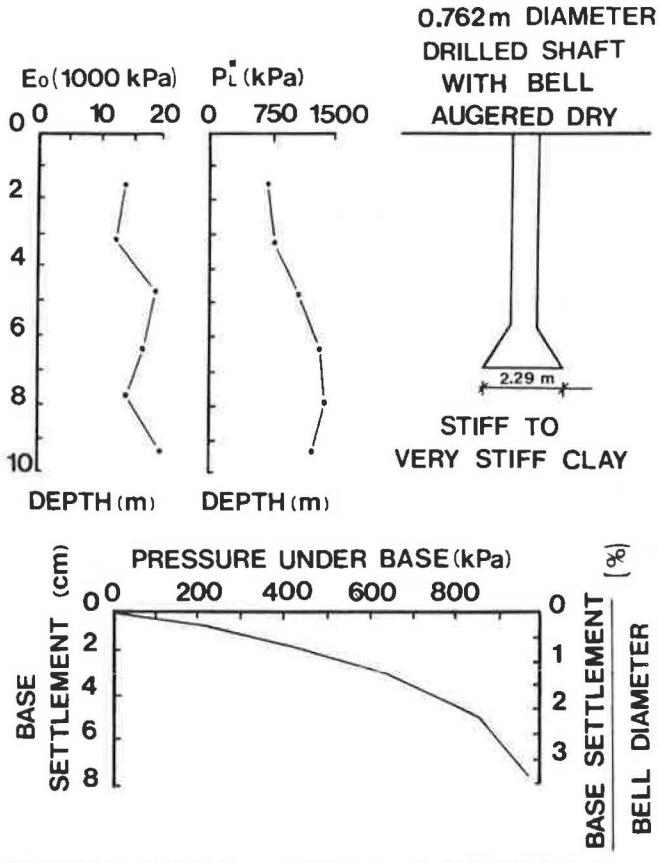

FIGURE 9 O'Neill-Reese-WCC test on belled drilled shaft *(12, 13)*.

3900 kPa (40 tsf); the pressuremeter test results are shown in Figures 8 and 9.

Tand et al. *(14)* reported the results of plate load tests at three sites (A, B, and C). The plate was 0.6 m (2 ft) in diameter and was placed at the bottom of a 0.6-m (2 ft) diameter, 1.5-m (5 ft) deep-cased hole (Figures 10, 11, and 12). At Site A, the soil was a stiff sandy clay with the following average properties: undrained shear strength from unconsolidated undrained triaxial tests 58.3 kPa (0.59 tsf), water content 20 percent and unit weight 19.5 kN/m^3 (124 pcf). At Site B, the soil was a medium sandy clay: undrained shear strength from unconsolidated undrained triaxial tests 38 kPa (0.39 tsf), water content 19.5 percent and unit weight 19.6 kN/m^3 (125 pcf). At Site C, the soil was a stiff clay: undrained shear strength from unconsolidated undrained triaxial tests 61.5 kPa (0.63 tsf), water content 25 percent, and unit weight 19.8 kN/m^3 (126 pcf). The test configuration and the load-settlement curves obtained are shown in Figures 10, 11, and 12. Briaud Engineers *(15)* reported the results of pressuremeter tests performed at Sites A, B, and C. These pressuremeter test results are shown in Figures 10, 11, and 12.

Marsland and Randolph *(16)* reported the results of plate load tests at four different depths in one uncased borehole (Table 1). The plate was 0.865 m (2.85 ft) in diameter. The soil was a very stiff fissured clay (London clay) with a unit weight of 19.6 kN/m^3 (125 pcf) and an undrained shear strength derived from the plate tests averaging 100 kPa (1 tsf). The pressuremeter test results are shown in Figure 13. Plate tests were performed at depths of 6.1, 12.2, 18.3, and 24 m (20, 40, 60, and 78.7 ft). The load settlement curve for the 18.3-m (60

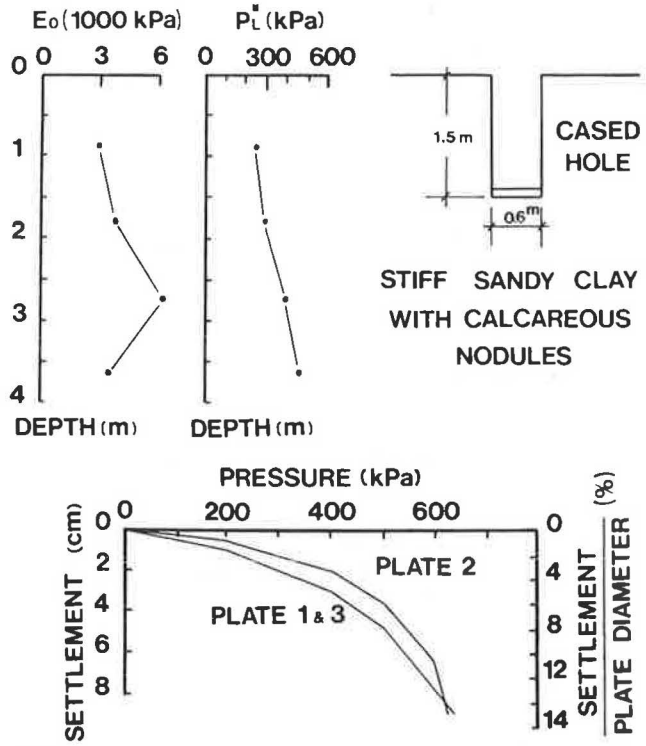

FIGURE 10 Tand-Funegard-Briaud plate tests (Texas City, Site A) *(14, 15)*.

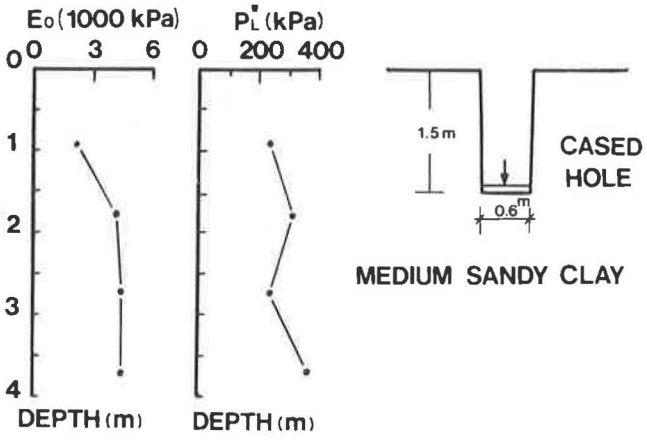

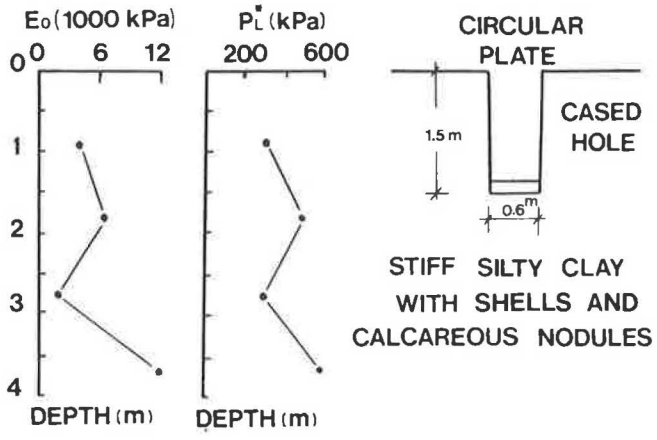

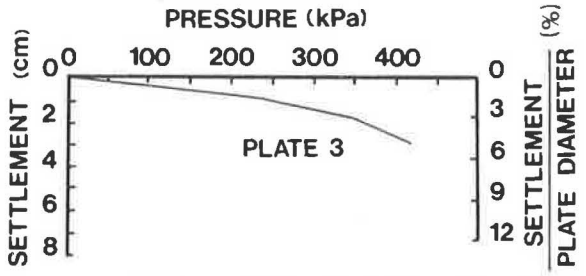

FIGURE 11 Tand-Funegard-Briaud tests (Texas City, Site B) *(14, 15)*.

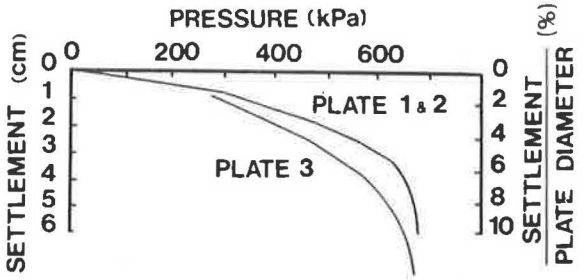

FIGURE 12 Tand-Funegard-Briaud tests (Chocolate Bayou, Site C) *(14, 15)*.

ft) deep plate test was reported only by Marsland and Randolph (Figure 13) *(16)*. Johnson *(17)* reported the results of a plate load test on a stiff clay. The plate was 0.762 m (30 in.) in diameter and was placed at the surface of the clay (Figure 14). The soil was a stiff clay with the following average properties: undrained shear strength from undrained triaxial tests 100 kPa (1 tsf), water content 28 percent, plasticity index 45 percent, and dry unit weight 15 kN/m^3 (96 pcf). The pressuremeter test results are shown in Figure 14. The plate was not brought to failure.

BEARING CAPACITY: PROPOSED DESIGN CURVES

The ultimate bearing pressure, q_L, is defined here as the pressure reached for a settlement equal to one-tenth of the footing width (B/10). This is consistent with failure criterions used for pile load test analysis. Sometimes, especially in sands, the pressure increases past this value of q_L; however, settlements larger than B/10 are rarely obtained in footing tests, and this definition provides a consistent way of defining the ultimate bearing pressure. For each of the footing test results described previously, q_L as defined earlier, was determined. The equivalent limit pressure p^*_{Le} was calculated according to Equation 10, the effective embedment depth H_e was calculated according to Equation 11, and the overburden pressure q_o at the footing depth was also calculated. The values of q_L, p^*_{Le}, H_e, and q_o are given in Table 2 with additional results for silt and sand.

Using Equation 9, it was then possible to backfigure the

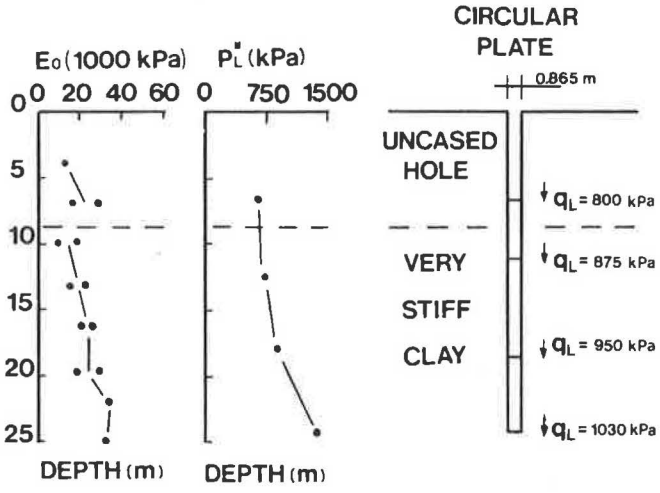

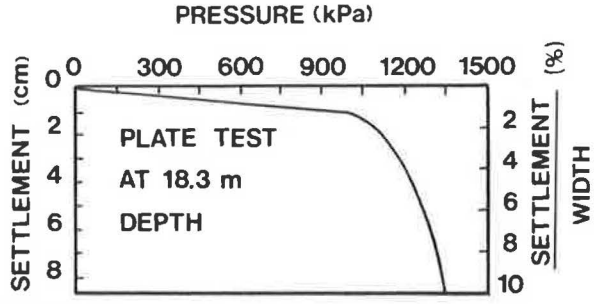

FIGURE 13 Marsland-Randolph plate tests *(16)*.

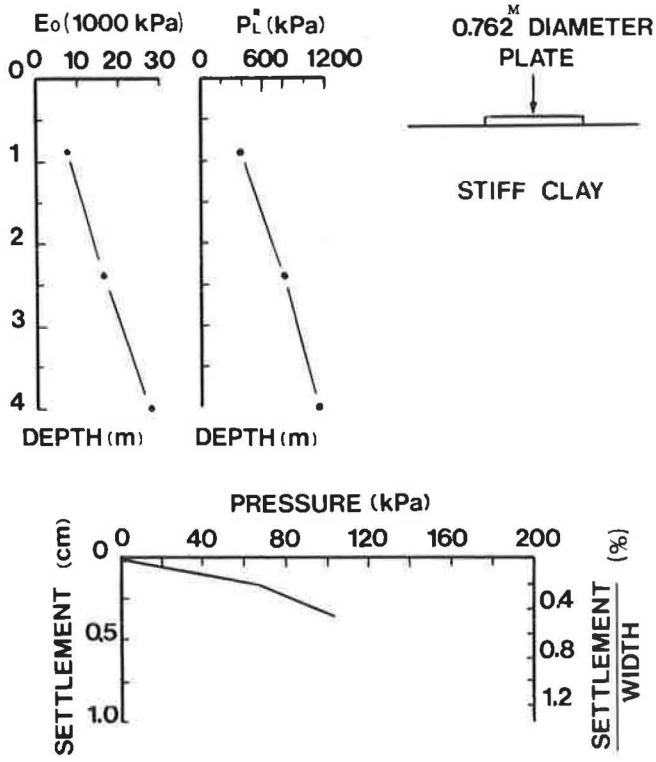

FIGURE 14 Johnson-Briaud plate test *(17)*.

measured bearing capacity factor k for each footing test (Table 2). The data points were then plotted as shown in Figure 15. After consideration of all the data available, the design curves shown in Figure 15 were selected. These curves correspond approximately to the curve that would split the data points in half (mean) minus one standard deviation of the scatter around the mean. It is emphasized that these curves are proposed to calculate the ultimate bearing pressure as defined by the one tenth of the width settlement criterion. It is also emphasized that the rules for obtaining p^*_{Le} and H_e must be followed rigorously.

By comparing Figures 3, 4, and 15, it can be seen that the proposed design curves are somewhat more conservative than the previous rules. The ratio of the ultimate bearing pressure predicted by these design curves to the measured ultimate bearing pressure varied between the extreme values of 0.60 to 1.24 for this data base. For comparison purposes, the precision of the method that consists of using the general bearing capacity equation to predict the ultimate bearing pressure is shown in Figure 16 for clay and in Figure 17 for sand. These figures come from a data base study conducted by Amar et al. *(18)*. As can be seen, the ratio of predicted overmeasured ultimate bearing pressure varies from 0.51 to 1.67 in clay and from 0.12 to 12 in sand. Therefore the pressuremeter may not improve significantly the bearing capacity predictions in clay but may improve dramatically the predictions in sand.

TABLE 2 SUMMARY OF ULTIMATE CAPACITY DATA FOR FOOTING LOAD TESTS

Study (1)		Soil (2)	Equivalent Net Limit Pressure p^*_{Le} (kPa) (3)	Bearing Pressure at B/10 Penetration q_L (kPa) (4)	Overburden Pressure q_o (kPa) (5)	Effective Embedment $H_{e/B}$ (6)	Measured Bearing Capacity Factor k (7)
1 Deschenes-Briaud *(24, 25)*	F1C	Sand	152(43)	130	0.0	0.0	0.86
	F2C	Sand	167(60)	165	4.5	0.94	0.96
	F3C	Sand	174(107)	430	9.0	1.81	2.42
	F4C	Sand	192(149)	430	13.5	2.61	2.17
2 Deschenes-Briaud *(24, 25)*	F1D	Sand	407(86)	450	0.0	0.0	1.1
	F2D	Sand	424(126)	510	4.8	0.87	1.19
	F3D	Sand	447(252)	640	9.6	1.90	1.41
3 Amar-Baguelin-Canepa *(18)*	F1	Silt	369	335	0.0	0.0	0.91
	F2	Silt	389	375	13.0	0.56	0.93
	F3	Silt	393	450	21.0	0.92	1.09
4 Shields-Bauer *(9)*	(.45)	Clay	600	550	0.0	0.0	0.86
	(3.1)	Clay	561	550	12.3	0.28	0.96
5 O'Neill-Sheikh-Briaud *(10, 11)*		Clay	515	820	46.2	0.61	1.50
6 O'Neill-Reese-WCC	(0.762)	Clay	1256	1250	137.2	6.76	0.89
(12, 13)	(0.29)	Clay	1130	1225	137.2	2.43	0.96
7 Tand-Funegard-Briaud	A	Clay	286	560	30.0	2.18	1.85
(14, 15)	B	Clay	266	525	30.0	2.21	1.86
	C	Clay	376	660	30.0	1.99	1.68
8 Menard *(5)*		Sand	-	-	-	-	-
9 Marsland-Randolph	6.1	Clay	640	920	120	6.6	1.25
(16)	12.2	Clay	725	1095	240	12.2	1.18
	18.3	Clay	885	1310	360	15.6	1.08
	24.0	Clay	1360	1510	480	16.3	0.75
10 Johnson *(17)*	PB4	Clay	475 1	-	0.0	0.0	-

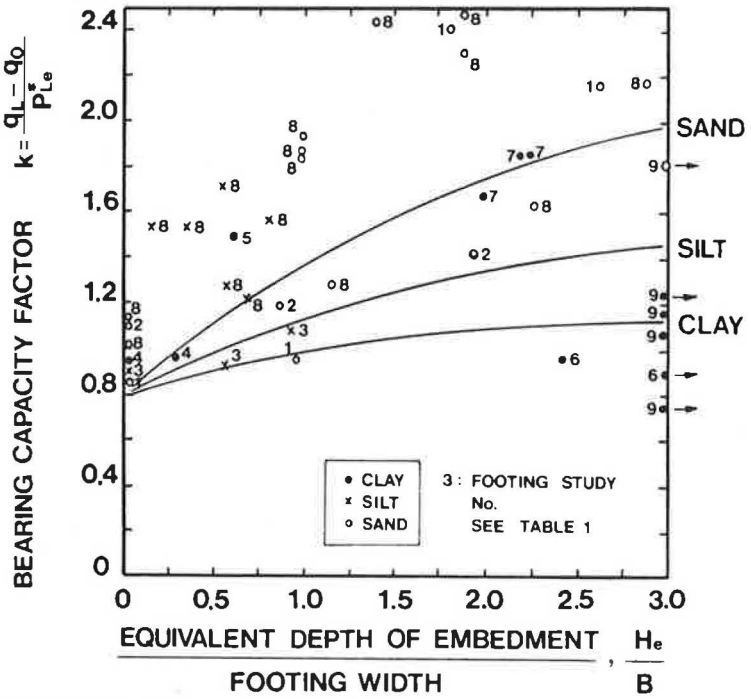

FIGURE 15 Recommended design curves for bearing capacity.

SETTLEMENT: MENARD'S APPROACH

In 1962, Menard and Rousseau *(19)* proposed a method of calculating the settlement of a footing on the basis of pressuremeter test results. The basis of Menard's settlement equation is related to the following theoretical background *(19, 8)*.

Two settlements can be considered: an undrained or no-volume change settlement, s_u, which takes place rapidly, and a drained or final settlement, s_T. In elasticity, s_u would be calculated by using undrained parameters (E_u, ν_u, G_u) and s_T by using drained-long-term parameters (E′, ν′, G), where E is Young's modulus, ν is Poisson's ratio, and G is the shear modulus.

The stress tensor (σ) at any point within the loaded mass of soil can be decomposed into its spherical (σ_s) and deviatoric component (σ_d):

$$\sigma = \sigma_s + \sigma_d \tag{14}$$

In elasticity the stress-strain relations can be written

$$\sigma_s = 3K\varepsilon_s = E/3\ (1 - 2\nu)\ \varepsilon_S \tag{15}$$

$$\sigma_d = 2G\varepsilon_d = E/1 + \nu\ \varepsilon_d \tag{16}$$

where K is bulk modulus, ε_s is spherical strain tensor, and ε_d is deviatoric strain tensor.

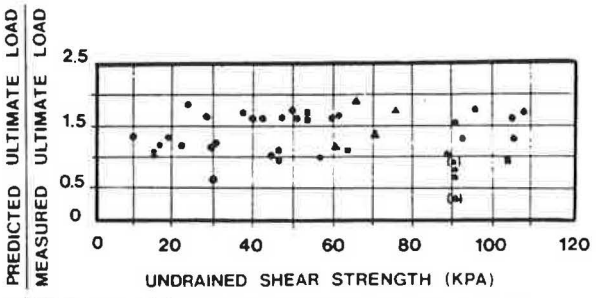

FIGURE 16 Measured versus predicted capacity by $q_u = N_c\ s_u + \gamma D$ for clay *(18)*.

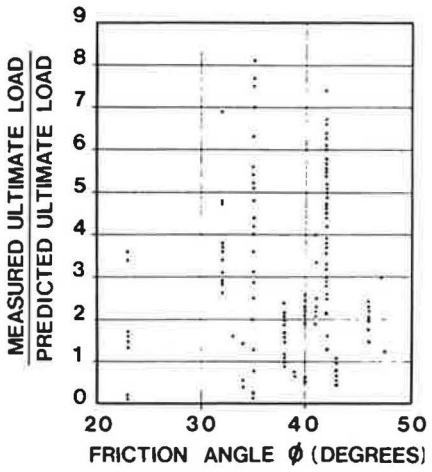

FIGURE 17 Measured versus predicted capacity by $q = 0.5\ \gamma B N_\gamma + \gamma D N_q$ for sand *(18)*.

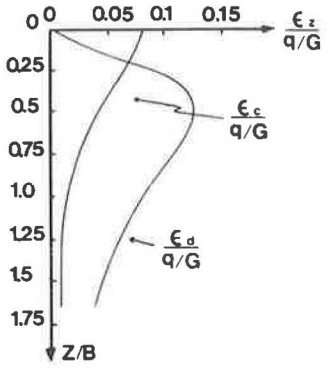

FIGURE 18 Deviatoric and spherical strains versus depth *(8).*

Variation of the components ε_s and ε_d of the vertical strains ε_z are shown in Figure 18. The deviatoric component of the stress tensor, σ_d, is the same whether it is expressed in effective stress or total stress. Therefore

$$\sigma_{du} = \sigma_d' = \sigma_d \tag{17}$$

Since

$$\sigma_{du} = 2G_u\varepsilon_d \tag{18}$$

and

$$\sigma_d' = 2G'\varepsilon_d \tag{19}$$

then

$$G_U = G' = G \tag{20}$$

Consider the settlement of a rigid circular plate on an elastic half space

$$s_T = (\pi/8)/(1 - \nu'/G)\ qB \tag{21}$$

$$s_u = (\pi/8)/(1 - 0.5/G)\ qB \tag{22}$$

The difference $s_T - s_u$ is the consolidation settlement s_c

$$s_u = (\pi/16)\ (qB/G) \tag{23}$$

$$s_c = \pi/16\ (1 - 2\nu')\ qB/G \tag{24}$$

$$s_T = (\pi/16)\ (qB/G) + \pi/16\ (1 - 2\nu')\ qB/G \tag{25}$$

For an average Poisson's ratio (ν') of 0.33, s_u is three times larger than s_c and therefore represents 75 percent of the total settlement, s_T; this shows that when the width of the foundation is small compared to the depth of the compressible layer (most common case for shallow footings), the undrained settlement is the major portion of the final settlement.

The foregoing discussion of the settlement problem is the backbone of the pressuremeter equation for settlement *(19)*:

$$s = \underbrace{2qB_o(\lambda_d\ B/B_o)^{\alpha}/9E_d}_{\text{deviatoric settlement}} + \underbrace{\alpha q\lambda_c\ B/9E_c}_{\text{spherical settlement}} \tag{26}$$

where

s = footing settlement,
E_d = pressuremeter modulus within the zone of influence of the deviatoric tensor,

TABLE 3 MENARD'S α FACTOR *(8, 20)*

Soil Type	Peat		Clay		Silt		Sand		Sand and Gravel	
	E/p^*_L	α	E/p^*_L	α	E/p^*_L	α	E/p^*_L	α	E/p^*_L	α
Over-consolidated			>16	1	>14	2/3	>12	1/3	>10	1/3
Normally consolidated	For all Values	1	9-16	2/3	8-14	1/2	7-12	1/3	6-10	1/4
Weathered and/or remoulded			7-9	1/2		1/2		1/3		1/4

Rock	Extremely Fractured	Other	Slightly Fractured or Extremely Weathered
	α = 1/3	α = 1/2	α = 2/3

q = footing net bearing pressure q_{net},
B_o = reference width of 2 ft or 60 cm,
B = footing width,
α = rheological factor (Table 3),
λ_d = shape factor for deviatoric term (Figure 19),
λ_c = shape factor for spherical term (Figure 19), and
E_c = pressuremeter modulus within the zone of influence of the spherical tensor.

This equation is the elasticity Equation 25, which has been altered to take into account the footing scale effect $B\alpha$ and the magnitude of the pressuremeter modulus.

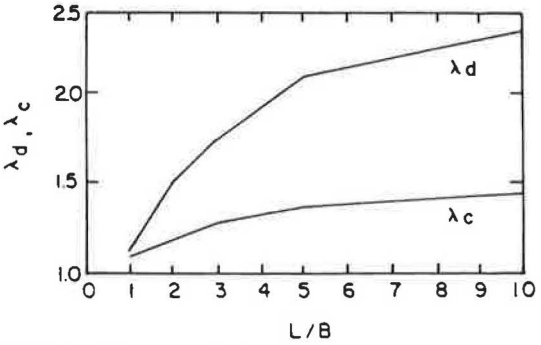

FIGURE 19 Shape factors *(19)*.

SETTLEMENT: PRESSUREMETER VERSUS CONSOLIDATION TEST APPROACH

Consolidation settlement is the result of the spherical part of the stress tensor. As can be seen from Figure 18, the spherical strain ε_c decreases rapidly with depth, indicating that consolidation settlement is prevalent at shallow depth only (e.g., one-half footing width, B/2, below the footing). On the other hand, the deviatoric strain, ε_d, remains significant down to at least 2B below the footing (Figure 18).

The consolidation test applies well to the prediction of ε_c, while the pressuremeter test, which is theoretically a pure deviatoric test, applies well to the prediction of ε_d. Therefore, for a wide foundation over a thin compressible layer where ε_c will predominate, the consolidation test approach is to be favored. For footings on deep relatively uniform deposits where ε_d will predominate, the pressuremeter test approach is to be favored.

Further acknowledging this distinction, Menard recommends that in Equation 26, E_d be taken as the average pressuremeter modulus over a significant depth below the footing, while E_c is the average modulus just below the footing. The averaging technique for E_d is based essentially on the ε_d distribution. The modulus E_c is empirically corrected into E_c/α in order to obtain a "consolidation" modulus. The details of the step-by-step procedure for calculating E_d and E_c can be found in discussions by Menard *(20)*, Briaud et al. *(2)*, and Baguelin et al. *(8)*.

SETTLEMENT: MENARD'S PREDICTION VERSUS LOAD TEST RESULTS

In 1978, Baguelin et al. *(8)* presented the results of 45 comparisons between predicted and measured settlements on various structures; the results are plotted in Figure 20.

The footing load tests presented earlier for bearing capacity evaluation were used to calculate the settlement by Menard's Equation 26. The procedure followed was to use the proposed design curves of Figure 15 in order to obtain a bearing capacity factor k, calculate the ultimate bearing capacity, and use a factor of safety of 3 to obtain the safe bearing pressure q_{safe} (Column 3, Table 4)

$$q_{safe} = k\, p^*_{Le}/3 + q_o \qquad (27)$$

The pressure q_{safe} was then used to calculate the footing settlement (Column 4, Table 4). This settlement was compared with the settlement measured at q_{safe} during the load tests (Column 6, Table 4). Figure 21 is a comparison of measured and predicted settlement for the load tests described in this

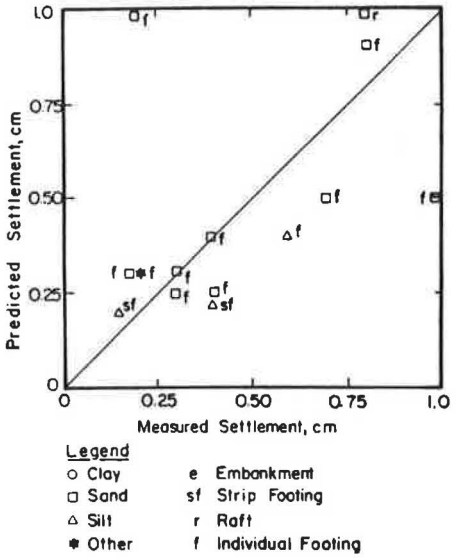

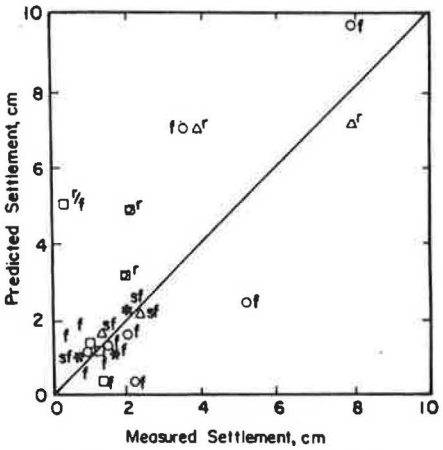

FIGURE 20 Measured versus predicted settlement by Menard's method *(8)*.

TABLE 4 SUMMARY OF SETTLEMENT DATA FOR FOOTING TESTS

Study		Soil	Calculated Safe Bearing Pressure q_{safe} (kPa)	Calculated Settlement (Menard) S_{CM} (cm)	Calculated Settlement (Elasticity) S_{CE} (cm)	Measured Settlement at q_{safe} (cm)	Factor of Safety (chosen)	Factor of Safety (true)
(1)		(2)	(3)	(4)	(5)	(6)	(7)	(8)
1 Deschenes-Briaud *(24, 25)*	F1C	Sand	40	0.58	1.45	0.5	3	3.25
	F2C	Sand	81	0.75	1.7	1.2	3	2.10
	F3C	Sand	108	0.8	1.48	0.4	3	4.25
	F4C	Sand	137	0.9	1.4	0.9	3	3.37
2 Deschenes-Briaud *(24, 25)*	F1D	Sand	108	0.75	1.69	0.6	3	4.17
	F2D	Sand	192	1.14	2	1.2	3	2.70
	F3D	Sand	266	1.28	2.16	1.3	3	2.46
3 Amar-Baguelin-Canepa *(18)*	F1	Silt	98	0.47	1.25	0.8	3	3.41
	F2	Silt	145	0.64	1.41	0.8	3	2.74
	F3	Silt	168	0.69	1.34	0.65	3	2.92
4 Shields-Bauer *(9)*	(0.46m)	Clay	160	0.24	0.33	0.14	3	3.44
	(3.1m)	Clay	171	1.9	2.25	1.0	3	3.39
5 O'Neill-Sheikh-Briaud *(10, 11)*		Clay	204	1.04	1.28	1.2	3	4.90
6 O'Neill-Reese-WCC *(12, 13)*	(0.762m)	Clay	639	0.77	1.08	0.95	3	2.22
	(2.29m)	Clay	557	1.6	2.43	2.5	3	2.59
7 Tand-Funegard-Briaud *(14, 15)*	A	Clay	133	0.55	0.66	0.5	3	5.14
	B	Clay	126	0.56	0.66	0.48	3	5.15
	C	Clay	165	0.56	0.61	0.48	3	4.67
8 Menard *(5)*		Sand	-	-	-	-	-	-
9 Marsland-Randolph *(16)*	18.3	Clay	702	0.81	0.70	0.79	3	2.78
10 Johnson *(17)*	PB4	Clay	126	0.35	0.50	0.50	3	-

paper, as well as additional tests in sand and silt. Figure 21 shows that a precision of ± 50 percent can be expected from Menard's rules.

Column 8 in Table 4 indicates the true factors of safety that were obtained by using the proposed bearing capacity design curves of Figure 15 and a chosen factor of safety of 3.

SETTLEMENT: ELASTICITY APPROACH

An alternative to Menard's settlement approach would be to use the elasticity formula *(21)*:

$$S = I_o I_1 (1 - \nu^2) q (B/E_o) \quad (28)$$

where

- S = the footing settlement,
- I_o and I_1 = influence factors,
- ν = Poisson's ratio,
- q = the bearing pressure,
- B = footing width, and
- E = pressuremeter modulus within the zone of influence.

Equation 28 was used to calculate the settlement of the footings under q_{safe} (Column 5, Table 4). The factors I_o and I_1 were obtained from Jambu et al. *(21)* using a length-to-diameter ratio of 20 for strip footings and a depth of hard-layer-to-diameter ratio of 20 for infinitely deep deposits (Figure 22). The average pressuremeter modulus, E_o, was obtained by following the averaging technique proposed by Schmertmann *(22)* together with his recommended strain distribution.

The resulting settlements are listed in Column 5 of Table 4. Figure 23 is a plot of predicted versus measured settlements. This figure shows that this elasticity approach predicts settlements for footings on stiff clay, which compare very well with the measured settlements.

The validity of the chart by Jambu et al. *(21)* has been challenged by Christian and Carrier *(23)*. The use of the modi-

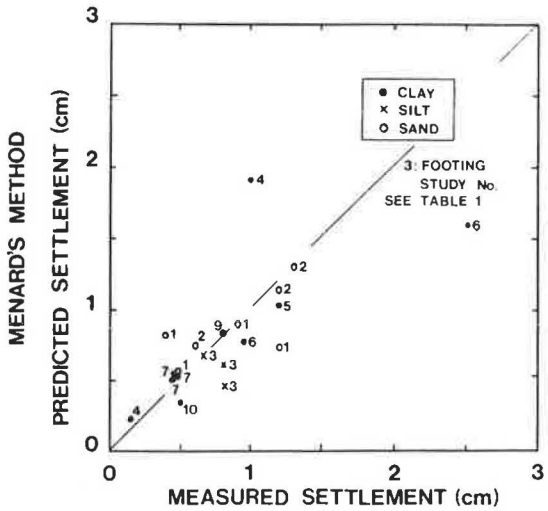

FIGURE 21 Measured versus predicted settlement by Menard's method.

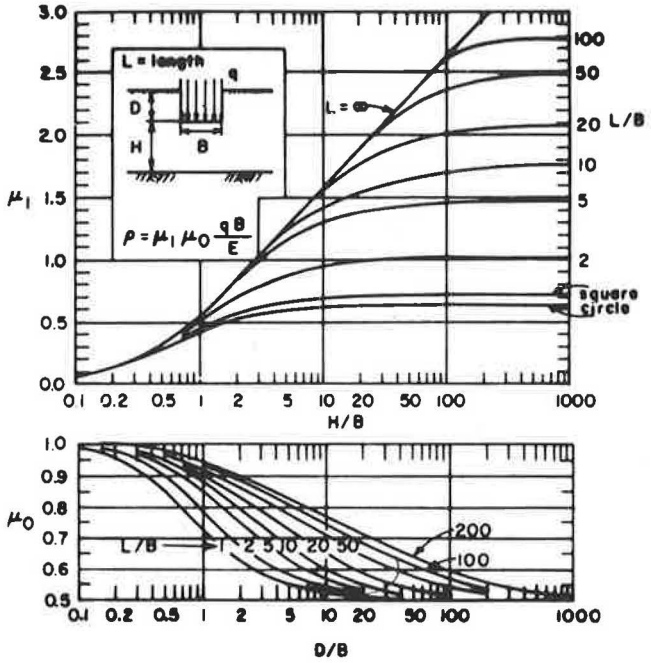

FIGURE 22 Jambu-Bjerrum-Kjaernsli chart *(21)*.

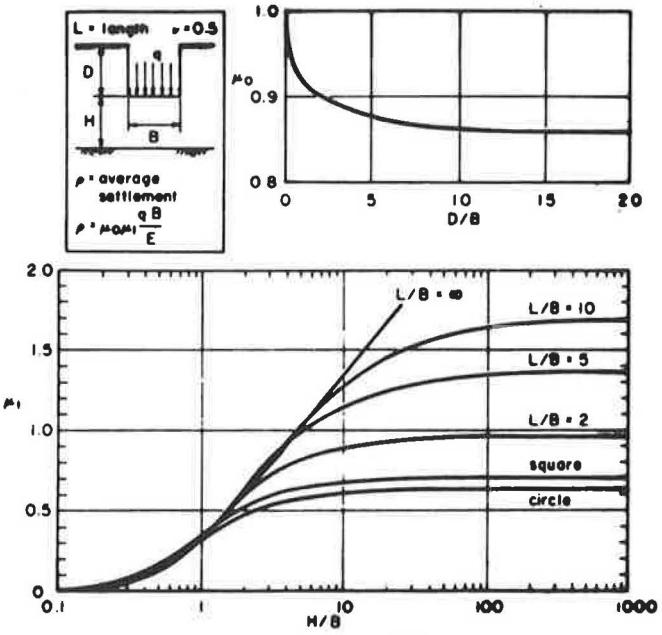

FIGURE 24 Christian carrier chart *(23)*.

fied chart proposed by Christian and Carrier (Figure 24) will generally lead to higher predicted settlement; note that this chart applies only to a Poisson's ratio of 0.5.

SETTLEMENT: GENERAL BEHAVIOR

The 17 load test results presented in Figures 5 to 14 can be regrouped on a normalized load settlement plot (Figure 25). The load is normalized to the ultimate load at a settlement of one-tenth of the footing width; the settlement is normalized to one-tenth of the footing width. The resulting curves fall within the band shown in Figure 25 indicating that with a factor of safety of 3, the settlements for the load tests on stiff clay were 0.5 to 1 percent of the footing width.

CONCLUSIONS

Load test results on shallow footings varying from 0.30 m to 2.41 m (1 ft to 7.9 ft) have been presented together with predicted behavior using preboring pressuremeter test results.

The ultimate bearing pressure is defined as the pressure reached at a settlement equal to one-tenth of the footing width, the measured values of ultimate bearing pressure allowed to propose new simplified bearing capacity design curves. These curves are somewhat more conservative than the previously existing design curves. The ratio of predicted overmeasured bearing capacity using new pressuremeter rules varies from 0.60 to 1.24 (Figure 15). The same ratio using the general bearing capacity equation varies from 0.51 to 1.67 in clay and from 0.12 to 12 in sand (Figures 16 and 17).

The settlement at one-third of the ultimate bearing pressure predicted by Menard's method compared relatively well with the measured settlement. The precision of the Menard settle-

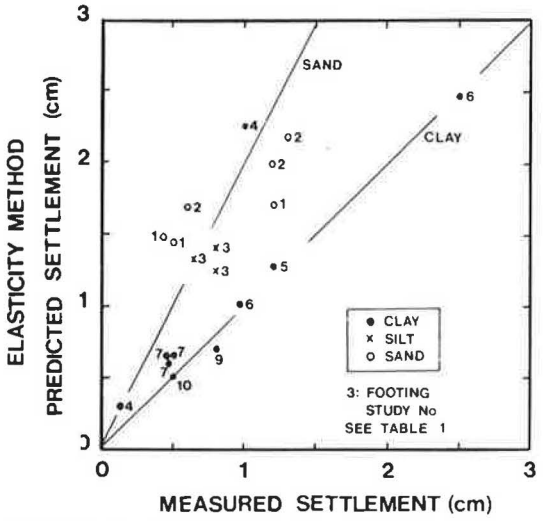

FIGURE 23 Measured versus predicted settlement by elasticity method.

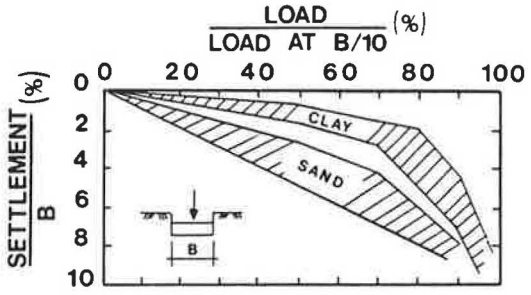

FIGURE 25 General behavior of footings.

ment predictions is about + 50 percent (Figures 20 and 21). An elasticity approach is proposed to predict settlement; this approach is promising (Figure 23), however, more work is required in order to fully evaluate its potential.

REFERENCES

1. J. L. Briaud and M. Gambin. Suggested Practice for Drilling Boreholes for Pressuremeter Testing. *ASTM Geotechnical Testing Journal*, Vol. 7, No. 1, 1984.
2. J. L. Briaud, L. M. Tucker, and R. S. Olsen. Pressuremeter and Foundation Design. Short Course Notes, Vol. 1, Civil Engineering Department, Texas A&M University, College Station, 1982.
3. E. Winter. Suggested Practice for Pressuremeter Testing in Soils. *ASTM Geotechnical Testing Journal*, Vol. 5, No. 3/4, 1982.
4. J. L. Briaud, A. Noubani, J. Kilgore, and L. M. Tucker. Correlations Between Pressuremeter Data and Other Soil Parameters. *Research Report*. Civil Engineering Department, Texas A&M University, College Station, Nov. 1985.
5. L. Menard. Calcul de la Force Portante des Fondations sur la Base des Resultats des Essais Pressiometriques. *Sols-Soils*, Vol. 2, Nos. 5 and 6, 1963.
6. A. W. Skempton. The Bearing Capacity of Clays. *Proc., Building Research Congress*, Vol. 1, 1951.
7. A. S. Vesic. Expansion of Cavities in Infinite Soil Mass. *Journal of the Soil Mechanics and Foundation Engineering Division, ASCE*, Vol. 98, No. SM3, 1972.
8. F. Baguelin, J. F. Jezequel, and D. H. Shields. *The Pressuremeter and Foundation Engineering*. Trans Tech Publications, Rockport, Mass., 1978.
9. D. H. Shields and G. E. Bauer. Determination of the Modulus of Deformation of a Sensitive Clay Using Laboratory and In Situ Tests. *ASCE Specialty Conference on In Situ Measurement of Soil Properties*. North Carolina State University, Raleigh, 1975.
10. M. W. O'Neill and S. A. Sheikh. Geotechnical Behavior of Underreams in Pleistocene Clay. *Proc., Session on Drilled Piers and Caisson II*, ASCE Convention, Denver, Colo., May 1985.
11. J. L. Briaud and K. Riner. A Study of Cyclic Pressuremeter Testing for Offshore Applications. *Research Report 4839*. Civil Engineering, Texas A&M University, College Station, 1984.
12. M. W. O'Neill and L. C. Reese. Behavior of Axially Loaded Drilled Shafts in Beaumont Clay. *Research Report 89-8*. Center for Highway Research, University of Texas, Austin, 1970.
13. Woodward Clyde Consultants. *Study to Investigate the Effects of Skin Friction on the Performance of Drilled Shafts in Cohesive Soils*. U.S. Army Waterways Experiment Station, Vicksburg, Miss., Aug. 1981.
14. K. E. Tand, E. G. Funegard, and J. L. Briaud. Bearing Capacity of Footings on Clay: CPT Method. *Use of In Situ Tests in Geotechnical Engineering*, ASCE Specialty Conference, Blacksburg, Va., 1986.
15. Briaud Engineers. Foundation Investigations Using Pressuremeter Testing at Chocolate Bayou and Texas City Amoco Plants. Kenneth E. Tand and Associates, Inc., Houston, Tex., Jan. 1984.
16. A. Marsland and M. F. Randolph. Comparison of the Results from Pressuremeter Tests and Large In Situ Plate Tests in London Clay. *Geotechnique*, Vol. 27, No. 2, 1977, pp. 217–243.
17. L. D. Johnson. Correlation of Soil Parameters from In Situ and Laboratory Tests for Building 333. *Use of In Situ Tests in Geotechnical Engineering*, ASCE Specialty Conference, Blacksburg, Va., 1986.
18. S. Amar, F. Baguelin, and Y. Canepa. Etude Experimentale du Comportement des Fondations Superficelles. *Annales de l' I.T.B.T.P. 427*. Serie Sols et Fondations 189, Sept. 1984.
19. L. Menard and J. Rousseau. L'Evaluation des Tassements-Tendances Nouvelles. *Sols-Soils*, Vol. 1, No. 1, 1962.
20. L. Menard. The Menard Pressuremeter: Interpretation and Application of Pressuremeter Test Results to Foundation Design. *Sols-Soils*, No. 26, 1975.
21. N. Jambu, L. Bjerrum, and B. Kjaernsli. *Guidance in the Solution of Foundation Problems*. Publication 16. Norwegian Geotechnical Institute, Oslo, 1956.
22. J. H. Schmertmann. Improved Strain Influence Factor Diagram. Technical Note. *Journal of the Soil Mechanics and Foundation Engineering Division, ASCE*, Vol. 104, No. BT8, 1978.
23. J. T. Christian and W. D. Carrier. Jambu, Bjerrum, and Kjaernsli's Chart Reinterpreted. *Canadian Geotechnical Journal*, Vol. 15, 1978, pp. 123–128.
24. J. H. Deschenes. *Bearing Capacity of Footings Close to Slopes of Cohesionless Soil*. Ph.D. dissertation. Civil Engineering, University of Ottawa, Canada, 1978.
25. J. L. Briaud. *The Pressuremeter: Application to Pavement Design*. Ph.D. dissertation. Department of Civil Engineering, University of Ottawa, Canada, 1979.

Publication of this paper sponsored by Committee on Foundations of Bridges and Other Structures.

Brighton Avenue Bridge Replacement Supported on Spread Foundations

PAUL F. BYRNE AND HUGH S. LACEY

The replacement of a 70-year-old railroad bridge with a new, longer span over an improved and widened urban street required an extensive geotechnical study to determine the optimum foundation type for the site. Traditional deep foundation solutions of driven piles and concrete caissons were investigated, along with the ultimate selection-spread foundations on a pressure-grouted bedrock, described as a thinly bedded calcerous shale with varying degrees of decomposition. Presented are planning, design, and construction considerations.

Discussed in this paper are the planning, design, and construction of a 94-ft span, through-girder, steel railroad bridge in a tightly confined urban setting, with emphasis on techniques to reduce foundation costs while maintaining traffic on adjacent transportation arteries. Described in particular is how pressure grouting was used to improve the existing bedrock foundation by filling voids and joints, thus avoiding the necessity of a more expensive pile foundation.

Demolition of an existing railroad bridge and construction of the new bridge and appurtenances at a cost of $1.1 million was one phase of a $9.2 million highway reconstruction project that also included replacement of another bridge, an upstation highway crossing of the same railroad.

NEED FOR PROJECT

The necessity of replacing the existing 70-year old, 45-ft, single-span, plate-girder railroad bridge over Brighton Avenue in Syracuse, New York, was dictated by the following conditions:

- Bridge condition: The steel plate girder superstructure with riveted joints was in serviceable condition, but after 70 years of weathering and quarry train traffic, there was severe rusting and loss of section on some secondary members. In addition, the roller joints were nonfunctional.
- Layout: The northbound highway traffic approached the structure on a 1,100-ft downgrade of 6 percent, and the southbound traffic passed under the grade separation on a 19.1-degree (300-ft radius) curve.
- Vertical clearance: The vertical clearance between Brighton Avenue and the lower flange of the existing bridge was 12 ft, whereas the maximum state legal vehicle height is 13 ft 6 in.
- Lateral clearance: In the northbound lane, the lateral clearance from the edge of the 20-ft roadway to the abutment was 1 ft. In the southbound lane, there was a 4-ft wide sidewalk without curb between the edge of pavement and the abutment. The paved roadway narrowed from 48 ft to 20 ft at the bridge within a distance of 120 ft.
- Roadway capacity: Under preconstruction (1980) conditions, the adjusted average daily traffic (AADT) of 12,200 vehicles exceeded the existing roadway capacity, and the prediction for the year 2010 showed an increase to 16,200 AADT. Thus, the bridge contributed to a traffic restriction, which, if left uncorrected would only become worse with the increased traffic associated with the anticipated population growth in the city's southern suburbs.
- Sight distances: Vehicles approaching the bridge from both directions had a substantially obstructed view of the road ahead.
- Safety: According to research conducted by the New York State Department of Transportation (NYSDOT), the accident rates in 1973 and 1974 on the stretch along Brighton Avenue near the bridge were 10.1 and 9.7 accidents per million vehicle miles, respectively. This rate is more than twice the statewide average of 3.68 accidents per million vehicle miles for two-lane urban roads. Inspections of the old stone block bridge abutments revealed evidence of numerous bridge-vehicle collisions, the majority of which occurred without being officially reported.

SITE CONSTRAINTS

The location of the bridge, spanning a major arterial into the city, was one of the elements dictating its replacement. Its location also contributed to logistical and construction difficulties. The project site is located in a congested urban neighborhood with mixed residential, light industrial, and commercial use. Brighton Avenue, the city street crossed by the bridge, carries a steady volume of local traffic (15 percent trucks), as well as commuter traffic between the city and the expanding southern suburbs.

The northbound lane of Interstate 81 is about 55 ft from the west wingwalls, and property had to be acquired from New York State for the construction of the abutments, wingwalls, and an adjacent retaining wall. The major physical constraint, however, was the Binghamton-Syracuse Branch line of the Consolidated Rail Corporation (Conrail). The new railroad main line was constructed less than 20 ft from the old main line without interruption of rail service, which was essential for the operation of the local Allied Chemical Corporation plant. Figure 1, which shows the new bridge abutments under construction, provides a perspective of Interstate-81 in the foreground and the existing railroad bridge in the background.

P. F. Byrne, Calocerinos & Spina Consulting Engineers, 1020 7th North St., New York, N.Y. 13088. H. S. Lacey, Mueser Rutledge Consulting Engineers, 708 Third Ave., New York, N.Y. 10017.

FIGURE 1 Brighton Avenue railroad bridge under construction.

BRIDGE SITE OPTIONS

During the planning stage, the following options were considered:

1. Change the alignment of Brighton Avenue so as to remove the steep grade and curve at the bridge and reuse the existing superstructure. This option was given only brief consideration because the existing 20-ft roadway was substandard for even a two-lane roadway, and the fixed distance between abutments would not permit a roadway that could adequately handle the anticipated traffic volume. Thus, the bottleneck would remain.
2. Under the second option, a temporary railroad bridge would be constructed, the existing bridge would be demolished, and the new bridge would be constructed on the site of the original bridge.
3. The third option provided for the construction of a new bridge adjacent to the old bridge while it remained in use.

After initial consideration, Option 1 was rejected and only Options 2 and 3 were seriously evaluated. Option 2 had the advantage of minimal additional track work beyond the bridge site. However, a cost comparison of the two options revealed that, despite the additional track work, the city would save approximately $1 million by eliminating the temporary structure and building the new structure adjacent to the existing bridge. In addition, critical construction time was reduced by approximately 3 months. Therefore, Option 3 as shown in Figure 2 was selected.

GEOTECHNICAL CONDITIONS

The field geotechnical investigation for this project was conducted in two stages:

1. In 1979, the Soil Mechanics Bureau of the New York State Department of Transportation took four borings in the vicinity of the bridge to a depth of between 30 and 40 ft.
2. In 1982, Geotechnical Drilling and Testing, Inc. of Castleton, New York, under the direction of Calocerinos & Spina, took an additional 11 borings. The majority of the borings were to a depth of 30 to 40 ft, with one deep boring advanced to 75 ft.

The additional borings confirmed the findings of the soil mechanics bureau and also provided data for the development of subgrade profiles and the determination of rock surface topography.

The geologic sections of the site, shown in Figures 3 and 4, reveal about 5 to 7 ft of loose to compact granular mixed fill

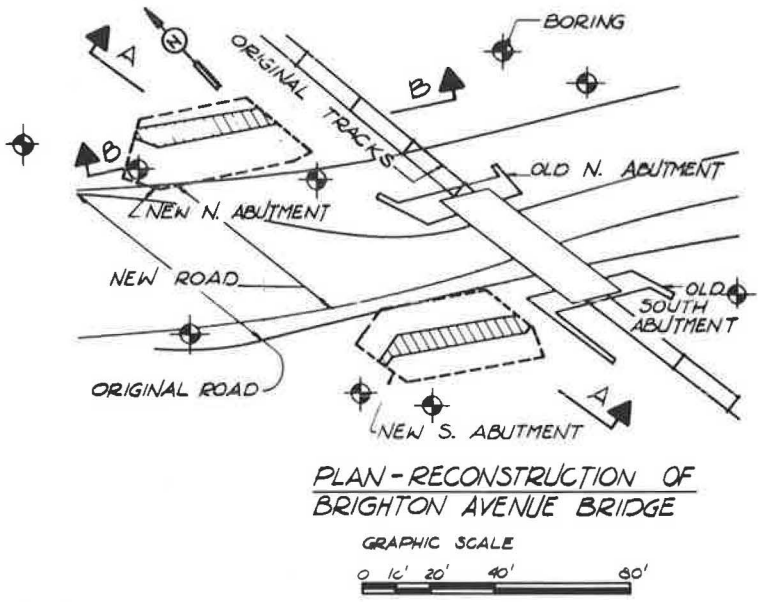

FIGURE 2 Site plan.

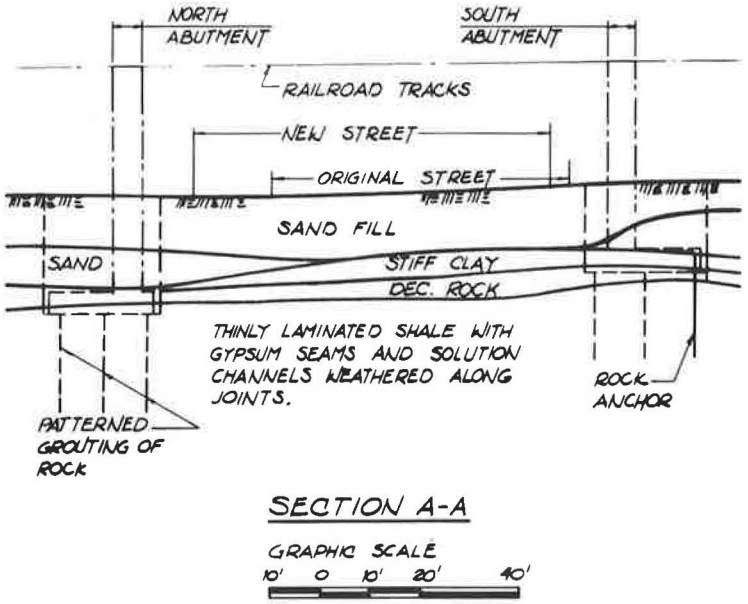

FIGURE 3 Geological section.

underlain by 8 to 18 ft of a compact till matrix containing silt and sand in the upper section and coarser materials and gravel at the greater depths. Shale bedrock is encountered at depths between 13 and 25 ft below the surface. The bedrock can be described as a thinly bedded calcerous shale, varying in degrees of weathering or decomposition. The shale is horizontally bedded with predominant joints in the horizontal and vertical planes. The voids encountered in drilling are primarily the result of the solution of gypsum seams, a property that is characteristic of the Camillus shale formation. Most of the core samples reacted to hydrochloric acid, indicating the presence of a carbonate in the shale bedrock. The thin resistant layers alternating with decomposed layers are apparently the result of a variable magnesium carbonate content (dolostone) in the bedrock.

As a result of being thinly bedded or in a decomposed condition, all rock cores recovered in the vicinity of the railroad bridge had a rock quality designation (RQD) value of 0. It is also noteworthy that the shale layers were friable in many cases. The ground water level was generally at or below the surface of bedrock; the borings indicated the possibility of perched water in the fill, but no significant sources were encountered during construction and only occasional pumping was required to remove surface water.

A supplementary phase was added to the geotechnical program in order to determine the depth of the existing stone masonry abutments, information required for the design of the adjacent sheeting pits. Because no as-built drawings of the original structure were available, this information was obtained by taking an angle boring through the face of the abutment at grade using a skid-mounted percussion drill.

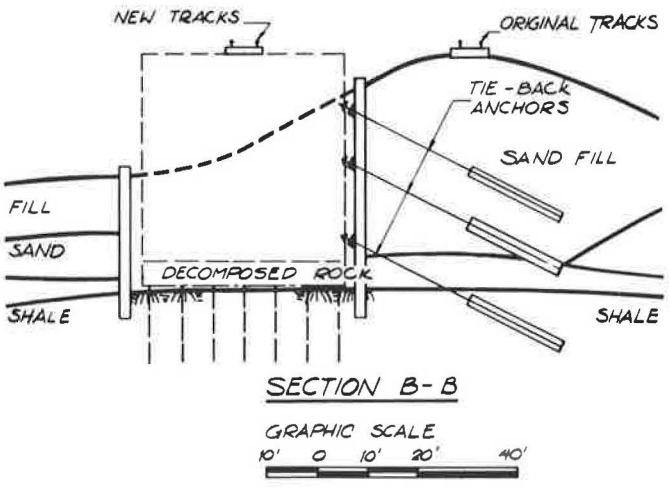

FIGURE 4 Tieback section.

FOUNDATION DESIGN CONSIDERATIONS

Several alternatives were investigated for the bridge abutment foundations. Initially, a deep foundation system of driven piles or concrete caissons was favored, but subsequent examination of the boring logs discouraged this approach because of the presence of erratic voids in the bedrock as shown by dropping of drill rods and loss of water during drilling; the actual cores examined had small holes, gypsum seams, and low recovery. The concentrated loads associated with piles or caissons might collapse the voids in the shale formation. Shallow footings supported on imported compacted sand were also considered, but with an allowable bearing capacity of 2 to 3 tsf, the footings would have been excessively large for the restricted site. Therefore, the type of abutment selected was a cantilevered retaining wall foundation with bearing on the shale bedrock just below the topmost weathered zone. Because of the slope in the bedrock in this area, the south abutment was scheduled to be founded at Elevation 447 and the north at Elevation 441; the existing and proposed grade of Brighton Avenue is approximately 465.

As an added precaution, pressure grouting was specified for

the bedrock at both abutments to permit an increase in the bearing capacity from 8 to 15 tsf and fill any collapse-susceptible voids and joints. The estimated possible settlement from collapsing voids was in the range of from 1 to 6 in., which was unacceptable. In addition, the drilling and grouting operation would provide an indication of the presence of large voids that might warrant further investigation. Selection of the 20-ft depth for rock drilling of grout holes was based on the level of the majority of the voids as indicated in the borings and on the goal to reduce the loading at the base of the grouted rock zone to less than 8 tsf.

The abutments were designed with a safety factor of 2.0 for overturning and 1.5 for sliding. This was easily achieved by the mass of the footing and the quantity of backfill on the northern abutment. However, for the shallower south abutment, there was no room to increase the toe length without encroaching on the existing road, which had to be kept in service for its full width. Analysis showed that, for the critical load condition during construction, before placement of bridge girders, the resultant was outside the middle third of the abutment. Although the allowable rock pressure was not exceeded under this condition, the safety factor against overturning was closer to 1 than 2. To increase the safety factor to the desired level, a row of rock anchors (embedded No. 11 bars) was specified for the heel end of the footing. The 20-ft long anchors with a 17.5-ton design load were sized using an allowable grout-rock bond stress of 20 psi and a length sufficient to mobilize a cone of rock equal to 110 percent of the design load. This contributed little additional cost because the drill rigs were already on-site for the pressure grouting of the bedrock. This approach saved additional rock excavation and an equivalent volume of reinforced concrete.

After the decision was made to keep the existing railroad bridge in service while constructing the new one adjacent to it, the major concern was providing temporary support for the existing abutments and embankments while advancing an adjacent 40-ft-deep excavation. Because of the critical need for rigid support of adjacent ground, Mueser Rutledge Consulting Engineers designed the system of temporary support for the excavation. The system was fully detailed on the contract drawings and vital time was saved by eliminating the usual contractor design and engineer review process. In addition, early approval from the reviewing agencies was facilitated.

The temporary support system was designed using active pressures redistributed for a braced excavation. The effects of the sloping embankment and the railroad surcharge were included. The final design of the excavation support system used several different techniques for an efficient and site-specific solution to the problem. As shown in Figures 5 through 8, HP 12 × 53 soldier piles at the south abutment and HP 14 × 73 soldier piles at the deeper north abutment were spaced at a maximum of 7 ft OC, with closer spacing adjacent to the tracks. In order to protect the existing tracks and embankment from the vibration effects normally associated with pile driving, it was specified that all piles within about 25 ℄ of the track centerline be installed by augering from existing grade to a depth 5 ft below the base of the abutments. Steel casing was used to keep the holes open and to prevent loss of ground. Full strength

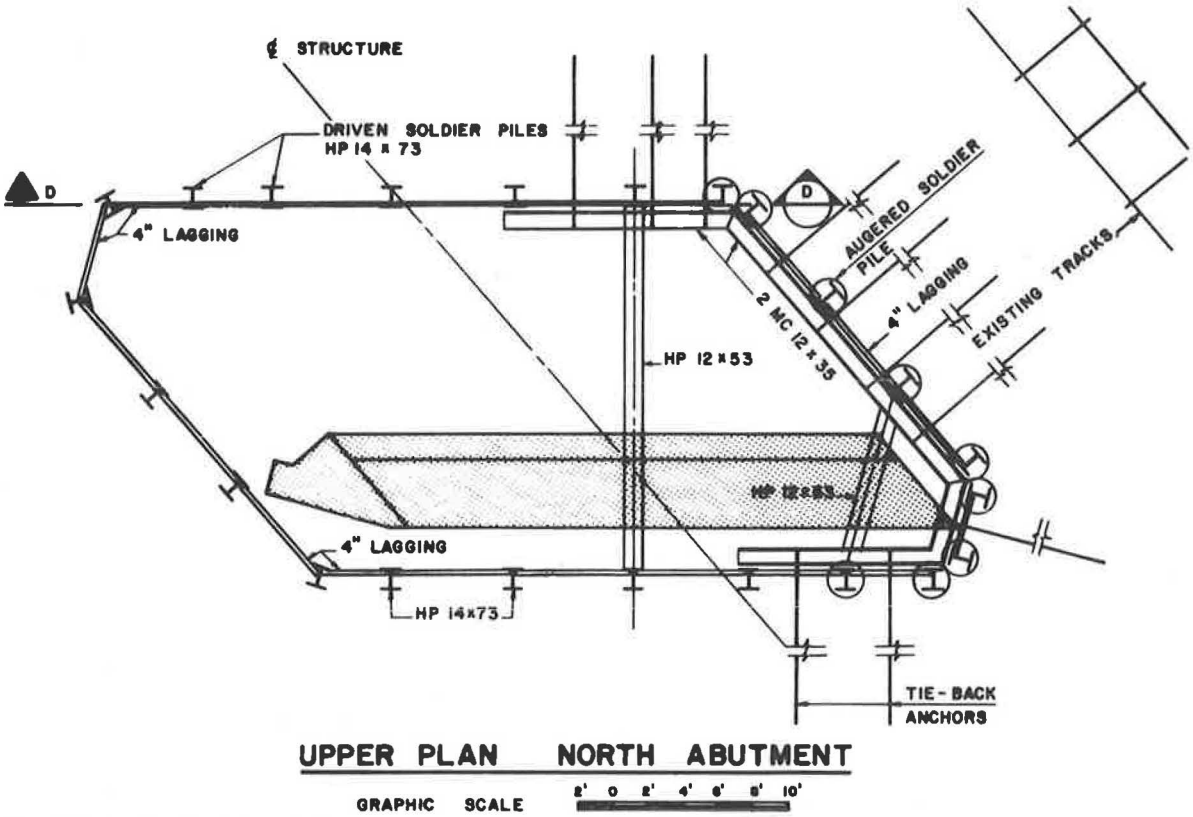

FIGURE 5 North abutment plan.

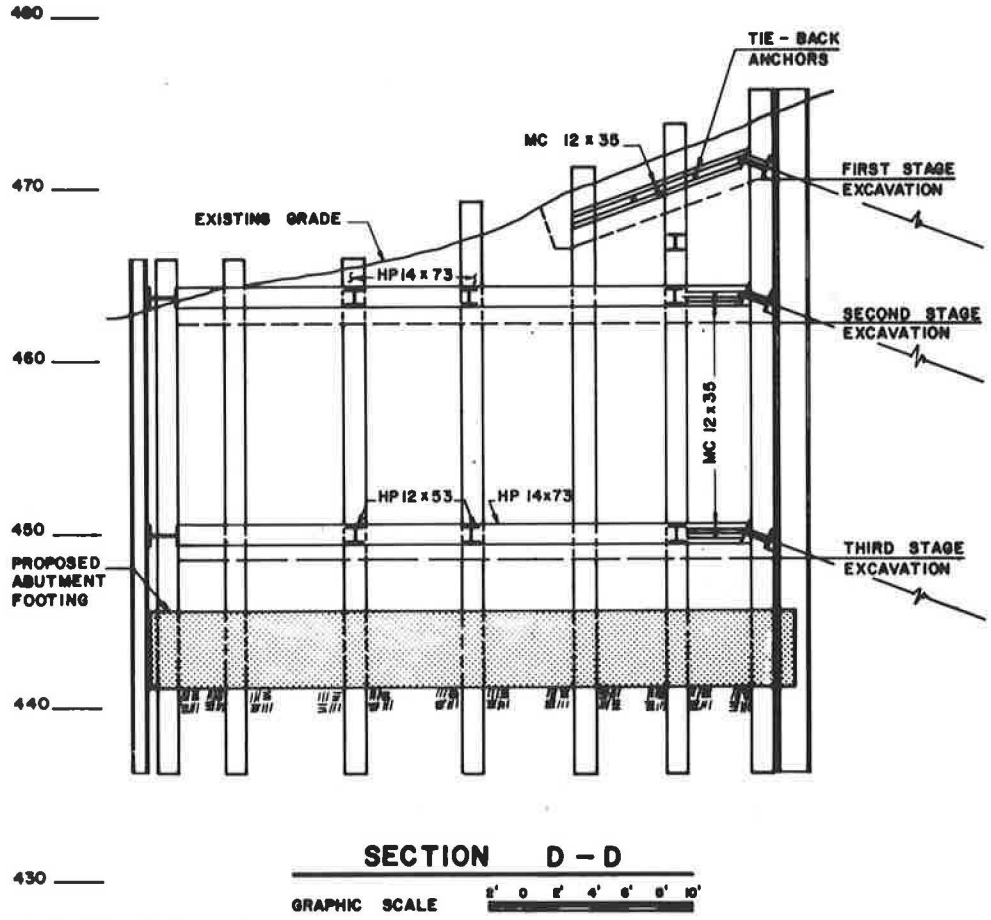

FIGURE 6 North abutment section.

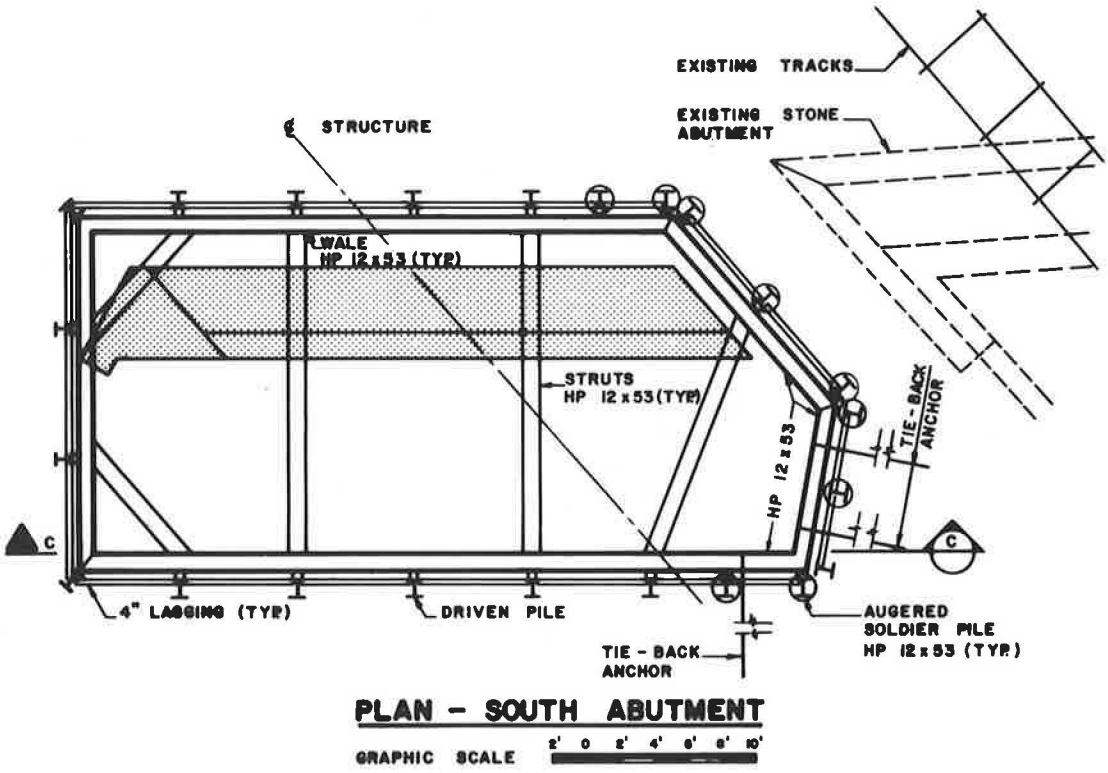

FIGURE 7 South abutment plan.

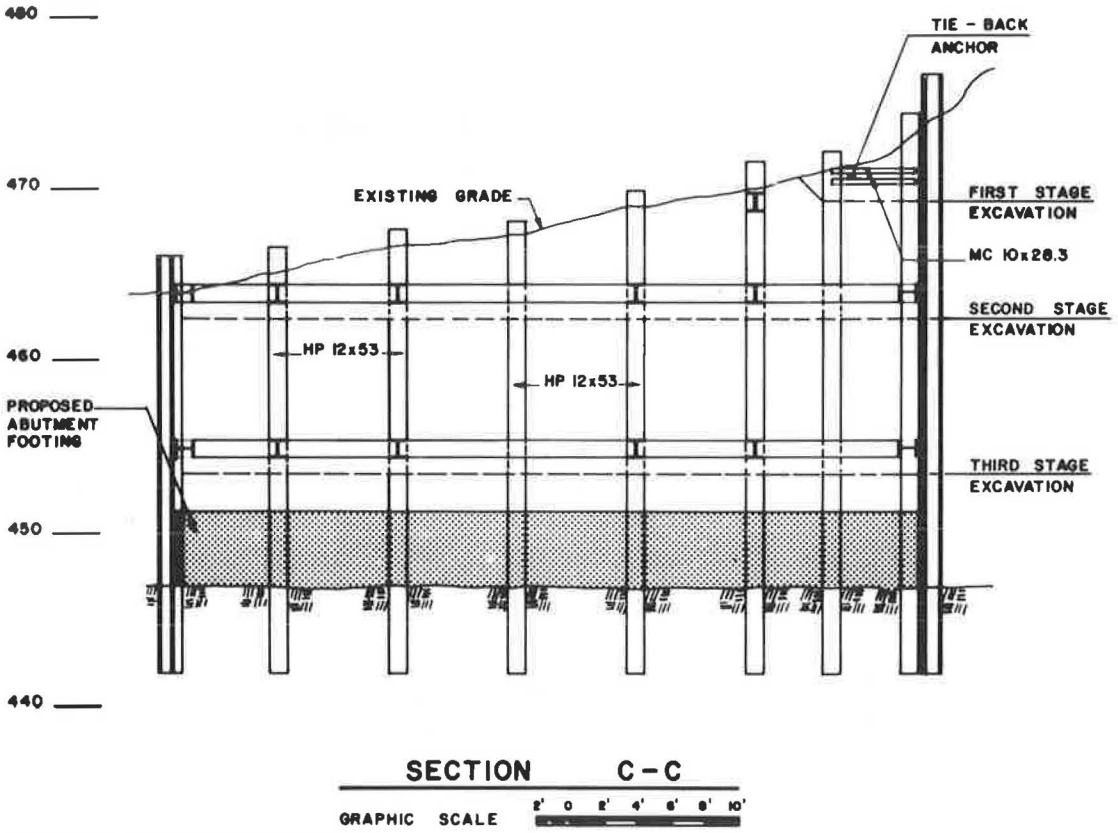

FIGURE 8 South abutment section.

(4,000 psi) concrete was used to anchor the piles for the bottom 5 ft; above this elevation, lean concrete (1 bag mix) was placed as the casing was withdrawn. Piles fartherest from the track were driven conventionally.

CONSTRUCTION

Following installation of the augered soldier piles with a truck-mounted rig, using a 36-in. auger in soil and a 24-in. bit in rock, vertical and horizontal control points were established on selected soldier piles, slope stakes, and track rails. These points were monitored twice daily during abutment construction in order to detect and correct any movement trends associated with the deep excavations within the existing railroad embankments. Figure 9 shows a location plan of the vertical control points along the railroad tracks. A time versus settlement plot of these points is presented in Figure 10 and shows that no significant settlement of track occurred during excavation. The slight differences in elevation over time are attributed to the effect of temperature variations and frost heave on the soil below the steel rails. Horizontal movement was insignificant.

With the monitoring system in place, the excavation support system construction proceeded. As the excavation advanced, the annular ring of lean concrete surrounding the soldier piles was easily removed with hand tools, thus permitting the installation of timber lagging from web to web of adjacent piles. Concurrent with the lagging, three stages of double channel wales (MC 12 × 35) were installed. Through each wale stage, corrosion-resistant tiebacks (120 K design load) were drilled and grouted in place along the embankment side of the

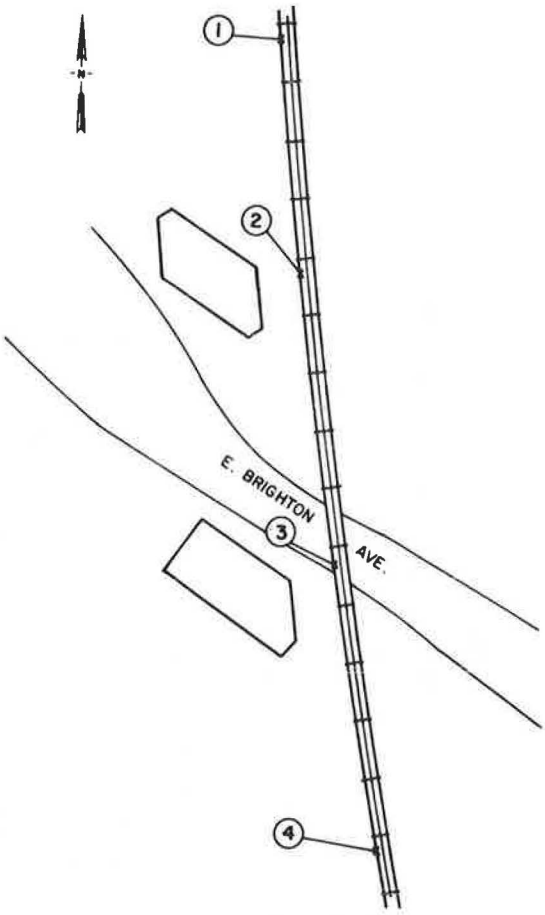

FIGURE 9 Vertical monitor points location plan.

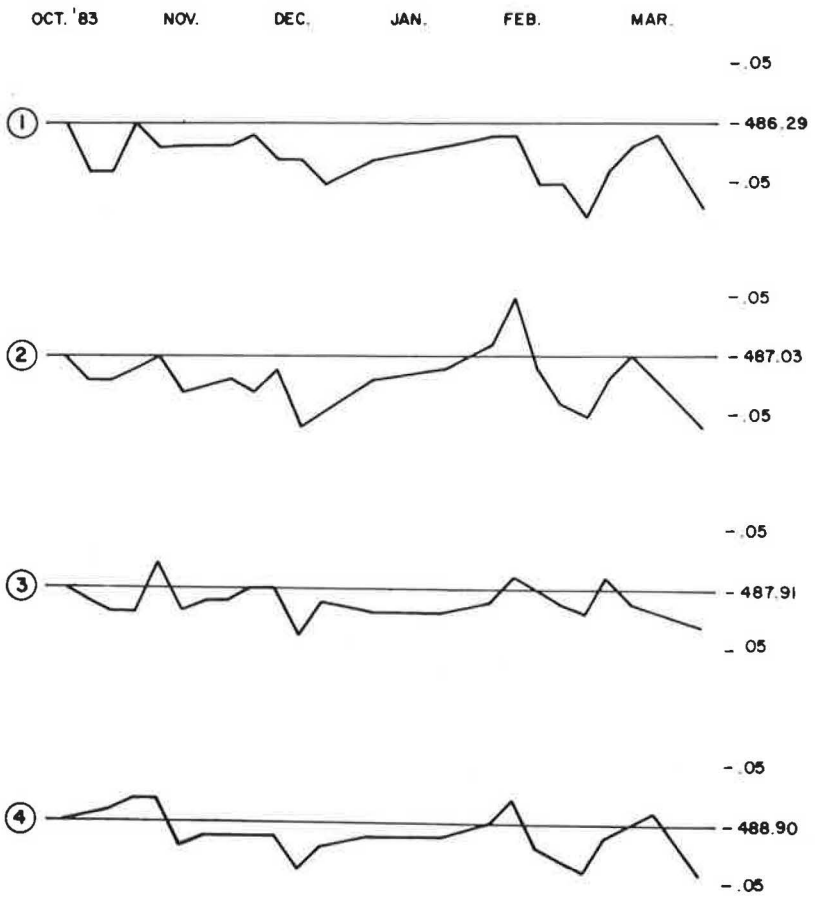

FIGURE 10 Time versus movement plot of vertical control points.

abutment excavation. The tiebacks were installed at an angle of 27 degrees from horizontal to avoid the accentuated rock weakness along the horizontal joints. The 3-in. diameter holes were drilled with a self-propelled air track. The holes that were temporarily supported through the soil with casing were flushed with water and grout was tremied, under pressure, using Type 3 portland cement. A prefabricated anchor consisting of five 1/2-in. diameter cables was installed using polyethylene tubing as sheathing over the unbonded length. Minimum anchor lengths were established beyond the unbonded sections using allowable bond stresses in the soil overburden and rock of 25 and 50 psi, respectively. Other failure modes were also checked. Load deflection measurements plotted consistently on lines nearly identical to elastic lines for the effective anchor lengths, indicating satisfactory installations. All tiebacks were proof-tested to 130 percent of the design load before being locked off at 80 percent of the design load. This system permitted tension loading of the tie back anchors with minimum soil excavation and with insignificant track settlement.

As shown in Figure 7, the proximity of the existing south abutment limited the space in which tiebacks could be effectively anchored. By the same token, the existing abutment served to shield soil loading from the excavation, and other braces were installed to prevent shifting of the existing abutment. Costs were further reduced by using cross-bracing struts to support the excavation parallel to Brighton Avenue where potential minor settlements were not as critical as on the Conrail tracks. The bracing was designed to be installed at elevations that would facilitate the use of construction joints and the placement of backfill. This permitted the progressive removal of bracing in advance of the placement of concrete for the abutment stems. The combination of augered soldier piles, timber lagging, channel wales, and grouted tiebacks produced an efficient excavation support system with minimal cross bracing, which simplified equipment access and excavation soil removal.

The south abutment was excavated according to plan at Elevation 447. The subgrade level for the north abutment was scheduled to be Elevation 441; however, examination of the subgrade at Elevation 444 showed a good quality Camillus shale bedrock. The decision was then made to establish the north abutment at this elevation. This resulted in a savings of approximately 71 yd^3 of footing excavation and 31 yd^3 of stem concrete, while maintaining acceptable safety factors.

The process of improving the bedrock by pressure grouting began on completion of excavation and subgrade rock surface cleaning. Holes of 2½-in. diameter and 20-ft depth were drilled into rock in the patterns shown in Figures 11 and 12. The holes were then pressure-washed until clean water was returned to the surface in order to remove any material that might clog cavities and fissures. In some holes, wash water did not return, indicating the possibility of far-reaching solution cavities or veins. A decision was then made to cease water testing on those holes that did not return wash water in a reasonably short time. It was believed that further washing under pressure might serve to enlarge some of the existing small drainage paths.

The neat cement grout consisting of Type II cement and

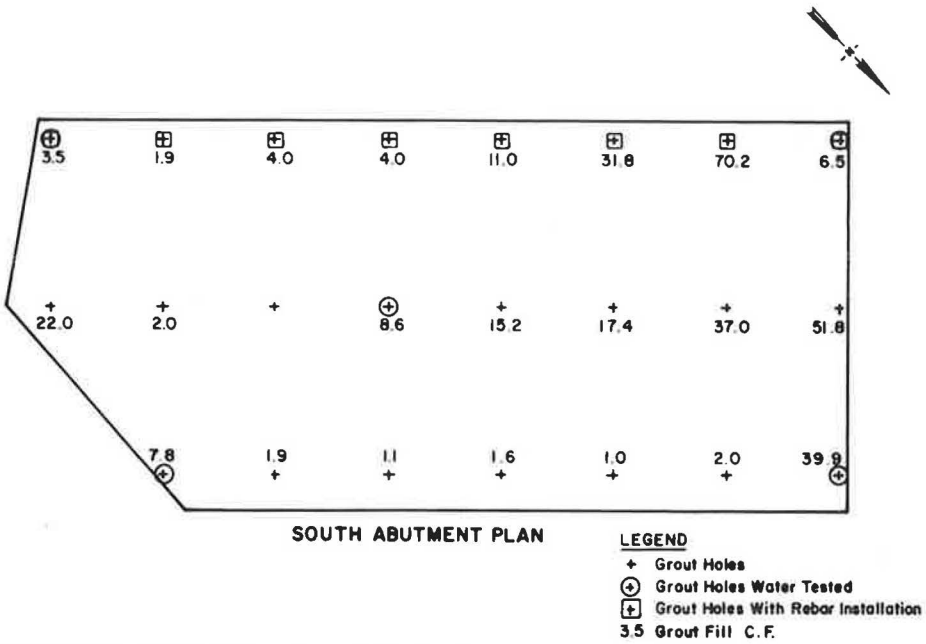

FIGURE 11 South abutment grout hole location plan.

potable water was mixed in an air-driven agitating tank and pumped to the holes with a progressing cavity pump (Moyno 3L6). Pressure, which varied with the depth from 5 to 20 psi, was monitored by a gauge mounted on an expandable membrane packer that surrounded the grout pipe in the hole. Grouting proceeded from the bottom up, with the packer positioned at two to three levels. The holes were grouted in an alternate sequence with frequent communication between adjacent holes. The remaining intermediate holes were then grouted, generally resulting in markedly reduced grout takes, thus demonstrating the effectiveness of the grouting program. The grout mix was field adjusted to vary from a lean 3 to 1 mix at the bottom of the hole where a lower viscosity promotes flow in smaller cracks, to a richer 1 to 1 mix near the rock surface. The grout take per hole is shown in Figures 11 and 12. A comparison of the total grout take per abutment shows that the north abutment took about 42 percent more grout than the south abutment. When this trend was recognized during the grouting of the north abutment, the operation was halted and a small supplementary rock coring program was undertaken to discover the reason for the higher than expected grout take. Two additional holes, designated C1 and C2, with depths of 25 and 27 ft, were advanced through the rock with an NX core (3-in. diameter). The drilling revealed no significant voids, as was initially suspected, but it was observed that there was a transition from a weathered intact shale to a more jointed decomposed shale. Because no additional action was required, the two drill holes were used as additional grout holes. The higher than

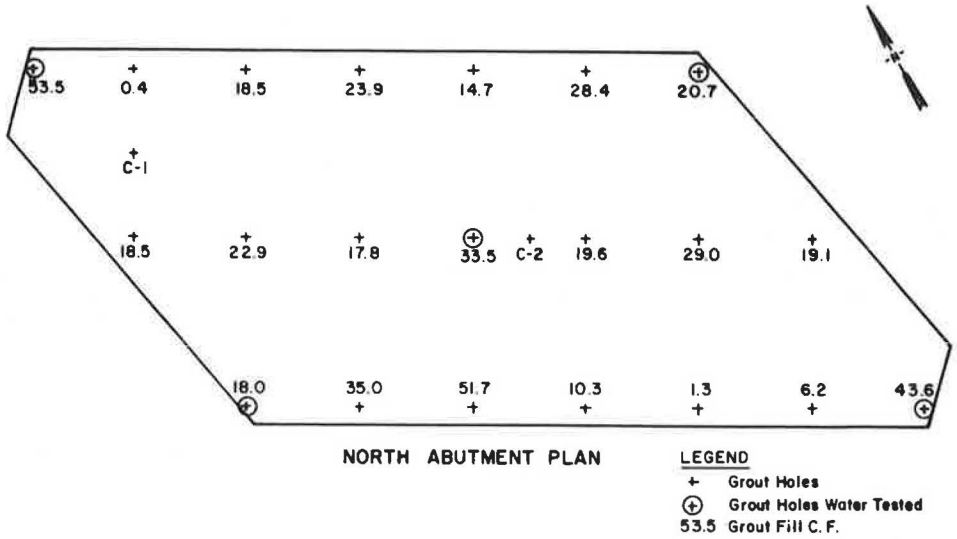

FIGURE 12 North abutment grout hole location plan.

expected grout take in each abutment did not have a significant adverse effect on the project budget, but it did validate and ameliorate the condition of voids in the bedrock formation.

SUMMARY

With construction on the bridge phase of the project recently completed, it can be reported that all major design elements of the foundation performed as anticipated, under both construction loading and railroad live loading. Equally important to the city and Conrail was the fact that rail traffic was unimpeded during construction and vehicular traffic on Brighton Avenue was maintained, even though occasionally reduced to one lane during foundation construction. The only stoppage and rerouting of traffic was limited to a portion of one day when superstructure main girder steel was set.

Publication of this paper sponsored by committee on Foundations of Bridges and Other Structures.

Geotechnical Error Analysis

GREGORY B. BAECHER

A simple method is presented for rationalizing the treatment of uncertainties in geotechnical engineering calculations. This method uses a reliability index to express the degree of confidence in a calculation. The reliability index combines the best estimate with a standard deviation reflecting four principal sources of uncertainty, spatial variability, measurement noise, model bias, and limited data. An example involving shallow footing design is used for illustration.

All engineers design in the face of uncertainties—uncertainty about material properties, conditions encountered in service, models used to predict performance, and many others. Traditionally, this uncertainty has been accounted for by conservative design, with the ratio of facility capacity to the demands placed on it—the factor of safety—chosen from common practice. As a general rule, the approach has been serviceable. Significant geotechnical failures occur at a rate of about 1,000 per year. The consequences of these failures, while important financially, are rarely catastrophic.

On the other hand, the strategy of fixed factors of safety has drawbacks. First, because uncertainty is not addressed directly, there is a tendency to be conservative about each of the estimates needed for design (soil properties, loads, etc.). The result is that the overall design factor of safety is unknown. Second, because the estimates of soil properties, loads, and so forth, are conservative and subjective, predictions of facility performance are often not repeatable. The result is poor quality assurance. Third, levels of uncertainty vary from situation to situation, because amounts and quality of data vary, facility uses vary, and so on. The result is that a fixed factor of safety leads to different likelihoods of adverse performance.

Department of Civil Engineering, Massachusetts Institute of Technology, Cambridge, Mass. 02139.

PURPOSE OF ERROR ANALYSIS

The purpose of error analysis is to improve current practice by expressly considering uncertainties. The term error analysis as used here is not what many now call probabilistic design. Geotechnical engineering involves many uncertainties only some of which are explicit. Therefore, probabilities resulting from analysis are not predictions of rates of failure to be experienced in the field. The majority of failures are attributable to unanticipated loads, gross errors, inadequate maintenance, and other factors not accounted for in design *(1)*.

Error analysis in the present context means a logical accounting for the uncertainties inherent in engineering calculations, and decisions that explicitly balance conservatism against those uncertainties. Specifically, error analysis addresses

1. Selection of design parameters from scattered, limited, and possibly biased data; and
2. Economic rationalization of design.

The method is nothing more than a form of accounting in which uncertainties are tabulated and their influence on engineering calculations combined according to well-defined rules.

UNCERTAINTY IN GEOTECHNICAL DESIGN

Uncertainties in geotechnical predictions are of many types. Some can be quantified, some cannot. In an approximate way they may be divided into five groups:

1. Site conditions,
2. Loads,
3. Model inaccuracies,
4. Construction and quality control, and
5. Omissions and gross errors.

The most important of these for engineering analysis are the first three, which are quantifiable and appear in calculations.

Uncertainties in Site Conditions and Models

If attention is restricted to only those uncertainties that affect calculations, namely site conditions and geotechnical models, a further and more specific subdivision of sources of error is possible. This leads to four sources that are the focus of error analysis:

1. Soil variability,
2. Measurement noise,
3. Measurement and model bias, and
4. Statistical error due to limited measurements.

These are the sources of uncertainty that affect calculated predictions. The first two, soil variability and measurement noise, appear as data scatter. The latter two, measurement and model bias and statistical error, cause systematic errors in predictions.

Data Scatter Equals Spatial Variability Plus Measurement Noise

The scatter among geotechnical measurements is often large. This scatter reflects two things: spatial variability of the soil and random measurement error (noise). A major purpose of statistical analysis is to separate real variability from noise, thereby lessening the magnitudes of data scatter and reducing uncertainty.

Systematic Error Equals Measurement Bias Plus Statistical Error

Bias is a systematic error. If strength is underestimated by a 10 percent bias error at one location, it is underestimated by the same 10 percent everywhere. The distinction between spatial variability and bias is important. For example, a 10 percent probability of failure due to soil variability implies that one-tenth of a long embankment will fail. The same probability due to bias implies a one in ten chance that the entire embankment will fail.

In geotechnical parameter estimation, bias is caused by *(a)* measurement techniques and *(b)* statistical estimation error. Measurement bias is common in geotechnical engineering; it is caused by soil disturbance or a difference between how a property is measured and how a structure imposes load. Statistical bias is also common; it is caused by limited data.

Separating the Sources of Uncertainty

Together, data scatter and systematic error constitute the uncertainty of geotechnical calculations. However, the effects of these components differ, as do the way each propagates through an engineering model. The most important concept of uncertainty analysis has nothing to do with mathematics, rather it has to do with separating source of uncertainty.

The methodology presented here is based on separating errors. It treats calculations and modeling. What results is a reliability index summarizing the confidence that can be placed in calculations.

DESCRIBING UNCERTAINTY

Assessments of soil properties for most purposes are adequately expressed by two numbers: a best estimate, and a measure of uncertainty. Here, the average value and standard deviation are used to express the two attributes. When more than one soil property is estimated, another attribute becomes important. This is the association between the uncertainties in different parameter estimates. Here, the correlation coefficient is used to express this association.

Average Equals Best Estimate

The average or mean of a set of measurements $x = (x_1,...,x_n)$ is denoted m_x, and defined as

$$m_x = 1/n \, \Sigma \, x_i = \text{mean} \tag{1}$$

In effect, the mean is the center of gravity of the measurements along the x-axis. It is used as the best single-valued estimate of x, being neither conservative nor unconservative.

Standard Deviation Equals Uncertainty

The standard deviation of the measurements x is their variation with respect to the mean, expressed as the square root of the sum-of-squared variations

$$s_x = [1/n - 1 \, \Sigma \, (x_i - m_x)^2]^{1/2} = \text{standard deviation} \tag{2}$$

In effect, the standard deviation is the root of the moment of inertia of the data about the mean. The proportional uncertainty or standard deviation normalized by the mean is called the coefficient of variation and denoted Ω_x,

$$\Omega_x = s_x/m_x = \text{coefficient of variation} \tag{3}$$

Just as in mechanics where it is convenient to deal with the moment of inertia rather than its square root, so, too, in analyz-

ing uncertainty is it convenient to deal with the square of the standard deviation rather than s_x itself. The square of the standard deviation is called the variance

$$V_x = s_x^2 = \text{variance} \tag{4}$$

Given the similarity of Equations 1 to 4 to mechanical moments, the mean and variance are often called the first and second moments of the uncertainty in an estimate of x.

Correlation Coefficient Equals Association Between Uncertainties

When dealing with two or more soil properties, the uncertainties in estimates may be associated with one another. That is, the uncertainty in one property estimate may not be independent of the uncertainty in the other estimate. Consider the problem of estimating the cohesion and friction parameters of a Mohr-Coulomb strength envelope based on a small number of tests. If the slope of the envelope to the Mohr circles is mistakenly estimated too steeply, then for the line to fit the data the intercept would have to be too small. The reverse is true if the slope is estimated too flat. Thus, uncertainties about the slope and intercept are not independent, they are related to one another.

The correlation coefficient for a set of paired data $x,y = [(x_1,y_1),\ldots,(x_n,y_n)]$ is denoted $r_{x,y}$, and defined as

$$r_{x,y} = 1/n - 2\ \Sigma\ (x_i - m_x/s_x)\ (y_i - m_y/s_y) = \text{correlation coefficient} \tag{5}$$

In effect, the correlation coefficient is equivalent to a normalized product of inertia in solid mechanics. It expresses the degree to which two parameters vary together. The correlation coefficient is nondimensional because deviations of x and y from their respective means are measured in units of the respective standard deviation. For these reasons $r_{x,y}$ is a convenient measure for expressing the degree of association or dependence between the uncertainties in two properties.

The value of $r_{x,y}$ may vary from +1 to −1; $r_{x,y} = +1$ implies a strict linear relation with a positive slope; $r_{x,y} = -1$ implies a strict linear relation with a negative slope; $r_{x,y} = 0$ implies no association at all.

The corresponding dimensional form of Equation 5, that is, using absolute deviations of x and y rather than normalized deviations, is called the covariance of x,y and denoted

$$C_{x,y} = 1/n - 2\ \Sigma\ (x_i - m_x)\ (y_i - m_y) = \text{covariance} \tag{6}$$

From Equations 5 and 6,

$$r_{x,y} = C_{x,y}/s_x s_y \tag{7}$$

Autocorrelation

Thus far the fact that soil properties are spatially variable has been ignored. They have not only magnitude but also location. The spatial quality of soils data has important implications, for it both strongly affects engineering predictions and increases the amount of information that can be squeezed from a testing program. Fortunately, the salient aspects of spatial variability from an error analysis view are easily analyzed using the statistical concept called autocovariance.

In an approximate way, spatial variability of data can be summarized by two measures: the variance of the data about their mean, and the waviness or frequency content of the variability in space. The longer the period of this waviness, the further data may be spatially extrapolated. Autocorrelation is used to measure waviness.

Autocorrelation measures the statistical association between data of the same type measured at separate locations. For example, the properties of two adjacent soil elements tend to be similar. If one is above average, the other tends to be above average, also; they are associated. Conversely, the properties of widely separated elements are not necessarily similar. If one is above average, the other may or may not be; they are not associated. This association of properties in space can be measured by the correlation coefficient of Equation 5. It is called autocorrelation because the data are all of the same type.

For data x_i, where i = the location of the measurement, the autocorrelation of data separated by interval, δ, is

$$R_x(\delta) = (1/V_x)\ (1/n_{\delta-1})\ \Sigma\ (x_i - m_x)\ (x_{i+\delta} - m_x) \tag{8}$$

the sum taken over all pairs of data having separation distance, δ, their number being n_δ. Autocovariance is related to autocorrelation as covariance is to correlation. The autocovariance of data at points separated by distance, δ is,

$$C_x(\delta) = (1/n_{\delta-1})\ \Sigma\ (x_i - m_x)\ (x_{i+\delta} - m_x) \tag{9}$$

Autocorrelation expressed as a function of separation distance, δ, is said to be the autocorrelation function, and autocovariance expressed as a function of distance, δ, is said to be the autocovariance function.

ESTIMATING UNCERTAINTY

Considered in this section are specific procedures for quantifying the uncertainties identified earlier.

Data Scatter: Soil Variability and Measurement Noise

Scatter in soil data reflects two things: real variability and noise. Yet, the amount of scatter is measured by a single number, namely the standard deviation of the data. It is not possible to separate soil variability from noise simply by inspection. Hence another approach to estimating the fraction of data scatter contributed by either of these sources must be used. The most convenient is through the autocovariance function. The autocovariance function reflects the spatial structure of variability in soil property measurements, and this structure differs depending on how the data scatter is divided between soil variability and noise. Each component has a characteristic signature that can be observed in the autocovariance function.

As a good approximation, measurements taken in the laboratory or field can be modeled as

$$z = x + e \tag{10}$$

where z is the measurement, x is the real soil property, and e is random measurement error. After some algebra, the autocovariance function of the set of measurements turns out to be related to the autocovariance functions of x and e by

$$C_z(\delta) = C_x(\delta) + C_e(\delta) \tag{11}$$

The autocovariance of x equals V_x at $\delta = 0$, and approaches 0 as δ increases. The autocovariance of e, on the other hand, equals V_e at $\delta = 0$, but equals 0 for any $\delta \neq 0$; that is, it is a spike. This is a result of the assumption that the error is independent from one test to another. Thus, for $\delta \neq 0$, the covariance of the e's is zero. Therefore, by extrapolating the observed autocovariance function back to the origin, an estimate of V_x and V_e is obtained directly. For typical in situ measurements on soil, measurement error variances have been found to contribute anywhere from 0 to as much as 70 percent of data scatter Baecher et al. *(2)*.

Systematic Error

Systematic error in the statistical estimation of soil parameters is directly calculated from statistical theory. The most significant of these errors is that in the mean of the soil property in the soil mass. As an approximation, although a robust one, the variance of the statistical error in this mean is

$$V_m = V_x/n \tag{12}$$

where n is the number of measurements. Note, although random measurement error can be eliminated from the data scatter variance to yield a reduced uncertainty, it does contribute to statistical error. Its effect on statistical error can only be lessened by making more measurements. The statistical error in other parameters usually has only second-order effect on predictions.

The last of the major sources of uncertainty, measurement bias, is the most difficult to estimate. Usually, the only way to estimate this component is by comparison of predicted with observed performance or by field-scale experiments. This has been done by Bjerrum *(3)* for field-vane strengths of normally consolidated clay, and has been attempted by other researchers for other applications. Such an approach aggregates a large number of uncertainties or biases together, including those due to inaccuracies of theory and method of analysis. Thus, measurement bias and model bias are usually inseparable.

In Bjerrum's work, the joint effect of bias in field-vane data and bias in 2D modified Bishop stability analysis leads to a correction factor, μ, which is the ratio of back-calculated, undrained strength to measured FV strength. The variation of back-calculated μ's about their mean is summarized in a variance, V_μ, which expresses the uncertainty of the bias term.

Estimating Autocovariance

In this section only a simple and often used approach to estimating autocovariances, the moment estimate, is considered. For readers with greater interest, a more detailed discussion of statistical aspects of estimating autocovariance, including maximum likelihood techniques, is presented by DeGroot *(4)*.

Consider the simple case of measurements at equally spaced intervals along a line, as for example in a boring. Presume that the measurements $x = \{x_1,...,x_n\}$ are uncorrupted by measurement error. The observed autocovariance of the measurements at separation, δ, is

$$c_x(\delta) = (1/n_{\delta-1}) \Sigma (x_i - m_x)(x_{i+\delta} - m_x) \tag{13}$$

where n_δ = the number of pairs of data at separation distance, δ.

This is called the sample autocovariance and is used as an estimator of the real autocovariance, $C_x(\delta)$, for separation distance, δ. Statistically, $c_x(\delta)$ is a moment of the sample data that is used to estimate the corresponding moment of the spatial model. Thus, $c_x(\delta)$ is said to be a moment estimator of $C_x(\delta)$, just as the sample variance is said to be a moment estimator of the real soil variance, V_x.

In the general case, measurements are seldom uniformly spaced and, at least in the horizontal plane, seldom lie on a line. For such situations the moment estimator of the autocorrelation function can still be used, but with some alteration. The most common way to accommodate nonuniformly placed measurements is by dividing separation distances into bands, and then taking averages of Equation 13 within those bands. This introduces some bias to the estimate but for most engineering purposes it is sufficiently accurate.

Combining Uncertainties in a Design Profile

The total uncertainty in engineering properties at a point in the soil profile reflects the combination of data scatter and systematic error. Algebraically, this total uncertainty, measured as a variance, is expressed as

$$V = V_1 + V_2 + V_3 + V_4 \tag{14}$$

where the four components of variance summarize, respectively, the four contributions of uncertainty:

V1 = Variance of the spatial variability, (15)

V2 = Variance of the measurement noise, (16)

V3 = Variance of the statistical error, and (17)

V4 = Variance of the measurement and model bias. (18)

For modeling purposes it is often convenient to draw a design profile of soil properties versus depth. About this profile are drawn two sets of standard deviation envelopes. One set describes point-to-point variability around the mean. This is the contribution of spatial variability. The other set describes uncertainty in the mean itself. This is the contribution of systematic error.

UNCERTAINTY IN CALCULATED PREDICTIONS

The preceding discussion used means, standard deviations, and correlations to describe best estimates and uncertainties about soil properties. For engineering analysis, these mean standard deviations and correlations must be accounted for in calculations. This leads to performance predictions that are described by means, standard deviations, and correlations.

The mathematics needed for relating a second-moment description of soil properties, loads, and other input parameters to a corresponding second-moment description of performance predictions are relatively uncomplicated. Schematically, the procedure is shown as follows:

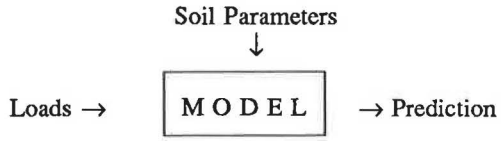

A model is chosen for calculating performance. For example, this might be Terzaghi's formula for predicting the bearing capacity of a footing. Next, means, standard deviation, and correlations are evaluated for all required input parameters. These means, standard deviations, and correlations are then translated through the model to determine the resulting means, standard deviations, and correlations on performance predictions.

Best Estimate (Mean) Prediction

Operationally, best estimates of soil properties are translated through a model using a first-order approximation. This is simply a linear approximation to the model in the vicinity of the best estimates of the soil parameters. Mathematically, the calculation of some performance prediction y based on a soil parameter x can be expressed as a function

$$y = g(x) \tag{19}$$

By taking a Taylor's series expansion of g(x) at the point m_x and then truncating all but the first two (i.e., linear) terms, the tangent plane at m_x is obtained. For most geotechnical purposes this linearization is sufficiently accurate. Applying rudimentary probability theory leads to the convenient result

$$m_y \doteq g(m_x) \tag{20}$$

where $\doteq$ indicates first-order approximation. In words, the mean or best estimate of the prediction y is the function of the mean or best estimate of the parameter x. This is the normal deterministic solution, using best-estimate soil properties as input.

Uncertainty (Standard Deviation) in Predictions

By similar reasoning, standard deviations on input soil properties x may also be translated through a model y = g(x) to find a corresponding standard deviation on the prediction y. The first-order approximation leads to the relation

$$s_y \doteq (dy/dx)\, s_x \tag{21}$$

where the derivative dy/dx is an influence factor. In words, the standard deviation of the prediction y is the product of the standard deviation of the parameter x and an influence factor equal to the derivative of y with respect to x. The relation is exact when g(x) is linear.

When the prediction y depends on a set of parameters, $x = \{x_1,...,x_n\}$, the equivalent forms of Equations 20 and 21 are

$$m_y \doteq g(m_{x1},...,m_{xn}) \tag{22}$$

$$s_y^2 \doteq \Sigma\,\Sigma\,(dy/dx_i)\,(dy/dx_j)\,C_{xi,xj} \tag{23}$$

Note, when x_i, x_j are mutually independent, $C_{xi,xj} = 0$ for $i \neq j$ and $C_{xi,xj} = s_x^2 = V_x$ for i = j, thus

$$s_y^2 \doteq \Sigma\,\Sigma\,(dy/dx)^2\, V_x \tag{24}$$

Two special cases deserve note because they are so common. When y is a linear combination of a set of independent parameters, $y = \Sigma a_i x_i$,

$$V_y = \Sigma\, a_i^2\, V_{xi} \tag{25}$$

when y is a power function of a set of independent parameters, $y = \Pi a_i x_i bi$,

$$\Omega_y^2 \doteq \Sigma\, b_i^2\, \Omega_{xi}^2 \tag{26}$$

Equation 26 pertains to small coefficients of variation, for example, less than 0.2 to 0.3.

Reliability Index, β

In traditional geotechnical analysis, the adequacy of a design is expressed by a factor of safety, defined as the ratio of capacity to demand

$$F = \text{capacity/demand} \tag{27}$$

The factor of safety makes no allowance for uncertainty. When performance is predicted by both a best estimate and a measure of uncertainty, a new and more complete safety index can be used. One such index that combines both best estimate and uncertainty is the reliability index, β

$$\beta = m_y - y_f/s_y \tag{28}$$

where y_f is the limiting state or failure value for the predicted performance, y. In essence, β measures the number of standard deviations separating the best estimate of performance from some unacceptable value. If the predicted variable, y, were, for example, a factor of safety against bearing capacity failure of a footing, then m_y = mean of F, s_y = standard deviation of F, and $y_f = 1.0$.

A lower value of β implies lower reliability. A β = 0 means

that the best estimate of performance just equals the failure criterion, that is, m_y would equal y_f. $\beta > 0$ means that $m_y > y_f$ because the standard deviation is always positive. Typical values of β for common geotechnical design range from about 2 to 3. The reliability index is a useful measure of safety because it balances the safety implied by a best estimate of facility performance against the uncertainty in that prediction. Thus, β can distinguish between the case of high estimated factor of safety with correspondingly high uncertainty and the case of a low estimated factor of safety with correspondingly low uncertainty. Thus, β allows a more comprehensive balancing of design conservatism against uncertainty than does FS alone, and can lead to significant economies on large projects *(5)*. The use of β rather than FS also allows design conservatism to be quantitatively related to the extent of site characterization and testing, thereby allowing a balance to be struck between information gathering and conservatism.

SETTLEMENT OF SHALLOW FOOTINGS ON SAND

The importance of uncertainties and errors is well illustrated by a field case involving shallow footings *(6)*. The case especially shows the usefulness of separating random measurement error from spatial variability when making predictions. The site overlies approximately 10 meters of uniform windblown sand on which a large number of footings were constructed. The site was characterized by SPT blow count measurements. Predictions were made of settlement, and subsequent settlements were measured.

Spatial Variation and Noise in Settlement Predictions

Inspection of the standard penetration test (SPT) data and subsequent settlements reveals an interesting discrepancy. Because footing settlements on sand tend to be proportional to the inverse of average blow count beneath the footing, from Equation 26 it would be expected that the coefficient of variation of the settlements be approximately that of the vertically averaged blow counts. Mathematically, settlement is predicted by a formula of the form

$$\rho \propto (\Delta q/N)\, g(B) \tag{29}$$

where

ρ = settlement,
Δq = net applied stress at the base of the footing,
N = average corrected blow count, and
$g(B)$ = a function of footing width.

Therefore, from Equation 26,

$$\Omega_\rho \doteq \Omega_N \tag{30}$$

but it is not. The coefficient of variation of the vertically averaged blow counts is about 0.50; the coefficient of variation of the settlements is only 0.37. Why the difference?

The best explanation for this apparent inconsistency is found in estimates of measurement noise in the blow count data. Figure 1 shows the horizontal autocorrelation function for the blow count data. By extrapolating this function to the origin, the noise (or high frequency) content of the data is estimated to be about 50 percent of the data scatter variance. This means that

$$(\Omega_{soil})^2 = (\Omega_{data})^2\,(0.5) = (0.35)^2 \tag{31}$$

which is close to the observed variability of the settlements.

Calculating Footing Settlement

Footing settlement can be predicted by any of a number of equations. Peck and Bazaara's equation is a modification of the Terzaghi and Peck upper envelope

$$\rho = [(2\Lambda q/m_N)\,(2B/1 + B)^2\,(1 - 1/4\ D/B)] \tag{32}$$

where

ρ = settlement (inches),
Δq = allowable applied stress (TSF),
m_N = (vertically) averaged corrected blow count, and
B = footing width (ft).

Water table elevation is ignored. The term involving D/B, where D = embedment depth, is a depth correction factor. In the present case D/B = 0.5. For square footings of design width B = 10 ft, the best estimate of ρ at the allowable stress of 3 TSF (6 ksf) is shown in Figure 2.

Spatial Component of Settlement Uncertainty

The variance of ρ due to uncertainty in m_N is calculated by noting that ρ is inversely proportional to m_N. Therefore, from Equation 26

$$\Omega_\rho \doteq \Omega_{mN} \tag{33}$$

m_N is the average blow count within a depth B of the footing and thus its variance and coefficient of variation are less than those of the point-by-point blow counts, N. For this site, blow counts are taken every 5 ft, thus m_N is the average of two measurements. As such, from Equation 12, $V_{mN} = V_N/2$, and Cov $m_N = \sqrt{1/2}\ \Omega_N = (0.71)\ (0.44) = 0.32$. Therefore, Ω_ρ is approximately 0.32. Alternately, Equation 21 could have been used to find the same result with more effort.

The coefficient of variation of ρ calculated above is that responding to spatial variation in the SPT data. This magnitude of variation should be observed among the various footings around the site. In comparison, the observed values of total

settlements for 268 footing at this site have a mean of about 0.35 ft, and a standard deviation of 0.12. Thus, $\Omega_\rho = 0.34$.

Systematic Component of Settlement Uncertainty

In addition to spatial variability, the limited number of borings causes statistical error in the prediction of average settlement. With 50 borings and hence 50 SPT measurements at any elevation, the statistical error in the estimated mean blow count at any elevation in the upper levels is $Vm_N \doteq V_N/50$. This reflects uncertainty on the average settlement of all the footings at the site.

The settlement model itself introduces bias that differs from site to site. For Equation 32 comparison data of predicted versus observed settlements yield a mean bias *(2)* of $m_b = 1.46$ and a standard deviation of $s_b = 1.32$, where b = observed settlement and predicted settlement. Correcting the earlier estimate for this model bias,

$$m'_\rho \doteq b\, m_\rho \tag{34}$$

where m_ρ is the corrected mean settlement. The variance of the corrected settlement is found using Equation 24 as

$$V_\rho \doteq V_b\, m_\rho^2 + m_b^2\, V_\rho \tag{35}$$

The poor correlation of the settlement model to actual footing performance introduces a large model error if data are unavail-

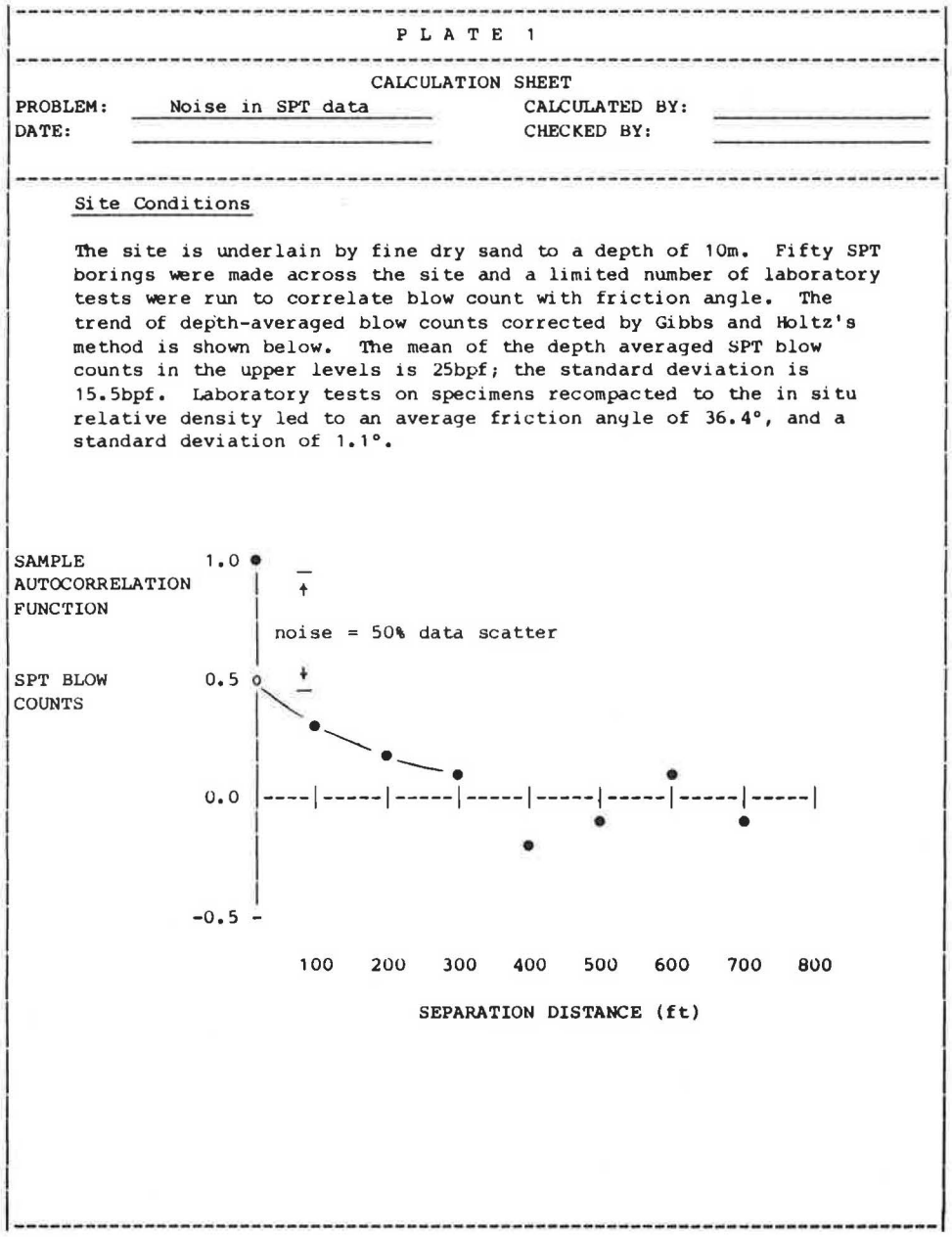

FIGURE 1 Calculation of noise in SPT data.

PLATE 2 1/3

CALCULATION SHEET

PROBLEM: Footing settlement CALCULATED BY: _____

DATE: _____ CHECKED BY: _____

PROBLEM

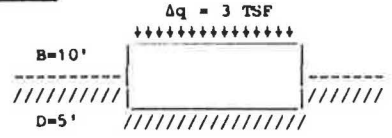

allowable ρ = 1"

SOIL PROPERTIES

m_N = vertically averaged SPT blow count, corr'd.

= 25 bpf

(a) BEST ESTIMTE (MEAN) OF SETTLEMENT

$$m_\rho \doteq \left(\frac{2\Delta q}{m_N}\right)\left(\frac{2B}{1+B}\right)^2 \left[1 - \frac{1}{4} D/B\right] = \left(\frac{2 \cdot 3}{25}\right)\left(\frac{2 \cdot 10}{1+10}\right)^2 \left[1 - \frac{1}{4} 5/10\right]$$

$$= 0.70"$$

$$m_\rho' \doteq b\, m_\rho$$

$$= (1.46)(0.70") = 1.02"$$

(b) UNCERTAINTY (VARIANCE) OF SETTLEMENT

Spatial Variability

from Eqn. 26, $\Omega_\rho = \Omega_{mN}$

$$\Omega_\rho = \Omega_N = \frac{\sqrt{V[N]}}{m_N} = \frac{\sqrt{V[N]/2}}{m_N} = \frac{\sqrt{1}1^2/2}{25} = 0.32$$

$$V_\rho = (\Omega_\rho\, m_\rho)^2 = [(0.32)(0.70")]^2 = (0.22")^2$$

$$V_\rho' = (\Omega_\rho\, m_\rho')^2 = [(0.32)(1.02")]^2 = (0.32")^2$$

Systematic Error

Statistical Estimation Error:

$$\Omega_{mN}^2 = \Omega_N^2/n = (0.32)^2 / 50 = (0.05)^2$$

$$\Omega_\rho = \Omega_{mN} = (0.05)^2$$

$$V_\rho = (\Omega_\rho\, m_\rho)^2 = [(0.05)(0.7)]^2 = (0.04)^2$$

$$V_\rho' = (\Omega_\rho\, m_\rho')^2 = [(0.05)(1.02)]^2 = (0.05)^2$$

Model Bias: $V_\rho' = V_b\, m_\rho^2 + m_b^2\, V_\rho$ |

$$= (1.32)^2\,(0.70")^2 + (1.46)^2(0.31 \times 0.70")^2$$

$$= 0.85 + 0.10 = (0.98)^2$$

(c) RELIABILITY INDEX

Spatial Variability Alone

$$\beta = \frac{m_\rho - \rho_o}{s_\rho} = \frac{|0.70" - 1"|}{0.22"}$$

= 1.364 spatial variability alone

Spatial Variability + Systematic Error

Total uncertainty = spatial variability + systematic error

$$V_\rho = (0.22)^2 + (0.04)^2 = (0.23)^2$$

$$V_\rho' = (0.32)^2 + (0.05)^2 + (0.98)^2 = (1.0)^2$$

$$\beta_\rho = \frac{\rho o - m_\rho}{s_\rho} = \frac{1.0" - 0.7"}{0.23"} = 1.30$$ without model uncertainty

$$\beta_{\rho'} = \frac{m_{\rho'} - \rho_o}{s_{\rho'}} = \frac{1.0" - 1.02"}{0.23"} = -0.09$$ with model uncertainty

FIGURE 2 Calculation of footing settlement.

able for calibrating the model to a particular site. This model error is difficult to divide into scatter and systematic parts because data of the type used in Figure 1 are mixtures from many sites and model tests. However, the calculations in Figure 2 attest to the importance of model uncertainty in settlement predictions.

In service, the footings were exposed only to 40 to 70 percent of the allowable load used for predicting settlements. Also, footing dimension and embedments varied. Therefore, the mean predicted settlement and the mean observed are not comparable. However, because Equation 30 is multiplicative, Ω_p should be unaffected by these differences.

CONCLUSION

The purpose of error analysis is to *(a)* identify the sources of uncertainty in engineering calculations, *(b)* estimate the magnitude of error contributed by each source, and *(c)* assess the confidence that should be attached to a calculated prediction. The methodology for performing error analyses is uncomplicated, and its routine use fosters improved quality control and reliability.

ACKNOWLEDGMENTS

The work presented in this paper was funded by the Federal Highway Administration, U.S. Department of Transportation. The author is grateful to Albert F. DiMillio and Jerry A. DiMaggio of the FHWA, and to Douglas Gifford of Haley and Aldrich, Inc. for their helpful comments and suggestions.

REFERENCES

1. L. C. P. Yam et al. *Study of Building Failures—A New Approach.* Document X-2.7. Construction Industry Research and Information Association, London, England, 1980.
2. G. B. Baecher, W. A. Marr, J. S. Lin, and J. Consla. *Critical Parameters for Mine Tailing Embankments.* Bureau of Mines, U.S. Department of the Interior, 1983.
3. L. Bjerrum. Embankments on Soft Ground. *Proc., ASCE Specialty Conference on Earth and Earth Supported Structures,* Vol. 2, Boulder, Colo., 1972, pp. 111–159.
4. D. DeGroot. Maximum Likelihood Estimation of Spatial Correlated Soil Properties. M.S. thesis. Massachusetts Institute of Technology, Cambridge, 1985.
5. Societe d'energie de la Baie James. *Report of the Committee of Specialists on Sensitive Clays of the NBR Complex.* Montreal, Canada, Aug. 1983.
6. C. Hilldale. *A Probabilistic Approach to Estimating Differential Settlement.* M.S. thesis. Massachusetts Institute of Technology, Cambridge, 1971.

Publication of this paper sponsored by Committee on Foundations of Bridges and Other Structures.

Review of Methods for Estimating Pile Capacity

EVERT C. LAWTON, RICHARD J. FRAGASZY, JERRY D. HIGGINS, ALAN P. KILIAN, AND ARTHUR J. PETERS

The first phase of an investigation of methods for construction control of pile driving and determination of pile capacity has been completed for the Washington State Department of Transportation. A literature review covering the use of dynamic pile driving equations, wave equation methods, and pile analyzers has been conducted. In addition, a survey of current practices by state transportation departments has been completed. The literature review has shown that dynamic formulas provide the least reliable pile capacity predictions. Of the numerous formulas studied, no single dynamic pile driving formula was found to be superior to all others. However, the Hiley, Janbu, and Gates equations appear to be among the best in published comparisons of formula predictions versus pile load test results. The *Engineering News* formula and its modified versions were found, with one exception, to be among the worst predictors of pile capacity. When wave equation methods were included in comparisons of predicted-to-measured capacity, the wave equation prediction was consistently equal to or better than the best formula. Pile analyzer results can be excellent; however, the ability of the operator is a crucial factor in its successful use. Recommendations have been made for the improvement of current procedures used by the Washington State Department of Transportation for construction control and estimation of pile capacity. These recommendations also are applicable to many other state transportation departments, as well as private contractors and consultants who are involved in the construction control of pile driving.

To determine if significant improvements can be made in the methods it uses for construction control of pile driving and estimation of pile capacity, the Washington State Department of Transportation (WSDOT) funded a research project entitled "Development of Guidelines for Construction Control of Pile Driving and Estimation of Pile Capacity." The results of this research are presented in this paper, including *(a)* a description of formulas and analysis techniques currently in use, with an evaluation of the strength and weaknesses of the most promising ones; *(b)* a determination of whether or not current WSDOT methods can be significantly improved; and *(c)* a recommendation of whether or not additional research is needed. To accomplish the project tasks, a survey of other state transportation departments was conducted to determine methods currently in use. Also, a review of the technical literature concerning dynamic formulas, wave equation methods, and pile analyzers was conducted with the help of the WSDOT library. Approximately 200 references were reviewed. Based on this literature, a discussion of dynamic methods of estimating static pile capacity (equations, wave analysis, and analyzers) is presented. The current practices of other state transportation departments are then described and compared with current WSDOT procedures.

Published comparisons between actual pile load test results and pile capacity predicted by various formulas, wave equation methods, and pile analyzers are also presented. This information, along with the information provided by the various state transportation departments, provides the bulk of the data used to formulate the conclusions and recommendations in this paper. Further details can be found in the final report prepared for WSDOT by the authors *(1)*.

E. C. Lawton. Current affiliation: Department of Civil and Architectural Engineering, University of Miami, P.O. Box 248294, Coral Gables, Fla. 33124. R. J. Fragaszy and J. D. Higgins, Department of Civil and Environmental Engineering, Washington State University, Pullman, Wash. 99164. A. P. Kilian and A. J. Peters, Materials Laboratory, Washington Department of Transportation, Olympia, Wash. 98504.

DESCRIPTION OF AVAILABLE METHODS

Dynamic Pile-Driving Formulas

Dynamic pile-driving formulas have been available for more than 160 years to predict the static bearing capacity of piles. Smith *(2)* states that in the early 1960s the editors of *Engineering News-Record* had 450 dynamic pile formulas on file. All these formulas are based on the assumption that the ultimate capacity of the pile under static loading is directly related to the driving resistance of the pile in its last stages of embedment.

The stress-strain relationship in a pile during driving is extremely complicated, making an exact theoretical treatment impractical. A small percentage of the available pile-driving formulas are empirical in their entirety; however, most formulas are based on Newton's law of impact and conservation of energy principles and are modified to account for energy losses during impact and during the propagation of stresses.

In 1859, Redtenbacher proposed the following formula that Jumikis *(3)* terms the "pure, classical, complete dynamic pile-driving formula:"

$$\underset{1}{e_h E_h} = \underset{2}{R_u s} + \underset{3}{e_h E_h [w(1 - n^2)/W + w]} + \underset{4}{[(R_u^2 L'/2A'E')} + \underset{5}{(R_u^2 L/2AE)} + \underset{6}{KR_u}] \quad (1)$$

where

1 = total applied energy;
2 = useful work, that is, energy used to move pile a distance s;

3 = loss in impact;
4 = loss in cap due to elastic compression;
5 = loss in pile due to elastic compression; and
6 = loss in soil due to elastic compression plus other losses.

The definition of individual terms is given in Table 1. Equation 1 can be solved for the ultimate bearing capacity, R_u; the safe bearing capacity of the pile, R_f, can be determined by dividing R_u by a factor of safety, F.

Except for those formulas based entirely on empirical results, all other dynamic pile-driving equations are simplifications of Redtenbacher's complete formula produced by introducing different assumptions on the energy loss terms. Redtenbacher presented a simplified formula in which a completely inelastic impact is assumed (n=0). This formula and others are given in Table 1, the most important of which are discussed in detail below.

Engineering News-Record

This formula was published in 1888 by A. M. Wellington, editor of *Engineering News Record* (ENR), and originally was developed for use in measuring the bearing capacity of light-

TABLE 1 COMMONLY USED DYNAMIC PILE DRIVING FORMULAS

Formula Name	Equation	Reference Number	Year	Recommended Safety Factor
Eytelwein (Dutch)	$R_u = \frac{e_h E_h}{s\left(1+\frac{w}{W}\right)}$ (drop hammers) $R_u = \frac{e_h E_h}{s+0.1\,\frac{w}{W}}$ (steam hammers)	(3) (4)	1820	6
Weisbach	$R_u = -\frac{sAE}{L} + \sqrt{\frac{2e_h E_h AE}{L} + \left(\frac{sAE}{L}\right)^2}$	(3)	1850	
Redtenbacher	$R_u = \frac{AE}{L}\left[-s + \sqrt{s^2 + e_h E_h \cdot \frac{W}{W+w} \cdot \frac{2L}{AE}}\right]$	(3) (5) (6)	1859	3
Engineering News-Record (ENR)	$R_u = \frac{e_h E_h}{s+z}$	(3) (4)	1888	6
Navy-McKay	$R_u = \frac{e_h E_h}{s\left(1+0.3\,\frac{w}{W}\right)}$	(4) (3)		
Gates	$R_u = 27\sqrt{e_h E_h}\,(1-\log s)$ $e_h = 0.75$ for drop hammers $e_h = 0.85$ for all other hammers R_u (kips), s (in), E_h (ft-kips)	(3) (4)	1957	3
Rankine	$R_u = \frac{2AEs}{L}\left[\sqrt{1+\frac{e_h E_h L}{s^2 EA}} - 1\right]$	(3)		
Hiley	$R_u = \frac{e_h E_h}{s+\frac{1}{2}(C_1+C_2+C_3)} \cdot \frac{W+n^2 w}{W+w}$	(7)		3
Janbu	$R_u = \frac{e_h E_h}{K_u s}$ $\quad K_u = C_d\left[1+\sqrt{1+\frac{\lambda}{C_d}}\right]$ $C_d = 0.75 + 0.15\,\frac{W}{W}$ $\lambda = \frac{e_h E_h L}{AEs^2}$	(4)	1951	3-6
Pacific Coast Uniform Building Code (PCUBC)	$R_u = \frac{e_h E_h \cdot \frac{W+Kw}{W+w}}{s+\frac{R_u L}{AE}}$ K = 0.25 for steel piles; = 0.10 for all other piles	(4) (6)		4
Gow	$R_u = \frac{e_h E_h}{s+z\cdot\frac{w}{W}}$	(7)		

TABLE 1 *continued*

Formula Name	Equation	Reference Number	Year	Recommended Safety Factor
Danish	$R_u = \dfrac{e_h E_h}{s + \sqrt{\dfrac{e_h E_h L}{2AE}}}$	*(7)*	1967	3-6
Rabe	$R_u = \dfrac{e_h E_h}{s + C} \cdot \dfrac{w}{w + \frac{W}{2}} \cdot B$	*(3)*	1946	2
Modified ENR*	$\dfrac{e_h E_h}{s + z} \quad \dfrac{W + n^2 w}{W + w}$	*(6)*	1965	6
Canadian National Building Code	$R_u = \dfrac{e_h E_h \cdot \dfrac{W + n^2(0.5w)}{W + w}}{s + \dfrac{R_u}{2A}\left(\dfrac{L}{E} + 0.0001\right)}$	*(4)* *(8)*		3

*There are several formulas that are modifications of the ENR formula and are known as Modified ENR. The Modified ENR presented here was proposed by the Michigan State Highway Commission in 1965.

Note: To be consitent, the net hammer energy is given in all equations as e_{hE} even though many of the formulas were developed for drop hammers where the hammer energy is given by Wh. No units are given for any terms (except for empirical formulas) so that any consistent set of units can be used.

- A = cross-sectional area of pile.
- A' = cross-sectional area of cushion block.
- B = static supplement factor in Rabe's formula *(10)* for clarification).
- C = temporary compression loss in the cap, pile, and soil; used in Rabe's formula (see *(10)* for clarification).
- C_1, C_2, C_3 = coefficients for Hiley equation.
- eh = efficiency of striking hammer *(<1.0)*.
- E = Young's modulus of elasticity of pile.
- E' = Young's modulus of elasticity of the cushion block.
- E_h = manufacturer's hammer energy rating.
- F = factor of safety.
- h = height of free fall of hammer.
- k = a coefficient to account for elastic compression plus other losses in Redtenbacher's classical formula.
- L = length of pile
- L' = axial length of cushion block.
- n = coefficient of restitution.
- R_u = ultimate bearing capacity of pile in soil.
- R_f = safe bearing capacity of pile.
- s = pile penetration for last blow, also called "set".
- w = weight of pile.
- W = weight of hammer.
- z = 0.1 for steam hammers; 1.0 for drop hammers.

weight timber piles with fairly uniform penetration driven by drop hammers. As indicated in Table 1, the formula was modified for use with steam hammers. Wellington derived the equation by equating the applied energy to the energy obtained by graphically integrating the area under typical load-settlement curves for timber piles driven by drop hammers, and all the losses are taken into account by a single factor, z. Usually e_n is assumed equal to 1 when using the ENR formula.

This formula probably is the most widely used dynamic pile-driving formula in the United States, mainly because of its simplicity. However, several investigators have noted the extremely wide range of safety factors determined when using this formula *(7–10)*. Details of field studies that report comparisons between pile capacity predicted by the ENR formula (and other formulas) and pile load test results are presented in the section titled "Comparative Studies."

Modified Engineering News-Record (Michigan)

This modified version of ENR was proposed in 1965 by the Michigan State Highway Department *(6)* as the product of an extensive study to compare the efficacy of several dynamic formulas to predict bearing capacity of piles.

This version modifies the ENR formula by multiplying it by the factor,

$$W + n^2 w / W + w$$

which gives a ratio of combined ram-pile kinetic energy before and after impact. This factor, when multiplied by the initial energy, $e_h E_h$, defines the available energy after impact.

Hiley

Olson and Flaate *(7)* reported that Hiley developed his formula in an attempt to eliminate some of the errors associated with the theoretical evaluation of energy absorption by a pile-soil system during driving. The factor 1/2 $(C_1 + C_2 + C_3)$ is analogous to the factor Z in the ENR formula. C_1 represents the peak temporary elastic compression in the pile head and cap. Chellis *(8)* has compiled values of C_1. The factor $C_2 + C_3$ represents the combined temporary compression of pile and supporting

ground and is based on field measurements. The Hiley formula is used extensively in Europe.

Janbu

This formula does not directly involve the law of impact. Janbu factored out of the conservation of energy equation a series of variables that are difficult to evaluate and combined them in his driving coefficient, C_d. The driving coefficient includes terms representing the difference between static and dynamic capacity, the rate of transferral of load into the soil with respect to depth, and hammer efficiency, and is correlated with the ratio of the pile weight to the hammer weight. The overall factor, K_u, modifies the driving coefficient by a term that includes λ, which incorporates the length and cross-sectional area of the pile, Young's modulus for the pile, the hammer energy, and the pile set.

Rabe

Rabe's formula is empirical, but is more complex than other empirical formulas. It is a combination static and dynamic formula that accounts for soil conditions as well as most of the other factors that influence pile capacity. This formula can be cumbersome to use because to solve it requires extensive computation and several trial estimates of load. It is necessary to perform many of the computations before driving; otherwise, it becomes difficult to use in the field.

Gates

The Gates formula is a strictly empirical relationship between hammer energy, final set, and test load results. It was developed by applying a statistical adjustment (based on approximately 100 load tests) to a significantly simplified form of existing equations. In his report, Gates *(11)* did not include the data on which his study was based and did not indicate the amount of scatter. It appears, however, that all soil types were included in the study.

Wave Equation Analysis

The problems associated with using dynamic pile-driving formulas to predict static bearing capacity of a pile are numerous. Many difficulties stem from the fact that pile driving is not a simple problem that can be solved by the direct application of Newton's laws *(12)*. With the exception of Rabe's formula, none of the other formulas listed in Table 1 even attempts to account for the soil types and soil conditions into which the pile is being driven. Other problems develop from the simplifying assumptions made in accounting for energy losses in the system. Empirical formulas can only be used in restricted applications because they generally are developed for specific pile types, driving equipment, soil types, and soil conditions and are of limited general use. Evidence of this can be found in the "Comparative Studies" section of this paper.

An alternate method of predicting static bearing capacity of piles involves analyzing the longitudinal wave transmission in piles by the wave equation. A wave equation computer program allows the user to predict the driving stresses induced in a pile for any blow of the hammer, determine the resulting motion of the pile during the impact, and determine the resistance of soil at the time of driving. This information allows the engineer to determine the compatibility of the driving equipment with the pile type, size, and soil conditions. From a theoretical standpoint, the wave equation models the development of bearing capacity in a pile driven into soil much more accurately than Newton's impact laws. However, because of the complex nature of pile-driving problems, the only solutions to this problem currently available are based on numerical methods. Although Isaacs *(13)* in 1931 and Glanville et al. *(14)* in 1938 related the wave equation to pile driving, the first practical form was not developed until the early 1960s by Smith *(2)*. Smith's solution consists of using a finite-difference method to numerically model the wave equation, thereby calculating the pile set for a given ultimate load. Since the publication of Smith's paper, a multitude of computer programs have been written that use a numerical model of the wave equation to analyze the pile-driving problem. Some of these programs incorporate finite-element methods rather than finite-difference methods. Two programs are of special interest in this paper and will be discussed next.

A wave equation was developed by Hirsch et al. *(15)* in the mid-1970s for determining the dynamic behavior of piles during driving. This program, commonly known as the Texas Transportation Institute (TTI) wave equation program, was developed by the Texas Transportation Institute under the auspices of the FHWA. The TTI program was intended for general practical use by highway departments and was meant to assist them in the understanding, use, and practical application of pile-driving analysis by the wave equation.

In the late 1970s and early 1980s, a wave equation program known as Wave Equation Analysis of Piles (WEAP) was developed by Goble and Rausche *(16)* under contract to FHWA. The motivation for the development of the WEAP program came from problems the New York State Department of Transportation (NYSDOT) encountered when it attempted to incorporate the TTI wave equation program into its pile-driving practice. NYSDOT experienced serious problems when TTI was used for piles driven by diesel hammers in that unrealistic values of driving stresses sometimes were obtained. The WEAP program improved on the TTI program by analyzing piles driven by diesel hammers using a thorough model of both the thermodynamic and mechanical hammer operation. WEAP also improved and refined existing techniques for wave analysis of piles driven by air-steam hammers.

Pile Analyzer

Two major shortcomings of most dynamic pile analyses are the uncertainty of the actual energy applied by the hammer to the

pile and the distribution of soil resistance along the pile. Research begun in 1964 at Case Western Reserve University under Goble initially concentrated on using electronic equipment to measure force and acceleration at the top of the pile for each blow of the hammer so that the actual applied energy could be determined. Using these data, Goble et al. were able to relate their dynamic measurements to static bearing capacity using a single force-balance theory *(17)*. Static bearing capacities predicted by the proposed theory were compared with model pile load tests, full-scale load tests, and load tests conducted in Michigan *(17)*, with the results indicating that the method showed promise as a means of predicting static bearing capacity of piles.

A later study extended the application of the force and acceleration methods to the calculation of the distribution of soil resistance along the pile *(18)*. The prediction of the magnitude of dynamic soil resistance is an important factor in choosing efficient hammer characteristics. In addition, two methods were used to predict static bearing capacity: *(a)* an improved version of the force-balance theory discussed earlier, and *(b)* a wave equation analysis method. The static capacities predicted by these two methods were compared with load test data, with the result that both methods yielded better correlation with the load test results than any of the energy formulas they used. The best predictions resulted from the wave equation analysis method as a result of the inclusion of both dynamic and static soil resistance.

Published in 1979 by Rausche and Goble *(19)* a further development using force and acceleration measurements suggested a procedure for detecting discontinuities and reductions in cross section at points along the pile below the ground surface. The theory behind this method is the use of one-dimensional wave propagation to predict the effect that stress waves produced by pile damage would have on force and acceleration records. The actual records are then examined to determine if evidence of pile damage exists.

A major drawback in the early use of this electronic measuring equipment was that personnel well trained in electronics were required to operate the equipment in order to achieve usable results *(16)*. In order to make this method feasible for routine use in the field, special-purpose computers were designed and constructed to perform all necessary computations and display the results. This equipment has been changed and improved through the years and is now available from Pile Dynamics, Inc., a privately owned company. The proprietary name of this equipment is the pile driving analyzer, but it is more commonly known as the pile analyzer or the "Goble" analyzer.

CURRENT PRACTICES OF STATE TRANSPORTATION DEPARTMENTS

To assess the current practices of state transportation departments, a letter was sent to each state and the District of Columbia requesting the following information:

1. Method(s) used for construction control of pile driving.
2. Any comparative studies of various pile driving formulas.
3. Any data comparing field load test results with results predicted from formulas or wave equation analyses.
4. Whether a pile analyzer had been used, and if so, whether the department was satisfied.

Thirty-five responses were obtained from the 50 letters sent. All regions of the country are represented and, although several replies were quite brief, it is believed that on the whole a reasonably detailed picture of current practice has been obtained. The following discussions are based on the responses received.

Construction Control of Pile Driving

Despite the multitude of dynamic methods available for estimation of pile capacity, only a handful appear to be used by transportation department engineers. Based on the responses received, several points are clear. First, the ENR formula, either in its original form or more often a modified version, is by far the most popular dynamic formula used. Second, wave equation methods, such as the WEAP computer program, are widely used also. Third, use of pile analyzers is growing, but is still not prevalent.

Twenty-two states replied that they use the ENR formula in its original or modified form and one state replied that "dynamic formulas" are used, but did not indicate which ones. No other formulas were mentioned.

Wave equation methods are used by 11 states. However, Florida uses them only to size the pile driving hammer, and North Carolina uses them to determine drivability. Both of these states use an ENR formula for estimation of pile capacity. Wyoming uses wave equation methods only for friction piles. New York and Pennsylvania both have extensive experience with wave equation methods. Both require a wave equation analysis for all pile jobs. New York uses the WEAP program; Pennsylvania did not indicate the specific method used. Rhode Island and Nevada both stated that they abandoned the ENR formula in favor of wave equation analyses. In the case of Nevada, piles were being overdriven with the ENR formula and correlation with load tests was poor.

New York and Wisconsin are the only two states that indicated that they use a pile analyzer in connection with construction control. On certain jobs, NYSDOT engineers perform their own dynamic pile load tests using the Goble pile analyzer. Using their own equipment, they have performed more than 100 pile load tests with the Goble pile analyzer. They find it quick and relatively inexpensive compared with static load testing. The Wisconsin reply merely stated that a pile analyzer is used in addition to a modified ENR formula.

Comparative Studies of Pile-Driving Formulas

Twelve states indicated that some comparative studies have been made. Unfortunately, most of the studies cited were either quite old and no data are available, or informal. Only Michigan and South Dakota were able to provide reports documenting their work. Three states volunteered opinions based on informal studies or experience. In New York's experience, WEAP is much better than any dynamic equation. In comparing WEAP predictions with the dynamic load test results, good agreement

is found "for certain soils and hammer types." When the WEAP program is inaccurate, it appears to be the result of either the assumed soil resistance distribution or the hammer model in WEAP. Diesel hammers present more problems than other types.

Wyoming's comparisons have shown that the modified ENR formula they use is overly conservative, whereas Oklahoma found that ENR and "more sophisticated formulas" vary only "under extreme conditions." The results of Michigan's study will be examined in detail in the following section.

Comparison of Pile Load Tests Results with Formulas and Wave Equation

Only four states referenced published comparisons they had made (Arkansas, Louisiana, Michigan, and South Dakota). However, California, Kansas, Maryland, Mississippi, and Pennsylvania are currently conducting tests or analyzing old test results, and Kentucky is contemplating a study in the near future. Details of the published comparisons are presented next.

Although the Pennsylvania study is not complete, officers stated that they are finding that both the wave equation and the pile analyzer underpredict capacity if there is no relaxation. The magnitude of the underprediction varies with the pile hammer system and appears to be greatest with light piles driven by heavy hammers. An example is cited of a Monotube driven with a Vulcan air hammer. They also stated that the driving stresses predicted by wave equation methods (WEAP, TTI) are reasonably accurate.

Use of a Pile Analyzer

Thirteen states indicated some experience with a pile analyzer and three plan to use one in the near future. Of those using an analyzer, New York and Pennsylvania appear to have the most experience. As discussed previously, New York has conducted more than 100 dynamic pile load tests using a Goble analyzer and is satisfied with the results. Pennsylvania also is satisfied with the analyzer but indicates that it underpredicts capacity, although not as much as a wave equation analysis.

Florida, Maryland, Idaho, North Dakota, and South Carolina have only limited experience with the analyzer (typically a FHWA demonstration project). Neither Idaho nor South Carolina was completely satisfied with the analyzer. Idaho stated that the analyzer failed to indicate damages that occurred to steel H-piles during driving, and South Carolina indicated that results were "uncertain." Maryland indicated satisfaction with the results from use of the analyzer, but expressed concern about finding trained personnel to monitor and evaluate the results if the analyzer were to be used exclusively.

Washington State Department of Transportation Practice

Washington State Department of Transportation (WSDOT) practice is similar to that in other states. For small pile-driving jobs the ENR formula is used for estimation of pile capacity and construction control of pile driving. The majority of pile driving projects fit into this category. For larger projects, especially Interstate construction, both wave equation analyses and pile analyzers are used. Wave equation analyses, which are conducted by WSDOT personnel, are used to qualify pile-driving hammers that do not meet standard specifications and when problems are encountered during pile driving. When a pile analyzer is used, contractors are employed because WSDOT currently has no in-house capability for this type of work.

COMPARATIVE STUDIES

Many researchers have attempted to determine which of the many pile-driving formulas is best by comparing formula predictions of pile capacity with pile load test results. Some of the more recent studies have included wave equation analyses and pile analyzer predictions. Because of the large number of formulas available, each study has concentrated on only a few of them. To further complicate the problem of determining the best formula, the method of static pile load testing used in each study is different. Also, the amount of information provided on soil conditions, type of pile-driving equipment, and selection of variables, such as coefficient of restitution or hammer efficiency, varies considerably. At best then, studies such as those discussed in the following paragraphs should be used primarily to indicate which formulas appear to be consistently among the better ones and to provide useful information on the variability of each formula.

Comparisons between predicted versus measured pile capacity are cited by Chellis *(8)*. He reports the results of comparisons using 45 individual piles in which the static capacity is predicted by ENR, Hiley, a modified ENR, a modified Eytelwein, Navy-McKay, Canadian National Building Code (Canadian NBC), and the Pacific Coast Uniform Building Code (PCUBC) formulas. The measured capacity is defined as the load on the net settlement versus load curve where the "rate of movement begins to increase sharply in proportion to the increase in load." The data include several different types of piles (thin, mandrel-driven corrugated shells, fluted steel shells, precast concrete, wood, and H-sections) and hammers (double acting, differential acting, and drop). The author used the ultimate capacity predicted by each formula.

The Hiley formula gave the best results, followed closely by the PCUBC and Canadian NBC formulas. The average predicted values of ultimate capacity were 92, 112, and 80 percent, respectively, of the measured pile capacities. Of equal importance is the range of predicted values measured as a percentage of actual pile capacity. The Hiley formula produced a range of 55 to 125 percent, the PCUBC formula range was 55 to 220 percent, and the Canadian NBC formula range was 55 to 140 percent. The other formulas were considerably worse. For example, the average for the ENR formula was 289 percent and the range was 100 to 700 percent, respectively.

The author concludes that the Hiley, Canadian NBC, and the PCUBC formulas provide sufficiently good agreement with load test values to be used with a safety factor of 2.5 to 3. He also states "there would not seem to be much point in continued use of the Engineering-News formula, except as a matter of interest in comparing it to results of more modern methods."

Spangler and Mumma *(10)* compared the predictions of four

formulas (ENR, Eytelwein, PCUBC, and Rabe) with load tests on 59 piles. A variety of pile types including H-piles, concrete, timber, Raymond step tapered, and pipe piles were included. The piles were located throughout the country and soil conditions varied considerably. The authors compared the working load predicted by the formula (for the PCUBC formula the predicted load was divided by 4) with the results of pile load tests and calculated a resulting safety factor. To obtain the ultimate load used in these comparisons, the authors calculated four failure loads for each test and averaged the results.

An examination of the data for the ENR formula indicates that all the piles with safety factors under 1.0 had a set of 0.10 in. or less, and those piles with a safety factor below 1.5 had sets of less than 0.25 in. The authors found no correlation between safety factor and type of pile material or length of penetration; however, friction piles tended to have higher safety factors then end-bearing piles.

There was more scatter in the results predicted by the Eytelwein formula, compared with the other three formulas. Like the ENR formula, the worst predictions came from small sets. When the pile hammer was heavier than the pile, safety factors were particularly low. Again, friction piles had higher safety factors than end-bearing piles.

The PCUBC formula was found to be most accurate for piles with deep penetration (greater than 45 ft) driven with a heavy hammer. For other cases, uneconomically high safety factors resulted.

The Rabe formula gave the best results of the four with no safety factor below 1.0 and only one above 4.0. As with the other formulas, friction piles had the highest safety factor. There was no apparent correlation between safety factor and pile set, pile type, material, or hammer weight ratio.

Agerschou *(9)* has compared load test results from 171 piles with predicted capacity based on 7 different formulas and the wave equation. The formulas used for comparison were the ENR, Eytelwein, Hiley, Janbu, Danish, [from Sorensen and Hansen *(20)*], and Weisbach. All of the piles extended into sand or gravel. The failure load was defined as the load at which the total settlement equals 10 percent of the pile diameter, except for those tests that involved hydraulic jacking, where failure was defined as the maximum load that could be reached by jacking. Three statistical evaluations of each formula were performed and the results are discussed in the next paragraph.

Of the seven formulas compared, the ENR and Eytelwein formulas had by far the largest standard deviations, 0.78 and 0.57, respectively. The wave equation analysis, although an early implementation not as accurate as current codes, had the lowest standard deviation, 0.23. Janbu and Hiley were also quite good with standard deviations of 0.25 and 0.27.

Agerschou *(9)* also calculated for each formula the safety factor that would have to be used to ensure that no more than 2 percent of the piles had an actual capacity less than the predicted capacity. For the ENR and Eytelwein formulas the necessary safety factors are 26 and 17, respectively. Janbu, Hiley, and the wave equation require much lower safety factors (3.6, 3.8, and 3.9, respectively).

As part of a larger scope investigation, Mansur and Hunter *(21)* compared the ultimate capacity based on pile load tests for 12 piles with computed capacities based on the PCUBC, Janbu, and ENR formulas. They used the average of four criteria to calculate ultimate capacity. The piles included four steel pipes, two concrete, two steel H-piles, and one timber pile. Excellent correlation was found between predicted loads and test failure loads for the PCUBC and Janbu equations. Significantly worse results were obtained using the ENR formula. The ratio of actual failure load to predicted failure load averaged 1.07 for both PCUBC and Janbu, and 0.64 for ENR. The range of ratios for PCUBC, Janbu, and ENR, respectively, are 0.85 to 1.34, 0.88 to 1.43, and 0.48 to 0.93. Both PCUBC and Janbu, on the average, underpredict the actual failure load, whereas the ENR formula overpredicted in all cases by factors ranging from approximately 1.1 to 2.1.

Poplin *(22)* studied test pile data collected by the Louisiana Department of Highways, concentrating on 14- and 16-in.^{2} precast concrete piles. Results of 24 load tests were compared with allowable capacity based on the ENR formula and a static soil mechanics analysis. The ultimate load based on load tests was the "load at onset of large displacement" or the load at which 1 in. of settlement occurs. On the average, predicted capacity based on static soil mechanics techniques was close to actual capacity. The average ratio of predicted-to-actual capacity was 0.964; however, the range was 0.40 to 1.84. The ENR formula, in the form that includes a safety factor of 6.0, provided an average safety factor of approximately 2.0 (average predicted-to-actual capacity = 0.506). The ratio of predicted allowable load to actual failure load ranged from 0.107 to 1.0, corresponding to actual safety factors between 1.0 and 9.4. As with other studies, the extreme variability of the ENR formula is demonstrated. Poplin was unable to find any correlation between actual safety factor and either pile weight or pile size.

Kazmierowski and Devata *(23)* report the results of a pile load testing program undertaken in Ontario, Canada. Five test piles were driven into a soil profile consisting of irregular cohesive layers of clayey silt and granular layers of silt to silty sand with some gravel. The five piles consisted of an H-section with a reinforced top flange, a closed-end steel pipe filled with concrete, two precast reinforced concrete piles, and a timber pile. All piles were driven by diesel hammers.

The ultimate capacity of each pile was predicted by the modified ENR formula (Michigan equation) and the Gates, Janbu, and Hiley formulas. In addition, a pile analyzer was used to predict ultimate bearing capacity and to measure the stress and energy developed in the pile during driving. Static analyses also were conducted using Meyerhof's method for the portion of the pile embedded in cohesionless soil and Tomlinson's method for the portion in cohesive soil.

Kazmierowski and Devata *(23)* calculate the ultimate pile capacity based on three different criteria (M.T.C., Davisson, and Flaate). The three criteria produced reasonably good agreement with a maximum deviation of 31 percent. Based on these comparisons, the authors concluded that the Hiley, Janbu, and Gates formulas all give acceptable consistency, with the Hiley formula generally predicting the highest capacity and the Gates prediction generally on the low side. The Janbu formula was best for concrete piles, Gates was best for pipe and timber piles, and the Hiley equation was closest for the H-section.

Three different estimates of ultimate capacity were made for each pile using the analyzer—an initial field prediction, an initial reanalysis before the load test, and a final reanalysis after

the load test. Except for the longer of the two concrete piles, the field predictions were very accurate. (The consultants who operated the analyzer attributed the large error in the longer concrete pile to incorrect wave speed estimates in the field.) However, because two reanalyses were deemed necessary by the analyzer consultants, it is difficult to have much confidence in the initial values. This illustrates an important consideration concerning use of a pile analyzer: the results are subject to interpretation and can be very sensitive to the assumptions made.

Olson and Flaate *(7)* measured the capacities of 93 piles driven into sandy soils and compared these values with predicted capacities using the ENR, Hiley, Gow, PCUBC, Janbu, Danish, and Gates formulas. Several different criteria were used to measure ultimate pile capacity from field tests. The authors state that this results in a scatter of about 15 percent in the results, but do not provide specific information on the load test results. Olson and Flaate performed linear regression analyses on the data to determine the slope and intercept of a straight line fit and calculated a correlation coefficient. Separate analyses were performed for timber piles (N=37), concrete piles (N=15), steel piles (N=41), and all 93 piles combined. The authors found that in all cases the ENR and the Gow formulas were clearly inferior to the others. Janbu's formula was found to be most accurate for timber and steel piles, but no formula was determined to be best for concrete piles, probably because of the small number of concrete piles analyzed. The Janbu, Danish, and Gates formulas had the highest average correlation coefficients, although the PCUBC and Hiley formulas were not much lower.

Ramey and Hudgins *(24)* compared pile load test results with predictions by five dynamic equations, a wave equation analysis, and static soil mechanics methods. The load tests were all on piles located in Alabama and adjacent southeastern states. The ultimate capacity was defined as the load at which the slope of the load-settlement curve reached 0.01 in./kip. The formulas used were the ENR, modified ENR, Hiley, Gates, and Danish formulas. A total of 153 pile load tests were used with the following breakdown according to pile type: steel-H (48), steel pipe (38), precast concrete (32), and timber (35). Forty-eight of the piles were driven into clayey soils, the remaining 105 were driven into predominately sandy soils. Statistical analyses were performed on the data in a manner similar to that done by Olson and Flaate *(7)*. The analyses were broken down into different pile types, hammer energy, and soil type. In reviewing their results, one finding is quite surprising and overshadows all the others. In direct contrast to all other investigations reviewed, the ENR formula was found to give the best overall correlation with pile load test results. The Gates formula was almost as good as the ENR formula, but the Hiley equation was found to be the worst.

Although the results described in the preceding paragraph may be surprising, the comparison of pile load tests with wave equation predictions is in line with the findings of other investigators. The authors found that the wave equation gave consistently better predictions of pile capacity compared with dynamic formulas. The authors state that they had little information regarding pile-driving accessories, capblocks, or condition of the hammer used, and therefore they expect that the accuracy of their wave equation analyses could be improved. The authors concluded that the wave equation method "should become a valuable tool for the foundation engineer."

Housel *(25)* presents the data gathered by the Michigan State Highway Department in its study of pile driving. The ENR formula and the modified ENR formula predicted capacities that were compared to failure loads of 19 test piles. Fourteen of the piles were 12-in. outer diameter (OD) steel pipes filled with concrete and driven closed-end; two were H-piles; three were open-end pipes, two of which were driven in clayey soils and one driven in granular soil.

Although the results of the comparison show that the modified ENR formula gives somewhat better results on the average, the authors conclude that "from the standpoint of a reliable estimate of capacity, the range of variation improved only slightly and there appears to be no practicable way of increasing the formula's accuracy in predicting pile capacity for the great variety of field conditions under which piles must be driven."

In a study conducted in Arkansas by Welch *(26)*, seven piles were tested and predictions of capacity based on a wave equation analysis, and the ENR, Hiley, and Danish formulas were compared with pile load test results. The Engineering News formula consistently overpredicted capacity by as much as 900 percent, whereas the Hiley formula and the wave equation predictions were quite accurate. The author recommends the use of both the Hiley equation and wave equation analyses.

The literature cited clearly shows that no one formula is consistently better than the others. Even when specific combinations of pile type, hammer, and soil conditions are considered, it is not possible to be sure which formula will be best. It does appear, however, that the Hiley, Janbu, and Gates equations are better, on average, than the others examined. The PCUBC formula also gives reasonable estimates of pile capacity. With a single exception, all investigators found the ENR and modified ENR formulas to be among the worst.

All investigators were consistent with regard to wave equation methods. A wave equation analysis of static pile capacity was consistently equal to or better than the best formula predictions, despite old versions of wave equation computer programs being used in many studies in which input information was not always accurate. It is likely that modern computer codes that include accurate information on specific hammers, combined with good geotechnical data, would compare even more favorably with dynamic formulas.

CONCLUSIONS

Based on the literature reviewed and the experiences of other state transportation departments, it appears that the current practice of many state transportation departments can be improved significantly. From a purely technical point of view, the use of a pile analyzer on all projects probably would be the best solution. The authors believe, however, that this is not practical for several reasons. An analyzer is expensive, difficult to maintain, and requires experienced personnel. For most pile driving jobs, the benefits would probably not justify the costs. Scheduling problems could occur if only one analyzer and crew were available and there were several pile driving projects spread out across the state. In those cases in which use of a pile

analyzer is justified, a private company specializing in pile analyzer work could be used.

Expanded use of wave equation analysis is recommended with the goal of performing such an analysis on all pile driving projects. This will require training programs for project engineering staff and should be phased in over a period of time.

The ENR formula has been shown to be inaccurate in most cases and can lead to unacceptably high and low safety factors. However, the use of pile driving formula as a construction control tool is extremely valuable in many instances. Therefore, it is recommended that all versions of the ENR be replaced by one or more of the following formulas: Hiley, Gates, Janbu, or PCUBC. Because it has been shown that the accuracy of any pile driving formula is dependent on soil type and pile type, no one formula can be recommended for all states under all conditions. Research and analysis should be done by the individual state transportation departments to determine which of the previously mentioned four formulas (or perhaps some other formula) is best for the soil conditions and types of piles encountered in each state.

ACKNOWLEDGMENTS

The research described in this paper was supported by the Washington State Department of Transportation (WSDOT) and the Federal Highway Administration, U.S. Department of Transportation. The contents of this paper reflect the views of the authors and do not necessarily reflect the official views or policies of WSDOT or FHWA.

REFERENCES

1. R. J. Fragaszy, J. D. Higgins, and E. Lawton. *Development of Guidelines for Construction Control of Pile Driving and Estimation of Pile Capacity.* Report WA–RD 68.1. Washington State Transportation Center, Olympia, Wash., June 1985, 83 pp.
2. E. A. L. Smith. Pile-Driving Analysis by the Wave Equation. *Transactions, ASCE,* Vol. 127, Part I, Proc. Paper 3306, 1962, pp. 1145–1193.
3. A. R. Jumikis. *Foundation Engineering.* International Textbook Co., New York, 1971, pp. 598–609.
4. J. E. Bowles. *Foundation Analysis and Design.* 3rd ed. McGraw-Hill Book Co., New York, 1982, pp. 638–670.
5. American Society of Civil Engineers. *Pile Foundations and Pile Structures.* Manual of Practice 27. New York, 1946, pp. 24–72.
6. Michigan State Highway Commission. *A Performance Investigation of Pile Driving Hammers and Piles.* Final Report. Research Project 61 F–60. Lansing, March 1965.
7. R. E. Olson and K. S. Flaate. Pile-Driving Formulas for Friction Piles in Sand. *Journal of Soil Mechanics and Foundation Division, ASCE,* Vol. 93, No. SM6, Proc. Paper 5604. Nov. 1967, pp. 279–296.
8. R. D. Chellis. The Relationship Between Pile Formulas and Load Tests. *Transactions, ASCE,* Vol. 114, Proc. Paper 2369, 1949, pp. 290–320.
9. H. A. Agerschou. Analysis of the Engineering News Pile Formula. *Journal of Soil Mechanics and Foundations Divisions, ASCE,* Vol. 88, No. SM5, Proc. Paper 3298, Oct. 1962, pp. 1–11.
10. M. G. Spangler and H. F. Mumma. Pile Test Loads Compared with Bearing Capacity Calculated by Formulas. *Proc., 37th Annual Meeting of the Highway Research Board,* National Research Council, Washington, D.C., 1958, pp. 119–149.
11. M. Gates. Empirical Formula for Predicting Pile Bearing Capacity. *Civil Engineering, ASCE,* Vol. 27, No. 3, March 1957, pp. 65–66.
12. A. E. Cummings. Dynamic Pile Driving Formulas. *Journal, Boston Society of Civil Engineers,* Jan. 1940, pp. 392–413.
13. D. V. Isaacs. Reinforced Concrete Pile Formulae. *Transactions of the Institution of Engineers,* Barton Act, Australia, Vol. 12, 1931, pp. 312–323.
14. W. H. Glanville, G. Grime, E. N. Fox, and W. W. Davies. *An Investigation of the Stresses in Reinforced Concrete Piles During Driving.* Department of Scientific and Industrial Research, British Building Research Board, Tech Paper 2. London, England, 1938.
15. T. J. Hirsch, L. Carr, and L. L. Lowery. *Pile Driving Analysis—Wave Equation Users Manual.* Vol. 1: Background. Texas Transportation Institute, College Station, April 1976.
16. G. G. Goble and F. Rausche. *Wave Equation Analysis of Pile Driving.* WEAP Program: Vol. 1, Background; Vol. 2, User's Manual; Vol. 3, Program Documentation; Vol. 4, Narrative Presentation. FHWA Report 76–14.1. U.S. Department of Transportation, 1976.
17. G. G. Goble, R. H. Scanlan, and J. J. Tomko. Dynamic Studies on the Bearing Capacity of Piles. In *Highway Research Record 167,* TRB, National Research Council, Washington, D.C., 1967, pp. 46–47.
18. F. Rausche, F. Moses, and G. G. Goble. Soil Resistance Predictions from Pile Dynamics. *Journal of Soil Mechanics and Foundation Division, ASCE,* Vol. 98, No. SM9, Proc. Paper 9220, Sept. 1972, pp. 917–937.
19. F. Rausche and G. G. Goble. Determination of Pile Damage by Top Measurements. *Behavior of Deep Foundations,* ASTM STP 670 (Raymond Lundgren, ed.), American Society for Testing and Materials, 1979, pp. 500–506.
20. T. Sorensen and B. Hansen. Pile Driving Formulae—An Investigation Based on Dimensional Considerations and a Statistical Analysis. *Proc., Fourth International Conference on Soil Mechanics and Foundation Engineering,* London, Vol. II, 1957, pp. 61–65.
21. C. I. Mansur and A. H. Hunter. Pile Tests—Arkansas River Project. *Journal of Soil Mechanics and Foundation Division, ASCE,* Vol. 96, No. SM5, Proc. Paper 7509, Sept. 1970, pp. 1545–1582.
22. J. K. Poplin. *Preliminary Evaluation of Test Pile Records for Highway Structures in Louisiana.* Engineering Research Bulletin 106. Louisiana Department of Highways, Baton Rouge, April 1971.
23. T. Kazmierowski and M. Devata. Pile Load Capacity Evaluation: *Highway 404 Structures.* Report EM–20. Ontario Ministry of Transportation and Communications, Canada, July 1978.
24. G. E. Ramey and A. P. Hudgins. *Modification of Pile Capacity and Length Prediction Equations Based on Historical Alabama Pile Test Data.* HPR Report 75. Bureau of Research and Development, State of Alabama Highway Department, Montgomery, June 1975.
25. W. S. Housel. Pile Load Capacity: Estimates and Test Results. *Journal of Soil Mechanics and Foundation Division, ASCE,* Vol. 92, No. SM4, Proc. Paper 4861, July 1966, pp. 1–30.
26. R. C. Welch. Evaluation of Rapid Pile Load Tests. Final Report. Highway Research Project 36. Arkansas State Highway and Transportation Department, Little Rock, June 1978.

Publication of this paper sponsored by Committee on Foundations of Bridges and Other Structures.

At-Rest to Active Earth Pressure Transition

S. BANG AND H. T. KIM

An approximate analytical procedure is described to estimate the developed lateral earth pressures behind a rigid retaining wall experiencing outward tilt about the base with horizontal cohesionless backfill soil. Included are various stages of wall tilt, starting from an at-rest condition to a full-active condition. The at-rest condition is defined as a stage of no-wall tilt, whereas the full-active condition occurs when the soil elements along the entire depth of the wall are in an active state. The predictions from the developed method of analysis are compared with model test measurements. The comparisons show very good agreement at various stages of retaining wall tilt. Finally, examples are provided to illustrate the transition of the lateral earth pressures behind a smooth and a rough retaining wall.

Estimation of the lateral earth pressure development has been one of the most important aspects in geotechnical engineering practice *(1–4)* because it governs the design of many engineering structures, including the retaining walls. Retaining walls are typically designed based on the active lateral earth pressures due to the tendency of outward tilt about the base. Classical lateral earth pressure theories, for example, Coulomb's and Rankine's *(5)*, have been widely used for this purpose.

Because a certain amount of strain must develop within the backfill soil mass in order that the shear stresses that help to support the soil mass may be fully mobilized, a certain amount of wall tilt must be allowed before the lateral earth pressure reduces to the value of the active lateral earth pressure *(6)*. However, when the movement of the wall is restricted or less than the magnitude necessary for the development of active condition, the developed lateral earth pressures could be greater than the active lateral earth pressures. Numerous such instances have been reported, indicating that the lateral earth pressure distribution behind the retaining structures must be associated not only with the type of structural movement taking place but also with the magnitude of the movement developed.

Described in this paper is a method of estimating the magnitude and distribution of the lateral earth pressure exerted by horizontal cohesionless backfill soil behind a vertical rigid retaining wall experiencing outward tilt about its base from an "at-rest" condition to an "initial-active" condition to a "full-active" condition. The description of an at-rest condition follows the conventional description, that is, the state of no-wall movement. The initial active condition refers to a stage of wall tilt when only the soil element at the ground surface experiences a sufficient lateral movement (limiting deformation) to achieve an active state defined by a Mohr-Coulomb stress relationship *(5)*. The full-active condition occurs when the entire zone of soil elements from the ground surface to the base of the wall are in an active state; that is, stresses are in a limiting condition at this stage. Between the at-rest and full-active conditions, "intermediate-active" conditions exist. The transition of the lateral earth pressures from an at-rest to a full active condition is discussed and the developed method of analysis is used to compare with the model test results. Finally, examples are presented to illustrate the transition of the lateral earth pressures.

Department of Civil Engineering, South Dakota School of Mines and Technology, Rapid City, S.D. 57701–3995.

FORMULATION

Stress equilibrium in two-dimensional plane strain state *(7)* can be written as

$$\partial\sigma_x/\partial x + \partial\tau_{xz}/\partial z = 0 \quad (1a)$$

$$\partial\tau_{xz}/\partial x + \partial\sigma_z/\partial z = \gamma \quad (1b)$$

where the coordinate x is measured positive from the top of the retaining wall toward the backfill and the coordinate z is measured positive from the top of the retaining wall toward the base; γ indicates the unit weight of the soil.

Because Equations 1a and 1b include three unknowns, σ_x, σ_z, and τ_{xz}, an additional equation needs to be introduced. Here the third equation assumes the relationship between the major and minor principal stresses, that is,

$$\sigma_3 = \sigma_1[(1 - \sin\psi)/(1 + \sin\psi)] \quad (2)$$

Figure 1 shows the schematic representation of Equation 2. Note that if ψ equals ϕ, where ϕ represents the internal friction angle of the cohesionless soil, then Equation 2 reduces to conventional Rankine's lateral earth pressure expression

$$\sigma_3 = \sigma_1[(1 - \sin\phi)/(1 + \sin\phi)] = \sigma_1 \tan^2[(\pi/4 - \phi/2)] \quad (3)$$

Solution of Equations 1a and 1b in conjunction with Equation 3

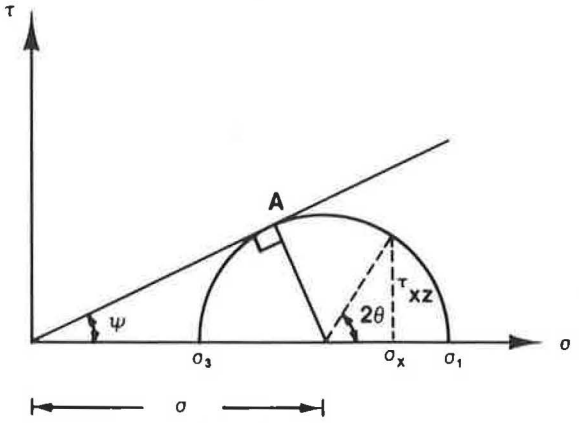

FIGURE 1 Stress relationship.

and boundary conditions will produce stress conditions at the limiting state, that is, full-active condition. This has already been solved by Sokolovskii in 1956 *(8)*.

To describe the transition of lateral earth pressures from at-rest to initial-active to full-active condition, Equation 3 has been modified. When the retaining wall is in an at-rest condition, no shear stress along the wall develops. Therefore in general

$$\sigma_3 = \sigma_x$$

$$\sigma_1 = \sigma_z$$

$$\sigma_3 = K_o \sigma_1 \tag{4}$$

where K_o indicates the at-rest lateral earth pressure coefficient. If K_o is known, the corresponding angle relating σ_3 and σ_1, ϕ_o, can be easily obtained

$$\sin\phi_o = (1 - K_o)/(1 + K_o) \tag{5}$$

Equation 4 then becomes

$$\sigma_3 = \sigma_1 [(1 - \sin\phi_o)/(1 + \sin\phi_o)] \tag{6}$$

If Jaky's equation *(9)*, $K_o = 1 - \sin\phi$, is used, then

$$\sin\phi_o = \sin\phi/(2 - \sin\phi) \tag{7}$$

By varying the angle, ψ, which describes the relationship between the major and minor principal stresses, from ϕ_o to ϕ, Equation 2 may represent both Equations 3 and 6, that is, from an at-rest to a full-active condition. Furthermore, the rotation of the wall about its base may produce different stress ratios at various depths depending on the stage of the wall tilt, for example, a portion of the soil whose deformation exceeds the limiting value may achieve $\psi = \phi$ state, whereas the remaining portion may still have $\phi_o < \psi < \phi$. Therefore, ψ may be described as a function of the depth, that is, $\psi = \psi(z)$. Note that in reality ψ may be a function of both x and z. However, the effect of x coordinate has been neglected for the purpose of obtaining an approximate solution. In other words, the physical model describing the function $\psi(z)$ can be visualized from a soil mass composed of an infinite number of infinitesimally thin horizontal layers with frictionless interfaces. Based on this assumption, Equations 1a and 1b and 2 can be rewritten.

Define, at any depth, z

$$\sigma = (\sigma_1 + \sigma_3)/2 = \text{average stress} \tag{8}$$

and θ = rotation angle from x-axis to the direction of the major principal stress, σ_1. These are indicated in Figure 1. The stresses can then be expressed as

$$\sigma_x = \sigma (1 + \sin\psi(z) \cos2\theta) \tag{9a}$$

$$\sigma_z = \sigma (1 - \sin\psi(z) \cos2\theta) \tag{9b}$$

$$\tau_{xz} = \sigma \sin\psi(z) \sin2\theta \tag{9c}$$

Substitution of Equations 9a, 9b, and 9c into Equations 1a and 1b yields

$$\partial\sigma/\partial x\,[1 + \sin\psi(z)\cos2\theta] + (\partial\sigma/\partial z)\sin\psi(z)\sin2\theta - 2\sigma\sin\psi(z)\,[\sin2\theta\,(\partial\theta/\partial x) - (1/2)\sin2\theta/\tan\psi(z)\,\partial\psi(z)/\partial z - \cos2\theta\,(\partial\theta/\partial z)] = 0 \tag{10}$$

$$\partial\sigma/\partial x\,[\sin\psi(z)\sin2\theta] + \partial\sigma/\partial z\,[1 - \sin\psi(z)\cos2\theta] + 2\sigma\sin\psi(z)[\cos2\theta\,(\partial\theta/\partial x) - (1/2)\cos2\theta/\tan\psi(z)\,\partial\psi(z)/\partial z + \sin2\theta\,(\partial\theta/\partial z)] = \gamma \tag{11}$$

The Point A in Figure 1 indicates an orientation of the plane, which satisfies $\sigma_n \tan\psi(z) = \tau_n$. The rotation angle, μ, from the direction of σ_1 to this "pseudo-slip" plane therefore becomes

$$\mu = [\pi/4 - \psi(z)/2] \tag{12}$$

as schematically shown in Figure 2. Therefore the slope of the pseudo-slip line, dz/dx, becomes

$$dz/dx = \tan(\theta \pm \mu) \tag{13}$$

Multiplying Equation 10 by $[\sin(\theta \pm \mu)/\cos\psi(z)]$, Equation 11 by $-[\cos(\theta \pm \mu)/\cos\psi(z)]$ and adding can yield

$$[\partial\sigma/\partial x \mp 2\sigma\tan\psi(z)\,\partial\theta/\partial x \pm \gamma\tan\psi(z) \pm \sigma\,\partial\psi(z)/\partial z]\cos(\theta \mp \mu) + [\partial\sigma/\partial z \mp 2\sigma\tan\psi(z)\,\partial\theta/\partial z - \gamma]\sin(\theta \mp \mu) = 0 \tag{14}$$

Multiplying Equation 14 by $[dx/\cos(\theta \pm \mu)]$ and using Equation 13, the following expressions are obtained.

$$d\sigma - 2\sigma\tan\psi(z)d\theta = \gamma[dz - \tan\psi(z)dx] - \sigma\,[\partial\psi(z)/\partial z]\,dx \tag{15}$$

$$d\sigma + 2\sigma\tan\psi(z)d\theta = \gamma[dz + \tan\psi(z)dx] + \sigma\,[\partial\psi(z)/\partial z]\,dx \tag{16}$$

Equations 13, 15, and 16 can be solved simultaneously for σ and θ at various coordinate points, which in turn can be used

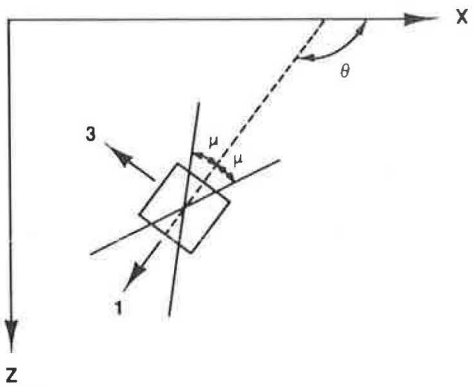

FIGURE 2 Orientation of pseudo-slip lines.

for the detailed calculation of the developed lateral earth pressures.

SOLUTION STEPS

Equations 13, 15, and 16 can be rewritten in different forms as

$$z_{i,j} - z_{i-1,j} = (x_{i,j} - x_{i-1,j}) \tan(\theta_{i-1,j} - \mu_{i-1,j}) \quad (17)$$

$$z_{i,j} - z_{i,j-1} = (x_{i,j} - x_{i,j-1}) \tan(\theta_{i,j-1} + \mu_{i,j-1}) \quad (18)$$

$$(\sigma_{i,j} - \sigma_{i-1,j}) - 2\,\sigma_{i-1,j}\,(\theta_{i,j} - \theta_{i-1,j}) \tan\psi_{i-1,j} = \gamma[(z_{i,j} - z_{i-1,j}) - (x_{i,j} - x_{i-1,j}) \tan\psi_{i-1,j}] - \sigma_{i-1,j}\,(x_{i,j} - x_{i-1,j})\,\partial\psi/\partial z|_{i-1,j} \quad (19)$$

$$(\sigma_{i,j} - \sigma_{i,j-1}) + 2\,\sigma_{i,j-1}\,(\theta_{i,j} - \theta_{i,j-1}) \tan\psi_{i,j-1} = \gamma[(z_{i,j} - z_{i,j-1}) + (x_{i,j} - x_{i,j-1}) \tan\psi_{i,j-1}] + \sigma_{i,j-1}\,(x_{i,j} - x_{i,j-1})\,\partial\psi/\partial z|_{i,j-1} \quad (20)$$

These equations completely described recursion formulas for the pseudo-slip line coordinates ($x_{i,j}$ and $z_{i,j}$), the pseudo-slip line slope ($\theta_{i,j} \pm \mu_{i,j}$), and the associated average stress ($\sigma_{i,j}$) in terms of previous values at coordinates (i–1,j) and (i,j–1). According to Sokolovskii *(8)*, the pseudo-slip lines form in general in three distinct regions as shown in Figure 3. The solution process starts from the line, 0_1A_o, that is, the ground surface whose coordinates and stress values are known, to the line 0_2A_3, that is, the rear face of the retaining wall through Regions I, II, and III. The detailed description of the solution procedure is beyond the scope of this paper; it is well described by Sokolovskii *(8)*.

Along the free surface 0_1A_o, all values are known as

$$\sigma_{i,j} = 0$$

$$\theta_{i,j} = \pi/2$$

$$x_{i,j} = x_{i,j}$$

$$z_{i,j} = 0 \quad (21)$$

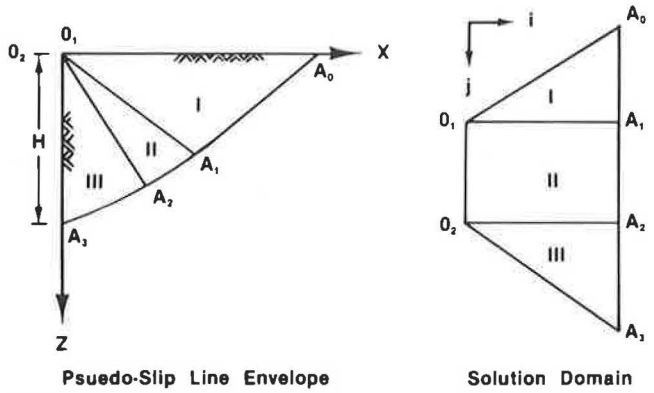

Psuedo-Slip Line Envelope Solution Domain

FIGURE 3 Schematics of solution procedure.

This leads to the complete solution of $x_{i,j}$, $z_{i,j}$, $\sigma_{i,j}$, and $\theta_{i,j}$ in Region I. For the solution of Region II, values of $\sigma_{i,j}$, $\theta_{i,j}$, $x_{i,j}$, and $z_{i,j}$ along $0_1 0_2$ are needed in addition to those values along 0_1A_1 obtained from the solution of Region I. Obviously at 0_1 or 0_2 (actually some point but separated conveniently for the solution), $\sigma_{i,j} = 0$, $x_{i,j} = 0$, and $z_{i,j} = 0$. However, $\theta_{i,j}$ varies from $\pi/2$ at 0_1 to some value at 0_2 where the wall friction may be considered. When the wall friction is considered, θ can be expressed, according to Sokolovskii *(8)*, as

$$\theta = \pi/2 + 1/2\,(\Delta - \delta) \quad (22)$$

where δ is the wall friction angle, and

$$\sin\Delta = \sin\delta/\sin\phi \quad (23)$$

Because angle $\psi(z)$ is introduced instead of ϕ, Equation 22 is also modified as

$$\theta = \pi/2 + 1/2\,[\Delta(z) - \delta(z)] \quad (24)$$

where $\delta(z)$ is the developed wall friction angle at depth z, and

$$\sin\Delta(z) = [\sin\delta(z)/\sin\psi(z)] \quad (25)$$

and $\delta(z)$ varies from zero at at-rest state to δ_{max} at active state with its variation in accordance with that of $\psi(z)$. The values of $\theta_{i,j}$ along $0_1 0_2$, therefore, can be taken as

$$\theta_{o_1} = \pi/2$$

$$\theta_{o_2} = \pi/2 + 1/2\,[\Delta(z) - \delta(z)]\,|_{z=0} \quad (26)$$

with linear variation between 0_1 and 0_2. This leads to the complete solution of Region II.

The solution of Region III requires at least two sets of initial values along 0_2A_3 in addition to solutions along 0_2A_2 obtained in Region II. Known initial values along 0_2A_3 are

$$x_{i,j} = 0$$

$$\theta_{i,j} = \pi/2 + 1/2\,[\Delta(z) - \delta(z)]\,|_{z=z_{i,j}} \quad (27)$$

Therefore a complete solution can be made possible. Once the values of $\sigma_{i,j}$ along 0_2A_3, that is, along the rear face of the retaining wall, are obtained, developed normal and shear stresses can be calculated from

$$\sigma_x = \sigma_{i,j}\,\{\sin[\Delta(z) - \delta(z)]/\sin\Delta(z)\}\,\cos\delta(z)\,|_{z=z_{i,j}}$$

$$\tau_{xz} = \sigma_x \tan\delta(z)\,|_{z=z_{i,j}} \quad (28)$$

The detailed solution steps, however, require a description of the function, $\psi(z)$, and its derivative, which describe the transition of lateral earth pressures from an at-rest to a full-active condition. As discussed before, the function varies from ϕ_o at at-rest condition to ϕ_o at full-active condition. The variation between these two extreme values is assumed as follows.

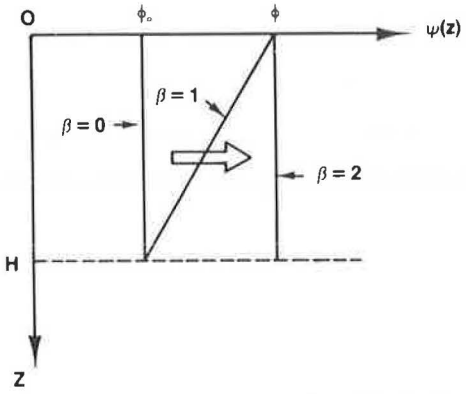

FIGURE 4 Transition of $\psi(z)$ from ϕ_o to ϕ.

Let β denote the stage of wall tilt so that $\beta = 0$ for at-rest condition, $\beta = 1.0$ for initial active condition, and $\beta = 2.0$ for full-active condition. In other words, for the values of β between 0 and 1.0, transition from an at-rest to an initial-active condition is described. Suppose that the behavior of the soil is elasto-fully plastic as defined by the limiting deformation, the values of β between 0 and 1.0 describe elastic behavior of the soil because the limiting deformation of the soil does not develop yet. Therefore it is assumed that the developed deformation of the soil for $0 \leq \beta \leq 1$ is directly proportional to β.

Values of β between 1.0 and 2.0 describe the transition from an initial-active to a full-active condition, where $(\beta - 1)H$ indicates the thickness of the soil from the ground surface, which experiences deformations exceeding the limiting value. Figure 4 shows the schematic variation of $\psi(z)$. At $\beta = 1.0$, the variation of $\psi(z)$ is assumed to be $\psi(z) = \phi$ at $z = 0$ and $\psi(z) = \phi_o$ at $z = H$, since by definition the initial-active condition describes a stage of wall tilt when only the soil element at $z = 0$ reaches a limiting condition defined by a friction angle ϕ. The original concept of this approach was first proposed by Dubrova (as translated by Harr) *(10)* in his "method of redistribution of pressures." Figure 5 shows the variations of $\psi(z)$ at various values of β assumed in the analysis. They can be expressed as for $0 \leq \beta \leq 1.0$, that is, elastic,

$$\psi(z) = \phi_o + (\phi - \phi_o)\,(1 - z/H)\beta$$

$$\partial\psi(z)/\partial z = -\beta(\phi - \phi_o)/H \qquad (29)$$

For $1.0 < \beta \leq 2.0$, within zone already in limiting condition $[0 \leq z \leq (\beta-1)]$, that is, in plastic region,

$$\psi(z) = \phi$$

$$\partial\psi(z)/\partial z = 0 \qquad (30)$$

within zone not yet in limiting condition $[(\beta-1)H < z \leq H]$, that is, in elastic region,

$$\psi(z) = (\phi - \phi_o)\,(\beta - z/H) + \phi_o$$

$$\partial\psi(z)/\partial z = -(\phi - \phi_o)1/H \qquad (31)$$

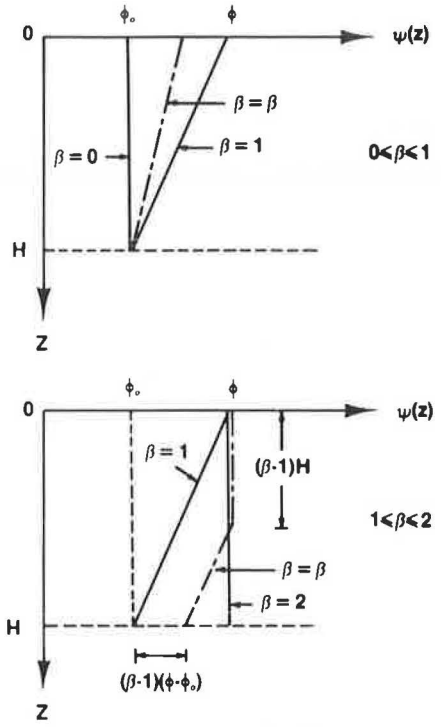

FIGURE 5 Variation of $\psi(z)$.

The following comparisons with model tests and example solutions are obtained using the preceding variations of $\psi(z)$ and $[\partial\psi(z)/\partial z]$.

MODEL COMPARISON

The developed method of analysis is used to compare with the model test results reported by Sherif et al. *(11)*. The model wall was 3.3 ft high and constructed of rigid structural aluminum. Air-dry Ottawa silica sand was used for backfill. Samples were compacted using a shaking table for various periods of time. The developed lateral earth pressures were measured continuously as the wall tilted outward about the base of the wall.

Figure 6 shows the detailed comparison of the lateral earth pressure developed at various amounts of wall tilt. The sand has an internal friction angle of 47 degrees, a wall friction angle of 24.6 degrees, K_o of 0.644, and a unit weight of 107.54 pcf. The solid line indicates the measured pressure values and dots indicate the calculated values at a depth of 0.5 ft. The initial active condition ($\beta = 1.0$) corresponds to a wall tilt of 3×10^{-4} radian. This is obtained from the conclusions of Sherif et al. *(11)*, which indicate that the horizontal displacement necessary to mobilize the active state of stress (limiting deformation) is independent of the soil friction angle or density, and that the amount corresponds to approximately 12×10^{-3} in.

Unfortunately the properties of the sand and the wall friction angle were not reported. The properties as indicated earlier were therefore obtained from the back-calculation with the initial stress at zero rotation (at-rest state) and the final stabilized stress at a very large rotation (active state), as well as friction angle-wall friction-unit weight relations reported by

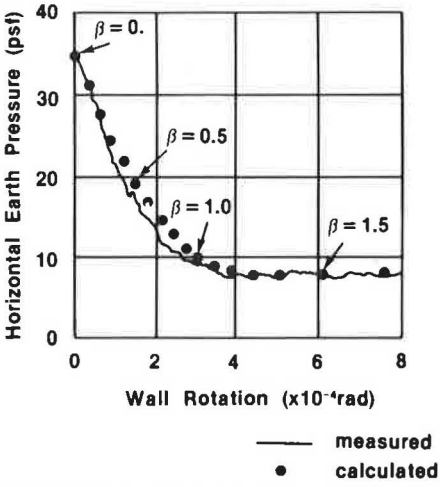

FIGURE 6 Model test Comparison 1.

Sherif et al. *(12)*. The comparison indicates that very good agreement exists between the measured and calculated lateral earth pressures in magnitude and variation at various degrees of wall tilt.

Sherif et al. *(11)* reported additional test results with the same model. Pressures were measured continuously at five different depths. Again, the detailed material properties were not indicated, therefore the same methods were used to obtain the material properties at corresponding depths of the measurements. The calculated soil friction angles vary from approximately 28 degrees at the lowermost pressure cell to approximately 46 degrees at the uppermost one. This wide variation in friction angle may raise a question. However, in the absence of direct measurements, these calculated friction angles could only be used for the comparison between experimental and analytical results. In the analysis, the soil is assumed to be composed of five layers whose material properties are represented by the values calculated at the mid-depths. The detailed lateral earth pressure comparisons, as well as the material properties, are shown in Figure 7 and Table 1, respectively. As

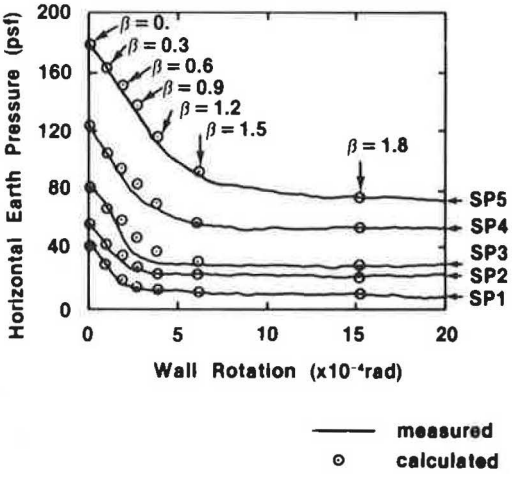

FIGURE 7 Model test Comparison 2.

TABLE 1 SAND PROPERTIES

Pressure Cell	Depth (ft)	ϕ (deg)	$\tan\sigma/\tan\phi$	K_o
SP1	0.5	46	0.52	0.89
SP2	0.99	38	0.52	0.44
SP3	1.53	40	0.52	0.47
SP4	2.06	31	0.52	0.56
SP5	2.60	28	0.52	0.72

can be observed in the figure, the method of analysis can predict the developed lateral earth pressures at various depths and at various degrees of wall tilt closely, with the exception of pressure cell SP3 near β of 1.0—the measurement indicates a very sharp drop of earth pressures in contrast to the other pressure cell measurements.

EXAMPLE

The lateral earth pressures behind a vertical retaining wall experiencing outward tilt about its base with uniform cohesionless backfill material are calculated at various values of β. Figure 8 shows the results of a smooth (frictionless) retaining wall. From at-rest (β = 0) to initial-active condition (β = 1.0), lateral earth pressures decrease more rapidly with β near the middle portion of the wall, whereas rapid reduction in pressure is observed within the lower portion of the wall from an initial-active (β = 1.0) to a full-active condition (β = 2.0). As expected,

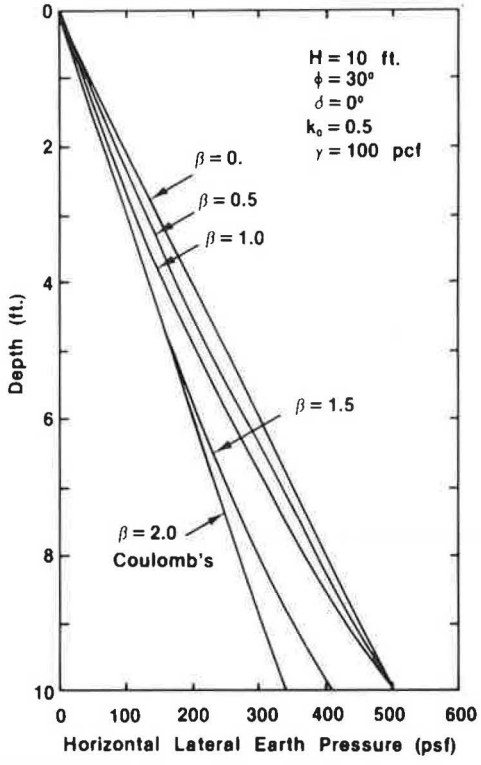

FIGURE 8 Transition of lateral earth pressures (smooth wall).

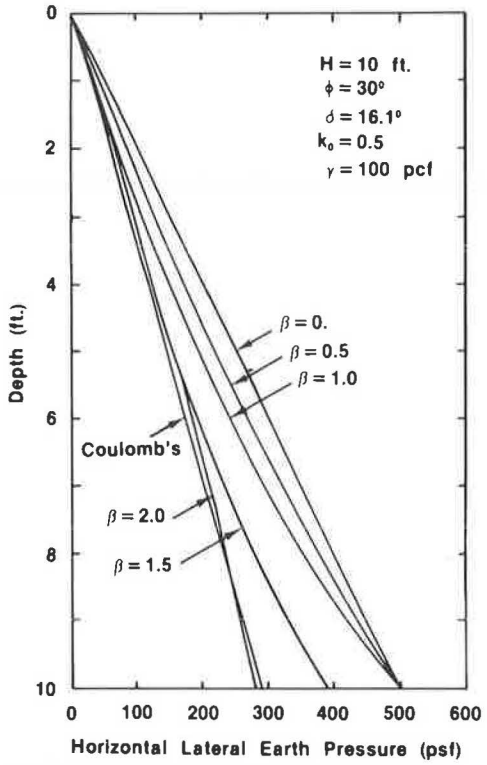

FIGURE 9 Transition of lateral earth pressures (rough wall).

the magnitude and variation of the lateral earth pressure at full-active condition ($\beta = 2.0$) exactly matches Coulomb's solution because the slip lines are identical between two methods for a frictionless wall. For a rough retaining wall (Figure 9), however, the developed method of analysis does not match exactly Coulomb's solution because of the differences in the orientation of the slip lines; Coulomb's solution is still based on linear slip lines, whereas the developed method of analysis involves curved slip lines near the retaining wall. The difference is very small, however.

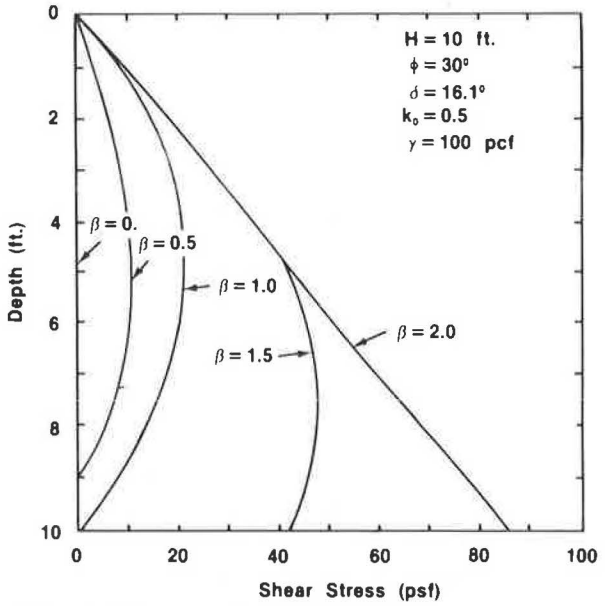

FIGURE 10 Transition of shear stresses.

Figure 10 shows the variations of the shear stresses behind the rough retaining wall from an at-rest to a full-active condition. The variation begins with zero shear stresses at at-rest condition, and reaches maximum values at full-active condition with transitions in accordance with the values of β. For instance, at $\beta = 1.5$, that is, when limiting condition reaches up to mid-depth, maximum possible shear stresses defined by the wall friction develop within the upper-half while the lower-half is yet to be within reach of full values.

CONCLUSIONS

An approximate analytical solution that describes the transition of the lateral earth pressures from an at-rest to a full-active condition behind a rigid retaining wall experiencing an outward tilt about the base has been developed. Comparisons with model test results have also been made. In general the developed method of analysis is capable of predicting not only the magnitudes but also the variations of the lateral earth pressures at various depths as well as at various amounts of wall tilt.

The developed analytical solution involves many assumptions, including the at-rest earth pressure coefficient. For many earth-retaining structures, backfill materials may be placed by various methods, resulting in an initial stress state other than at-rest condition. In such cases the induced initial stress state could be represented in the analysis by appropriately expressing the initial friction angle, ϕ_o, so that the resulting earth pressure ratio in Equation 6 represents the actual induced initial stress state.

The developed method of analysis can be easily expanded to include the cohesion of the soil, various geometry of the wall and the ground surface, and the depth-dependent soil strength characteristics, as well as other modes of wall movements. Further research is necessary, however, if other factors such as the large deformation effect, slippage between the structure and the soil, and the flexibility of the retaining structures are to be considered.

REFERENCES

1. M. Fukuoka, T. Akatsu, S. Datagiri, T. Iseda, A. Shimazu, and M. Makagake. Earth Pressure Measurements on Retaining Walls. *Proc., Ninth International Conference on Soil Mechanics and Foundation Engineering*, Tokyo, Japan, 1977.
2. I. K. Lee and J. R. Herington. Effect of Wall Movement on Active and Passive Pressures. *Journal of the Soil Mechanics and Foundations Division, ASCE*, Vol. 98, No. SM6, June 1972.
3. S. Okabe. General Theory of Earth Pressure. *Journal of Japanese Society of Civil Engineers*, Vol. 12, No. 1, 1924.
4. K. Terzaghi. General Wedge Theory of Earth Pressure. *Transaction, ASCE*, 1941.
5. T. W. Lambe and R. V. Whitman. *Soil Mechanics*, John Wiley and Sons, Inc., New York, 1969.
6. M. G. Spangler and R. L. Handy. *Soil Engineering*, 4th ed. Harper and Row, New York, 1982.
7. S. P. Timoshenko and J. N. Goodier. *Theory of Elasticity*. 3rd ed. McGraw-Hill Book Co., New York, 1970.

8. V. V. Sokolovskii. *Statics of Granular Media.* Pergamon Press, New York, 1965.
9. J. Jaky. The Coefficient of Earth Pressure at Rest. *Journal of the Society of Hungarian Architects and Engineers,* 1944.
10. M. E. Harr. *Foundations of Theoretical Soil Mechanics.* McGraw-Hill Book Co., New York, 1966.
11. M. A. Sherif, Y. S. Fang, and R. I. Sherif. K_a and K_o Behind Rotating and Non-Yielding Walls. *Journal of Geotechnical Engineering,* Vol. 110, No. 1, Jan. 1984.
12. M. A. Sherif, I. Ishibashi, and C. D. Lee. *Dynamic Earth Pressures Against Retaining Structures.* Soil Engineering Research Report 21, University of Washington, Seattle, Jan. 1981.

Publication of this paper sponsored by Committee on Subsurface Soil–Structure Interaction.

Initial Response of Foundations on Mixed Stratigraphies

CHARLES E. WILLIAMS

A procedure for easily computing the initial settlement of shallow foundations on mixed stratigraphies has been developed. Applicable soil conditions are primarily stiff to hard clays with horizontal layers of dense to very dense sand. The Revised Gibson Model makes use of a simple equation for elastic settlement of axisymmetric footings. An equivalent modulus that accounts for the variations in soil modulus with depth beneath the footing is one of the primary input parameters to the equation. The effect of a sand layer within the foundation soils on initial settlements is included in the procedure by means of an additional factor obtained from parametric charts. Twelve case histories, including elevated and ground storage tanks and multistory buildings, are used to evaluate the effectiveness of the new initial settlement computational method.

The initial settlement component of the response of foundations to applied load is an important design consideration when the supporting soil media are comprised of stiff to hard clays. The presence of competent sand layers within the foundation stratum can effectively "stiffen" the foundation response and should be considered in design.

The Equivalent Gibson Model *(1)* has been shown to be a useful procedure for properly characterizing cohesive foundation media in the Houston, Texas, area and computing expected initial settlements for a large range of foundation sizes. The Equivalent Gibson Model has been expanded to consider the presence of competent sand layers within the supporting soils. The simplicity of the original procedure is maintained by adding only one additional design step involving the use of parametric plots.

The new procedure was evaluated by application to 12 new projects ranging from elevated and ground storage tanks to multistory buildings. Measured initial settlements are compared with those predicted by the Revised Gibson procedure.

McBride-Ratcliff and Associates, Inc., 7220 Langtry, Houston, Texas 77040.

PREVIOUS WORK

Initial settlement represents the immediate foundation response to induced shear stresses at constant volume. The remaining two components of settlement due to consolidation and secondary compression involve time-related volume change. For stratigraphies containing moderately to heavily overconsolidated clays, the initial settlement component can account for 30 to 70 percent of the total settlement response *(2)*. Consequently, the expected magnitude of initial settlement for foundations on soil strata with a large percentage of stiff to hard clay layers is a major design consideration. Development of the initial settlement component within the total response of a building foundation to applied load is shown in Figure 1.

Proper design of foundations typically results in contact pressures for footings or mats that do not produce yield zones in the foundation soils. The foundation response is to the left of the "first yield" location shown in Figure 2, which makes it possible to use elastic or linear methods of analysis to predict initial settlements.

Williams and Focht (*1*) recognized that Pleistocene clays in the Houston area typically exhibit an increase in undrained modulus with depth, and that the soil model proposed by

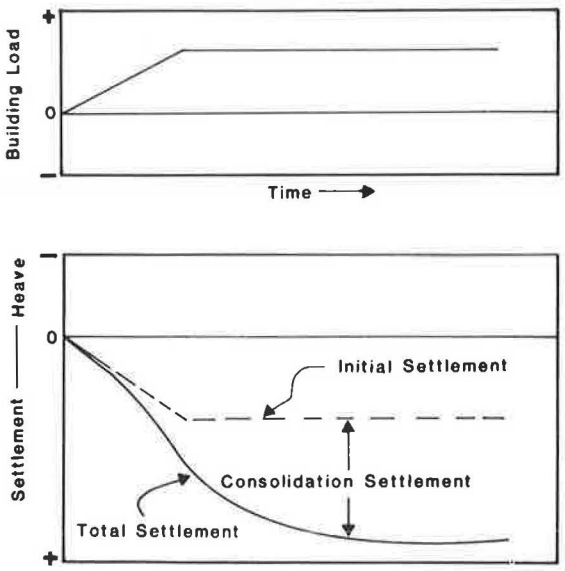

FIGURE 1 Time-settlement response.

Brown and Gibson *(3)* has possible application to such soils. They used the Gibson Soil Model shown in Figure 3 to produce an equivalent constant undrained modulus, $\bar{E}$, for a given foundation width. The equivalent modulus, $\bar{E}$, is defined as the average modulus for a given footing of width, B, which produces the same computed initial settlement as obtained using the Brown and Gibson procedure involving the modulus increasing with depth. The equivalent constant modulus could be input into the classical elastic settlement equation given below to develop an estimate of initial settlement for a given foundation width and applied contact pressure for axisymmetric foundations *(4)*:

$$\rho = PBI/\bar{E} \quad (1)$$

where

ρ = initial settlement,
P = contact pressure,
B = foundation width or diameter, and
I = geometric influence factor.

The Williams and Focht study *(1)* produced the curve shown in Figure 4 in which the equivalent modulus $\bar{E}$ is normalized with respect to the typical undrained shear strength for the foundation soils and related to the width of the foundation. Typical undrained shear strength is defined as the average undrained shear strength over a depth interval of twice the foundation width, with depth measured relative to the foundation bearing level. The band in Figure 4 is converted to a modulus profile with depth and compared in Figure 5 to modulus profiles obtained on similar soils in the Houston area using pressure meter, cyclic triaxial, and reduced cross-hole test data *(1)*.

Several case histories were applied to the model and are plotted in Figure 4. A review of that figure shows a consistent trend toward equivalent modulus values that are 50 to 100 percent higher than the Gibson curves would indicate, for cases in which significant sand layers were present within a depth range of twice the foundation width below the bearing level. Significant sand layers would be defined as relatively continuous cohesionless soil units located within the 2B depth interval beneath the foundation exhibiting a thickness of at least 10 percent of the foundation width. The most logical explanation for the improved settlement response was that the sand layers were mobilizing much higher modulus magnitudes than could be realized in the cohesive strata. The results clearly showed

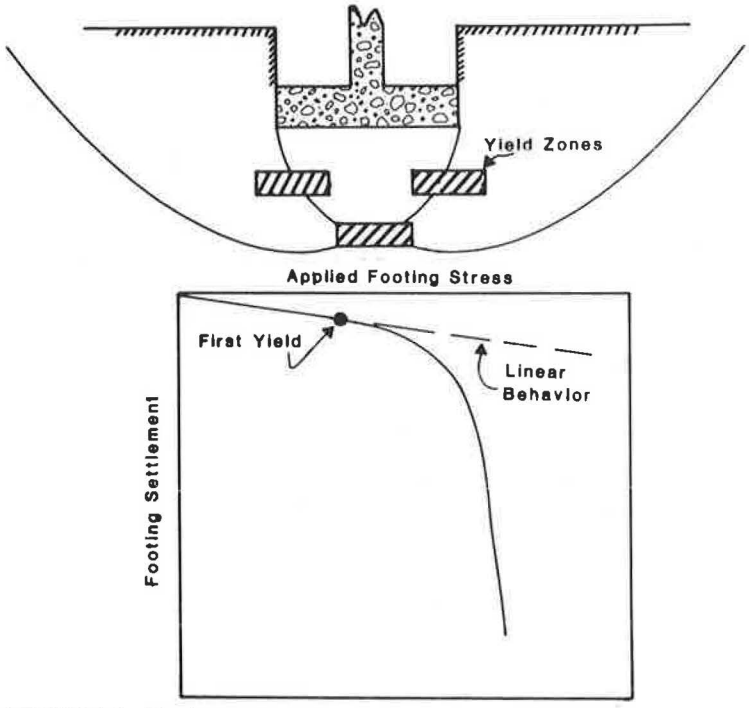

FIGURE 2 Typical load-settlement curve.

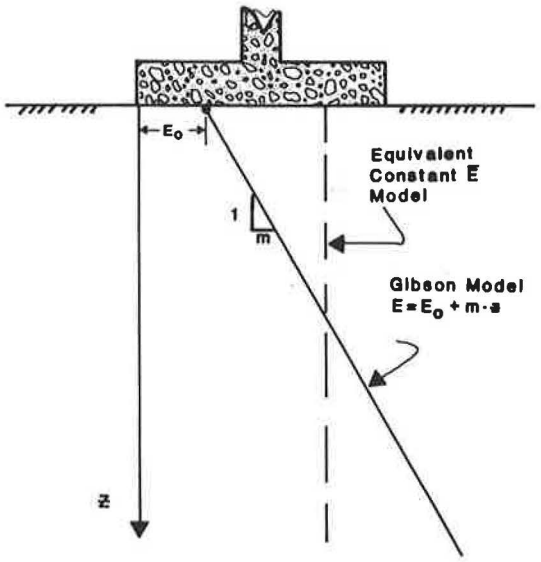

FIGURE 3 Gibson soil model.

that the presence of sand layers could improve foundation response and should be considered in design.

SAND DATA

The silty fine sands typically encountered within Pleistocene sediments in the Houston area are alluvial or deltaic in origin. The buried distributary sands are SM or SP according to the Unified Soils Classification System and may contain fines fractions (silt and clay) of 5 to 40 percent. Generally, less than 10 percent of the sand gradation is coarser than the No. 60 sieve size.

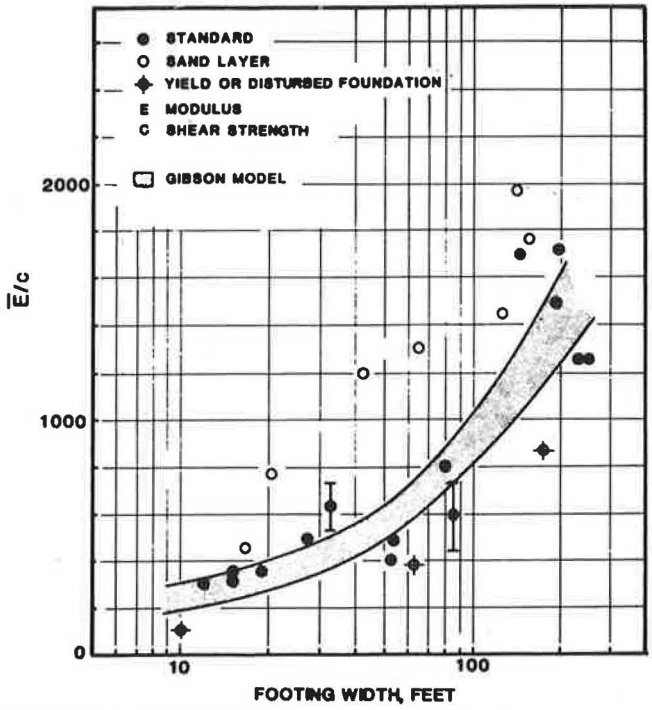

FIGURE 4 Normalized modulus versus foundation width.

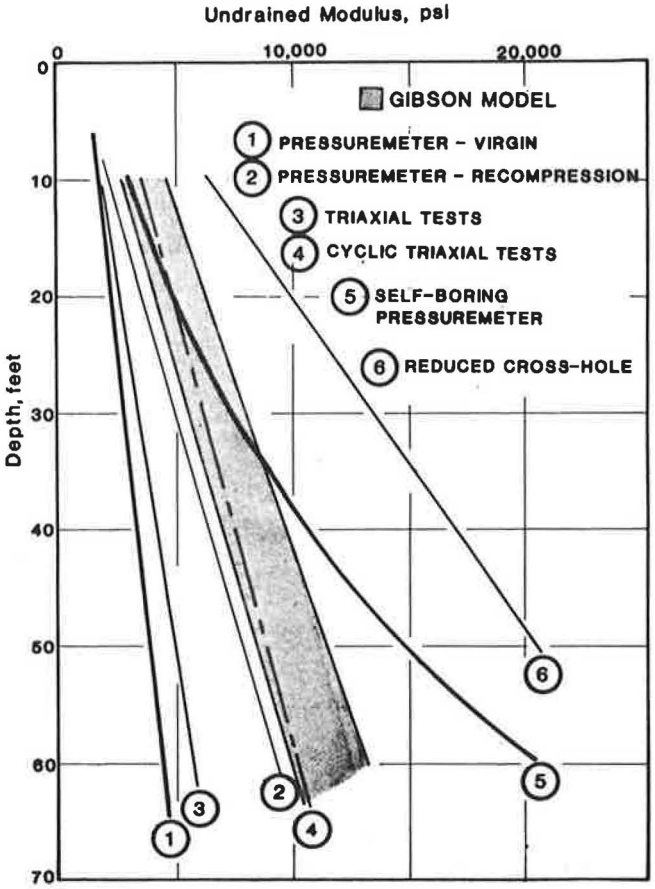

FIGURE 5 Comparison of Gibson model with test data.

Profiles of standard penetration test (SPT) resistance data on sand strata assembled from various subsurface studies in the Houston area are shown in Figure 6. The "dense" category is most commonly encountered and corresponds to a relative density range of 60 to 90 percent based on an empirical correlation between relative density, SPT resistance data, and effective

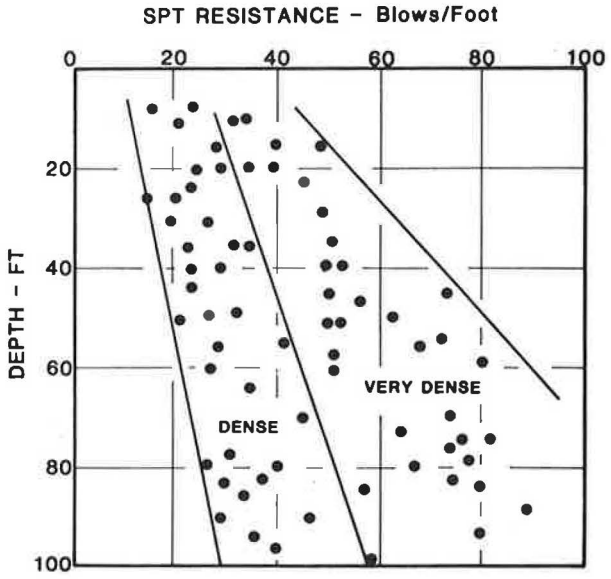

FIGURE 6 Typical sand data.

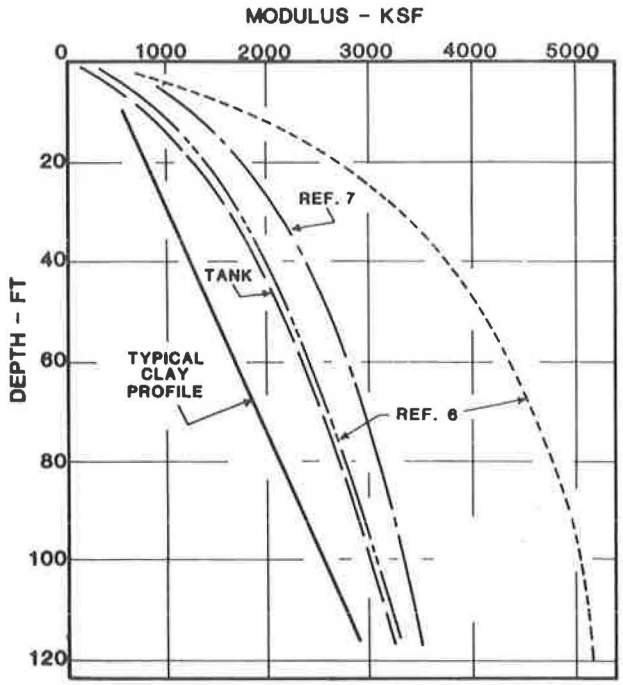

FIGURE 7 Clay and sand modulus profiles.

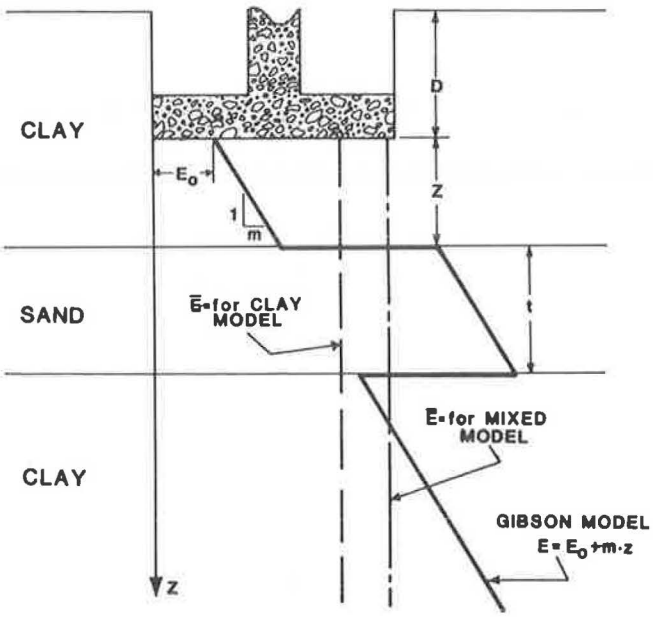

FIGURE 8 Mixed stratigraphy model.

overburden pressure *(5)*. The "very dense" category corresponds to a relative density range above 90 percent and is not encountered as frequently.

The silty sand strata are typically encountered as isolated horizontal soil layers within a primarily cohesive stratigraphy. Commonly observed sand stratum thicknesses range from 5 to 25 ft but can approach 30 to 40 ft near the center of a buried distributary channel. There are areas where two and three buried channels are geologically "stacked" upon each other and produce a total sand stratum thickness in excess of 100 ft.

Profiles of sand modulus with depth developed from a number of sources are shown in Figure 7. The curve labeled "tank" corresponds to a modulus profile backfigured from settlement measurements on a ground storage tank supported on more than 80 ft of sand from the "dense" category. The corresponding factor of safety for this foundation system was in excess of 5. The shape of the modulus profile is in accordance with the classical distribution found to be acceptable for many sands *(6)*. Also shown in Figure 7 is a curve labeled "Reference 7" corresponding to extensive cyclic triaxial and field cross-hole testing of a dense sand *(7)*. The cross-hole modulus values were reduced to 30 percent of calculated magnitudes to account for strain levels typically mobilized by loaded foundations *(8)*. The remaining two profiles are labeled "Reference 6" and correspond to dense and very dense typical sands selected by Hartman for extensive study of sand modulus *(6)*.

A typical clay modulus profile obtained from the Williams and Focht study *(1)* is also shown in Figure 7. Modulus magnitudes at a given depth for the clay profile are much smaller than the dense sands and less than one-half the very dense modulus values.

SAND FOUNDATION MODELS

The Revised Gibson Model is shown schematically in Figure 8. The primarily clay soil profile exhibits an increasing modulus with depth. The sand substratum is characterized in terms of depth below the foundation bearing level and sand layer thickness, and yields a modulus magnitude greater than that for a clay stratum at comparable depth. The equivalent constant modulus, $\bar{E}$, obtained from the mixed stratigraphy model is correspondingly higher than that computed for the homogeneous clay condition for a foundation of given size.

The various methods for computation of settlements of a foundation on sand were reviewed for possible utilization in the Revised Gibson Model procedure. The methods considered are given in Table 1 and are discussed as follows:

- Empirical procedures. The empirical procedures based on SPT or cone data generally model the soil with one representative variable and are not suited to consider layered models.
- Simple elastic models. Simple elastic models are based on a single modulus value for the foundation and cannot handle layered systems.
- Stress-based elastic models. The layered models of Webb and Oweis are useful procedures that have a theoretical base and substantial flexibility in application. However, layer distributions based on stress are greatly affected by differences in layer stiffness.
- Strain-based elastic model. The Schmertmann strain factor procedure is theoretically based and can handle layered systems. The strain influence factor approach is well documented, simple to use, and is relatively insensitive to the effects of embedment on layered soil stratifications.

TABLE 1 METHODS FOR COMPUTING SETTLEMENTS ON SAND FOUNDATIONS

Method	Description	Remarks
Terzaghi and Peck *(9)*	Empirical procedure	Very conservative
Meyerhof *(10, 11)*	Based on SPT data	Moderately conservative
Peck and Bazaraa *(12)*		
Peck et al. *(13)*		
Debeer *(14)*	Semiempirical procedure Based on cone data	Very conservative
D'Appolonia et al. *(15, 16)*	Elastic method with constant modulus	Considers modulus
Webb *(14, 17)*	Elastic layer method, stress-based	Considers modulus with depth
Schultze and Sherif *(14)*	Quasi-elastic method with empirical correlation based on SPT data	Indirectly considers modulus
Oweis *(18)*	Elm elastic model Considers layers, empirically uses SPT data	Complex procedure
Schmertmann *(5, 10, 20)*	Uses strain influence factors and considers layers	Theoretical base, model flexibility, variable modulus

The Schmertmann strain factor approach for computing settlements of foundations on sand is shown in Figure 9. The strain factor is a parameter that characterizes the distribution of vertical strain with depth beneath a footing. The unique strain factor distribution for an axisymmetric footing and the variation of modulus with depth beneath the footing can be input into Schmertmann's equation to compute expected footing settlements. The equation in Figure 9 uses a summation procedure over a depth of twice the footing width and average values of modulus and strain factor for each layer being considered. The equation also uses a factor for embedment and a separate factor for creep; however, these two parameters do not play a role in the utilization of the equation in this paper and have been, correspondingly, deleted.

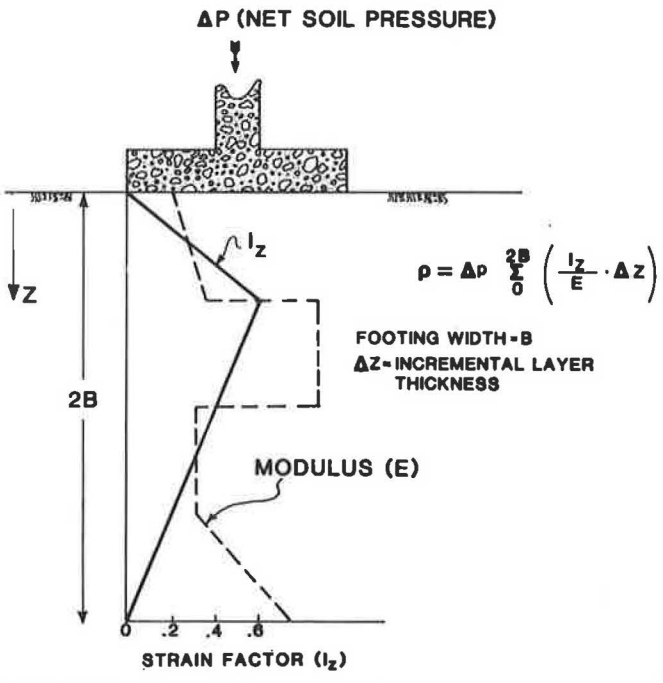

FIGURE 9 Strain factor approach.

Hartman *(6)* evaluated the Schmertmann strain factor approach in detail and found it to be applicable for soils exhibiting modulus magnitudes that increase with depth. Correspondingly, the model should be appropriate for Houston-area stiff to hard clays as well as sand strata. Hartman's findings concerning the insensitivity of the model to footing embedment and relative stiffness effects in layered soils, along with its general applicability to the Revised Gibson Model are summarized as follows:

- Triangular strain factor distribution is appropriate for soils with a nonlinear stress-dependent modulus.
- Mixed stratigraphies with "stiff" layers do not significantly affect strain factor distribution.
- Foundation embedment does not significantly affect strain factor distribution.
- There are "unique" strain factor distributions for rigid and flexible foundation units with axisymmetric geometry.

COMPUTATIONAL PROCEDURE

The Schmertmann procedure is powerful and, using the model shown in Figure 8, could compute settlements for mixed stratigraphies directly, provided detailed modulus data for the given design case were available. However, the intent of this paper is to revise the Equivalent Gibson Model and develop a conceptually simple procedure for computing initial settlements for foundations on mixed soils with a minimal amount of input data. Development of the new procedure involves the following steps:

1. Parametric characterization of a given design condition by foundation width (B), embedment of foundation (D), depth to top of sand layer (Z), thickness of sand layer (t), and competency of the sand layer.

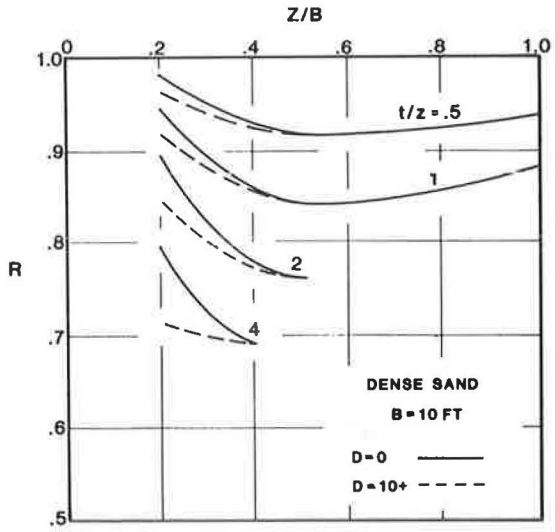

FIGURE 10 Reduction factor (dense sand, B = 10 ft).

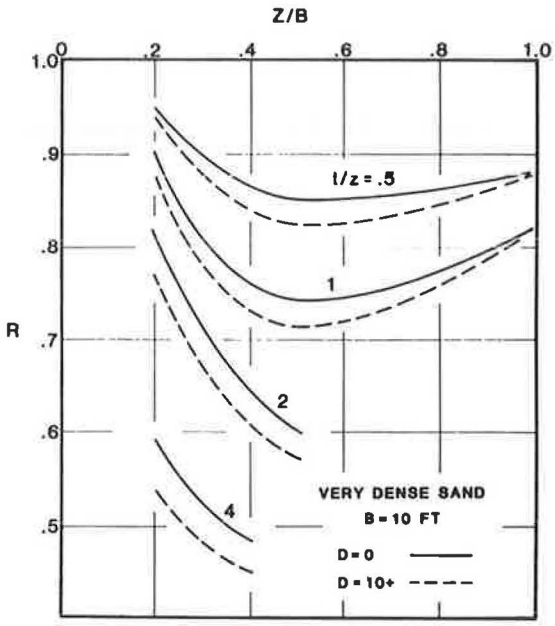

FIGURE 12 Reduction factor (very dense sand, B = 10 ft).

2. Computation of initial settlements for homogeneous clay profile with given foundation width (B) and embedment (D) using the Schmertmann procedure.
3. Computation of initial settlements for the various mixed soil conditions grouped on the basis of the ratios (Z/B) and (t/Z).
4. Development of a ratio (R) expressed as the initial settlement computed from Step 3 for a mixed soil condition divided by the homogeneous clay initial settlement from Step 2.

Figures 10 through 13 show developed relationships between the ratio (R) and the lumped parameters for depth to sand (Z/B) and sand-layer thickness (t/Z). The curves are grouped into four charts based on competency of the sand layer and size of the foundation. The Poisson's ratio used throughout the development of the computational procedure was 0.40. Parametric studies have revealed this magnitude to yield reasonable results for competent sands *(6)*.

The curves in Figures 10 through 13 are generally parallel to the strain factor distribution shown in Figure 9. The maximum effect of the sand layer, interpreted as the lowest ratio (R), is found near a depth to sand (Z) of about 0.5B. The effects of shallower or deeper sands are correspondingly less. Sand layer thickness and competency of the sand also have a direct effect on the ratio (R), with (t/Z) values near 4 in very dense sands producing R values below 0.5.

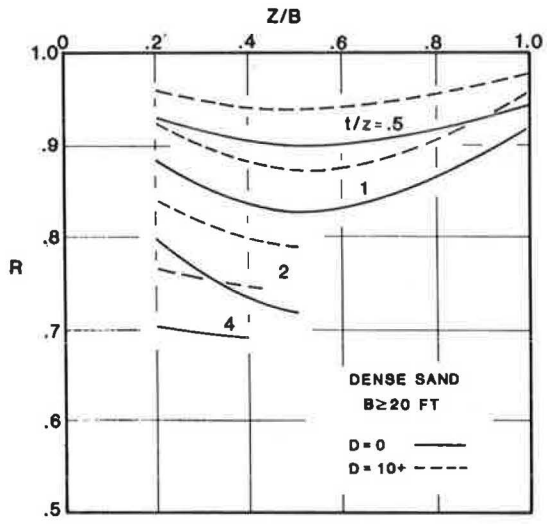

FIGURE 11 Reduction factor (dense sand, B ≥ 20 ft).

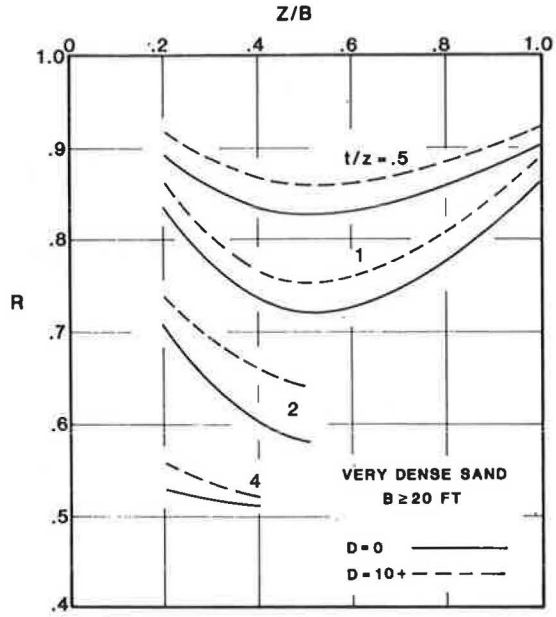

FIGURE 13 Reduction factor (very dense sand, B ≥ 20 ft).

TABLE 2 TEST CASES

Case	B (ft)	Z (ft)	T (ft)	Remarks
Ground tank	52	22	30	Very dense sand
Ground tanks	24–59	13	32	Three tanks
Elevated tank	53	12	24	
Elevated tank	53.5	12	9	
Elevated tank	53.5	12	37	Very dense sand
7-story garage	12	7	27+	Very dense sand, deep footings
9-story building	8–15	3	5.5–11.5	Very dense sand, 12 footings
17-story building	34–81	22	7	Two footings
19-story building	16–95	16	20	Very dense sand, 12 footings, deep footings
25-story building	134	15	20	Deep mat
25-story building	141	7	27	Deep mat
28-story building	175	30	20	Shallow mat

The effects of foundation size and embedment are more subtle and are primarily due to the parabolic shape of the sand modulus profile relative to the linear profile adopted for the clay strata. Shallow sands exhibit relatively small modulus magnitudes, which results in surface foundations with no embedment mobilizing larger R values. The effect is most pronounced for small footings and thick, shallow sands. For larger footings, embedment serves to increase R values because the sand and clay modulus profiles converge at depth.

PROCEDURE UTILIZATION

The procedure for utilization of the Revised Gibson Model is as follows:

1. Determine the average foundation width, representative undrained shear strength (c) for the cohesive strata to a depth of twice the footing width, and net increase in soil pressure at the foundation level due to the applied foundation loading.
2. Enter Figure 4 and obtain a representative value of $\bar{E}/c$, which in turn can be converted to an equivalent modulus ($\bar{E}$) by multiplying by the average undrained shear strength (c).
3. Determine an appropriate geometric influence factor (I) and compute a settlement (ρ) based on Equation 1 for initial settlements on half spaces.
4. Characterize the sand substratum as dense or very dense and compute the parameters (Z/B) and (t/Z).
5. Enter the appropriate chart in Figures 10 through 13 and select an R value.
6. Multiply the previously computed settlement by the R value to obtain a modified settlement for the mixed soil condition.
7. The procedure is structured to address only one sand layer. If two distinct sand layers are present within a depth range of 2B beneath the footing, both cases should be addressed separately and the individual R factors should be multiplied together to obtain a final R factor for the entire system.

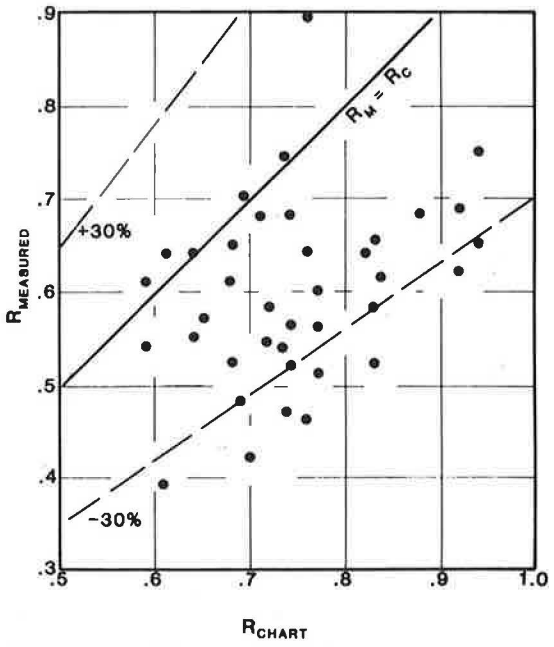

FIGURE 14 Method evaluation.

SETTLEMENT DATA

Twelve projects ranging from elevated and ground storage tanks to multistory buildings were monitored for initial settlements to provide a means for evaluating the new procedure. In some cases the projects were complete and the appropriate data were on file, and in others the new procedure was used to predict settlements during the design phase. Table 2 gives a tabulation of the 12 case histories and the parameters required for input into the Revised Gibson Model.

Values of R were computed for each of the 38 foundations monitored for settlements within the 12 case histories. These R values denoted as R CHART are plotted versus R MEASURED, the R values backfigured from the measured settlements. The comparisons are shown in Figure 14. The distribution of the data points is very encouraging in that most of the results are within 30 percent of R CHART = R MEASURED. A majority of the data points located below the R CHART = R MEASURED line indicate that the Revised

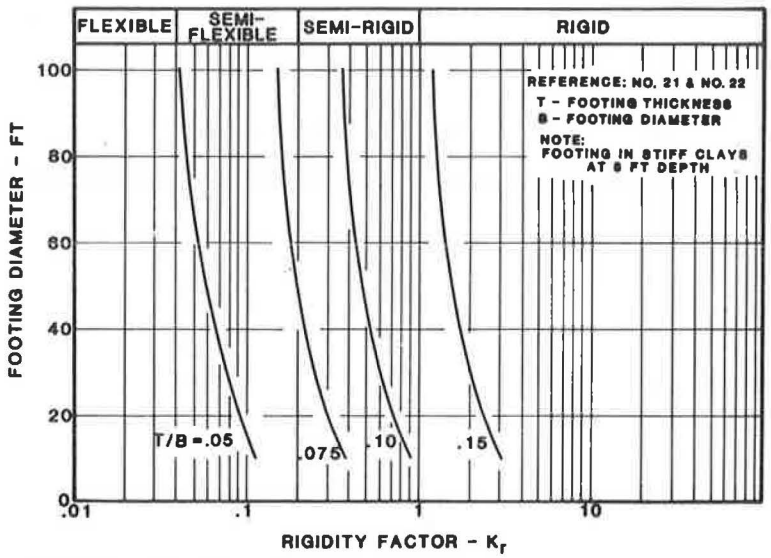

FIGURE 15 Rigidity factor – K_r.

Gibson Model for mixed stratigraphies generally underpredicts the beneficial effects of the sand substratum.

RESULTS OF THE STUDY

The Equivalent Gibson Model procedure has proven to be a simple but systematic approach to computation of initial settlements for foundations on stiff to hard clay stratigraphies that exhibit an increasing undrained modulus with depth. The Revised Gibson Model for layered stratigraphies provides an appropriate extension to the original method. The procedure has a strong theoretical base and is sufficiently detailed to address the major considerations within a foundation engineering design situation, but continues to provide the simplicity of the original Equivalent Gibson Model.

The results in Figure 14 show that the Revised Gibson Model is an effective but conservative procedure for the design cases considered to date. Of the 38 data points, 79 percent are within the ± 30 percent band; and 87 percent of the data base lies below the R CHART = R MEASURED line.

With predicted R values ranging from 0.59 to 0.94 and backfigured R values of 0.39 to 0.90, it is apparent that settlement reductions due to the presence of sand strata are real and can have an effect on foundation planning and design. In one particular case involving value engineering redesign during construction, it was possible to closely map the variable sand substratum thickness with additional subsurface work and custom tailor the individual footing bearing pressures on the basis of the Revised Gibson Model. Had it not been possible to quantify the beneficial effects of the sand stratum on reduced settlements, the redesign would not have been possible.

The new design procedure is most applicable to individual foundation units of less than 50 ft wide and with embedments of 20 ft or less. Larger mat foundations in excess of 100 ft wide were addressed in the case history study; however, understanding of the relative trends of the sand and clay modulus profiles below 100 ft depth is not strong. The semirigid response and complex loading patterns of most large mat foundations justify more detailed analytical procedures involving soil-structure interaction considerations.

It is possible to use data and procedures in this paper as a planning tool for large mat foundations loaded in a complex manner. Modulus profiles can be constructed from information contained in Figure 7, modified as required to reflect specific conditions for the given design case. Figure 15, developed from procedures offered by Terzaghi *(21)* and Brown *(22)*, can be referenced to determine the relative rigidity of the mat foundation, and the flexible and rigid strain factor envelopes in Figure 16 given relative weights based on the rigidity factor computed.

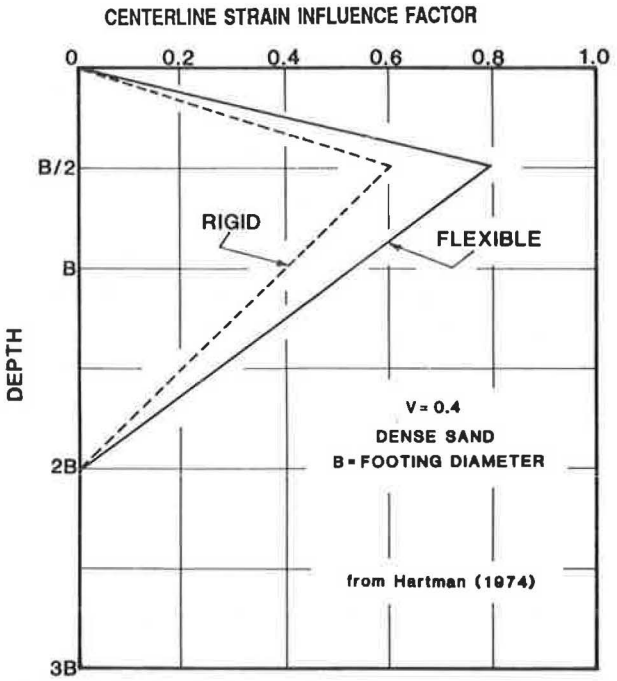

FIGURE 16 Strain factors for axisymmetric loading.

The Schmertmann procedure can then be employed to develop preliminary estimates of expected initial settlements for the mat. This information will be useful for planning purposes and for selection of subgrade modulus values required for the more detailed soil-structure interaction analysis of the mat system.

CONCLUSIONS

The Revised Gibson Model provides a strong extension to the original Equivalent Gibson Model procedure for axisymmetric loading conditions. The procedure has been shown to produce representative but conservative settlement estimates for a wide range of foundation sizes and layered stratigraphies in the Houston area.

The revised method is applicable to mixed stratigraphies comprised of stiff to very stiff clays with dense to very dense sand substrata. Different subsurface conditions will require modifications based on judgment.

The Revised Gibson Model is best suited to individual rigid foundation units of less than 50 ft wide and with embedments of 20 ft or less. Larger mat foundations with semirigid behavior and complex loading patterns should be analyzed by appropriate soil-structure interaction models. However, the procedures given in this paper can be useful in the initial planning of such mat foundation systems. As is the case for most new methods, additional calibration with more case histories would be highly beneficial to verification and expansion of the Revised Gibson Model.

REFERENCES

1. C. E. Williams and J. A. Focht, III. Initial Response of Foundations on Stiff Clay. ASCE National Convention, New Orleans, La., 1982.
2. J. B. Burland, B. B. Broms, J. Legrand, and V. F. B. de Mello. Behavior of Foundations and Structures. State-of-the-Art Reports, Session 2. *Proc., Ninth International Conference on Soil Mechanics and Foundation Engineering*, Tokyo, Japan, 1977.
3. P. T. Brown and R. E. Gibson. Surface Settlement of a Deep Elastic Stratum Whose Modulus Increases Linearly with Depth. *Canadian Geotechnical Journal*, Vol. 9, No. 4, 1972, pp. 467–476.
4. H. G. Poulos and E. H. Davis. *Elastic Solutions for Soil and Rock Mechanics*, John Wiley and Sons, Inc., New York, 1974.
5. W. F. Marcuson and W. A. Bieganousky. Laboratory Standard Penetration Tests on Fine Sands. *Geotechnical Engineering Division, ASCE*, Vol. 103, No. GT6, June 1977, pp. 565–588.
6. J. P. Hartman. *Finite Element Parametric Study of Vertical Strain Influence Factors and the Pressuremeter Test to Estimate the Settlement of Footings in Sand*. Ph.D. dissertation. University of Florida, Gainesville, 1974.
7. Woodward Clyde Consultants. *Basic Soil Data, Vol. I: Soil Parameters, South Texas Project*. Brown & Root, Inc., Houston, Tex., July 14, 1975.
8. W. F. Swiger. Evaluation of Soil Moduli, *Proc., ASCE Conference on Analysis and Design in Geotechnical Engineering*, Vol. II, Austin, Tex., 1974, pp. 79–92.
9. K. T. Terzaghi and R. B. Peck. *Soil Mechanics in Engineering Practice*, John Wiley and Sons, Inc., New York, 1967.
10. G. G. Meyerhof. Penetration Tests and Bearing Capacity of Cohesionless Soils. *Journal of the Soil Mechanics and Foundations Division, ASCE*, No. SM1, Jan. 1956, pp. 1–19.
11. G. G. Meyerhof. Shallow Foundations. *Journal of the Soil Mechanics and Foundations Division, ASCE*, No. SM2, March 1956, pp. 507–520.
12. R. B. Peck and A. B. S. Bazaraa. Discussion of Settlement of Spread Footings on Sand. *Journal of the Soil Mechanics and Foundations Division, ASCE*, No. SM3, May 1969, pp. 905–909.
13. R. B. Peck, W. E. Hanson, and T. H. Thornburn. *Foundation Engineering*, John Wiley and Sons, Inc., New York, 1974.
14. H. B. Sutherland. Granular Soils, Session I: Settlement of Structures. *Proc., British Geotechnical Society*, Cambridge, England, 1974, pp. 473–499.
15. D. J. D'Appolonia, E. D'Appolonia, and R. F. Brisette. Settlement of Spread Footings on Sand. *Journal of the Soil Mechanics and Foundations Division, ASCE*, May 1968, pp. 735–760.
16. D. J. D'Appolonia, E. D'Appolonia, and R. F. Brisette. Closure of Settlement of Spread Footings on Sand. *Journal of the Soil Mechanics and Foundations Division, ASCE*, No. SM2, March 1970, pp. 754–761.
17. J. K. Mitchell and W. S. Gardner. In Situ Measurement of Volume Change Characteristics. *Proc., of the Conference on In Situ Measurement of Soil Properties*, Vol. II, *Geotechnical Engineering Division, ASCE*, June 1975, pp. 279–345.
18. I. S. Oweis. Equivalent Linear Model for Predicting Settlements of Sand Bases. *Geotechnical Engineering Division, ASCE*, No. GT12, Dec. 1979, pp. 1525–1544.
19. J. H. Schmertmann. Static Cone to Compute Static Settlement Over Sand. *Journal of the Soil Mechanics and Foundations Division, ASCE*, Vol. 96, No. SM3, 1970, pp. 1011–1043.
20. J. H. Schmertmann, J. P. Hartman, and P. R. Brown. Improved Strain Influence Diagrams. *Journal of Geotechnical Engineering Division, ASCE*, Vol. 104, No. GT8, pp. 1131–1135.
21. K. T. Terzaghi. *Theoretical Soil Mechanics*. John Wiley and Sons, Inc., New York, 1943.
22. G. G. Meyerhof. Soil-Structure Interaction and Foundations. General Report, Main Session II. *Proc., Sixth Panamerican Conference*, Lima, Peru, 1979, pp. 109–140.

Publication of this paper sponsored by Committee on Foundations of Bridges and Other Structures.

Abridgment

Increasing Communication Between Bridge and Geotechnical Engineers

PHILIP KEENE AND JOSEPH J. BULBA

Geotechnical engineering is a new field compared with bridge engineering. During the early stages of the former, various methods were developed to implement geotechnical applications to bridge foundation design and construction. Several reviews have been conducted of the organizational structure in the state transportation agencies and district federal offices of the Federal Highway Administration (FHWA). The interaction of the many disciplines within these offices needs further improvement. Geotechnical engineers have not always been able to incorporate new methodology into current bridge foundation design practices. The reasons for this are reviewed to improve communication between these units and top management. The conclusion reached is that cooperation between independent geotechnical, bridge design, and construction units, best serves the interest of the agencies.

Treated as a science since the days of Leonardo da Vinci, bridge engineering is an old discipline, dating back to early civilizations. It has been taught in universities for several centuries. Geotechnical engineering, on the other hand, is a relatively new discipline; its scientific form may be said to date back to Terzaghi, Casagrande, and other pioneers early in the present century. In 1940 only a handful of engineering schools taught soil mechanics; after World War II the number increased rapidly, and today there are many excellent geotechnical engineering programs offered in the United States and elsewhere. Its wide appeal is reflected, for example, in the membership of the American Society of Civil Engineers, where it ranks second to structural engineering in popularity.

Bridge engineering has developed rapidly; recent innovations in design concepts and materials include prestressed concrete, orthotropic superstructures, integral abutments, weathering steel, cantilevered end spans, jointless decks on multispan superstructures, and so on. The bridge engineer's growing confidence in superstructure design has also been abetted by the more sophisticated analyses of soil condition available. The more adventurous bridge engineers will design with anticipated settlements, total and differential, into their structures.

Various methods of analyses of soil and rock behavior have been developed in geotechnical engineering and the field has advanced from the use of a basically theoretical approach to supplementary field observations and instrumentation that modify or confirm the theoretical. For some situations, long-term monitoring is important. Thus, the geotechnical engineer is developing a more solid base for his recommendations. In addition, as geotechnical engineering has become recognized as a separate entity in the field of civil engineering, it has also become accepted in highway engineering.

P. Keene, 34 Home Ave., Middletown, Conn. 06457. J. J. Bulba, Storch Engineers, 161 Main St., Wethersfield, Conn. 06109.

CURRENT ORGANIZATIONAL STUDIES

In 1976 the FHWA conducted a nationwide management survey of the organizational position and functions of the geotechnical groups in each state transportation department *(1)*. From 1977 to 1981, the FHWA conducted a study of foundation engineering practices in state transportation agencies and FHWA district offices. The study entitled *Foundation Engineering Management Reviews (2)*, was published along with *Foundation Engineering Improvement Program FY 1983–1987 (3)* in 1983. The principal objectives of the study were to

1. Determine current agency procedures related to the design and construction of structural foundations;
2. Assess the effectiveness of these procedures in constructing safe, economical, and environmentally acceptable facilities;
3. Document innovative foundation practices that could be transferred to other agencies; and
4. Establish needs necessary to improve the foundation engineering capabilities of the agencies by providing follow-up technical assistance and training.

Among the state and federal departments, consulting engineers, and others involved in highways and railroads, the organization of the bridge and geotechnical groups and their relationship vary widely, for a number of reasons. The bridge group is usually a separate division in the agency. The geotechnical group may be a separate division, part of the materials laboratory, or divided between the bridge and roadway divisions and the materials division. In some cases, the agency may rely solely on consultant services.

The earlier FHWA report *(1)* was based on a nationwide study conducted by officials of FHWA and each state. Originally requested by some states, the study was expanded and made a part of a foundation engineering improvement program *(3)* initiated by the U.S. Secretary of Transportation. After the reviews were completed, a draft report, prepared from the reviews, was forwarded to each state and FHWA regional office for comment. The final report to the states was well received. The findings indicated that nine years ago, six states had a separate geotechnical division in the central office and five more were considering one. In six additional states geotechnical work was divided between the bridge division and the materials laboratory. In the remainder of the states geotechnical work was done in the materials laboratory. Currently, workshops are being held by FHWA to improve the geotechnical organizational setups, as well as certain technical engineering practices *(4)*.

According to the FHWA, the current organizational location

of the foundation design units in state agencies is as follows: a few units (10 percent) are involved in all phases of subsurface investigation, design, and construction. Some are separated from the subsurface investigation entirely (10 percent), and 68 percent are included only in the subsurface investigation and design phases *(2, 3)*. These percentages were extracted from questionnaires in which multiple responses were permitted.

Geotechnical engineering is primarily a specialized technical function that serves planning, bridge design, roadway design, construction, and maintenance. As shown in the FHWA management studies *(1)* and *Foundation Engineering Management Reviews (2)* it serves not for testing or quality control but as an engineering function for subsurface investigation, design, construction, or combinations of the three.

In the executive summary of *Foundation Engineering Management Reviews (2)*, the FHWA states that "foundations for all civil engineering facilities are significantly less expensive when designed by a rational and scientific approach than when they are determined solely by rules of thumb and past experience." Unfortunately, the current practices of many of the agencies reviewed do not reflect modern state-of-the-art technology, nor do they resemble the practices of most of the private sector. In such agencies, it is the duty of top management (commissioner, chief engineer, etc.) to correct this situation, which is often the result of a lack of communication between the bridge and geotechnical engineers.

Although the reasons for this technological lag are undoubtedly many, several became obvious during the reviews: *(a)* low salary level, *(b)* insufficient technical personnel, *(c)* physical separation between geotechnical and bridge design facilities, *(d)* poor communication between design and construction personnel, *(e)* increased use of consultants, *(f)* lack of incentives for promotion of cost-effective designs, and *(g)* insufficient opportunities for technical training.

In addition to the foregoing list, it must be added that bridge design units are often under pressure to produce designs as rapidly as possible with limited manpower. This may result in costly overdesign of bridge foundations, as well as over design of the entire structure, but the excessive cost is buried in the construction cost. The public may believe that it is getting state-of-the-art design in its new construction, but this is often an illusion.

It is perhaps the direct and highly visible counting of personnel and funds that prevents the establishment of a separate geotechnical unit. Heads and dollars in a transportation agency budget cannot be hidden, but the cost of construction inefficiencies can. Despite the obvious reasons for technological lag and delay in the establishment of a more specialized approach to foundation design, probably the most frustrating aspect is the maintenance of the status quo in the system, which may inhibit the use of new methodologies. As already stated, top management has the opportunity to step in and bring the organizational structure up to date.

The FHWA recommendation can be summarized as follows:

> The need for continual geotechnical engineering involvement throughout all activities of foundation design and construction is absolutely necessary for a cost-effective end product.... This concept of project involvement from beginning to end is primarily related to the fact that soils are not man-made as are other construction materials such as concrete and steel; therefore, no matter how many borings are performed for a project, there will be a considerable amount of engineering judgement in the design which makes it likely that some modifications and adjustments will be necessary during the final structure design and construction.

Another deterrent to the proper use of geotechnical engineering in bridge foundations is the reluctance of many bridge engineers to accept modern and proven foundation design practices. This resistance is probably due chiefly to inertia and to well-intentioned conservatism. Other possible reasons are suggested by Keene *(5)*. For example, according to Wahls *(6)*, "recent surveys by FHWA indicate that in many states spread footings rarely are used for support of highway bridges. In some states, spread footings are not considered unless they can be founded on rock." In the words of the late O. J. Porter in 1953 *(7)*, "While we have had many mistakes due to inadequate foundations, we have also had many buried treasures of money due to using an expensive pile foundation where spread footings could be safely used." Often this situation can be corrected only through the intervention of top management, for example, the chief engineer.

Examples of savings realized where spread footings were used—even though piles would have been the "safe" choice—are given by Keene *(5)* and Wahls *(6)*. Part of this conservatism may also result from geotechnical engineers' involvement in public sector projects. As stated by Wahls *(6)*, in the private sector building foundation designs are typically more realistic and less costly, even though buildings are more delicate structurally than highway bridges. Most buildings are constructed with private funds, and unnecessarily costly design and construction would not be tolerated. Another example of the reluctance to change bridge design is the antiquated specification used in interpreting pile load test results *(8)*. One example indicates that the allowable load, from the test on a pile, should be 50 percent of the gross load, which results in a net settlement of ¼ in. This was specified in the original manual of the American Association of State Highway Officials (AASHO), Committee on Bridges and Structures published in 1931; it has not been changed in the 53 years of the manual's existence. Today, however, some agencies are ignoring this specification.

MODERN FOUNDATION DESIGN PROCEDURES

A separate soils and foundations unit was established in Connecticut in 1940, thus initiating a scientific approach to foundation analyses for roadways and structures. At the direction of the highway commissioner, this unit gave special attention to bridge foundations because of the number of bridges in the state. A list of items to be covered in foundation design was developed that included the geotechnical engineer's recommendations. This list, with discussion of items, is given by Keene *(9–11)*. A shorter list without discussion is given in the *Manual on Foundation Investigations (12)*. A good working relationship developed because the bridge designer was relieved of responsibility in an area where most bridge engineers had only limited knowledge. Piled foundations no longer needed to be used in the conservative approach to a majority of foundations, nor was a too-liberal approach needed for others. Inventive substructures could be designed with assurance that

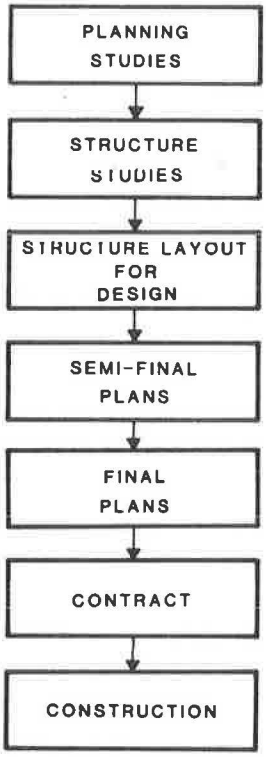

FIGURE 1 Communication procedures used to aid project design.

the developing soils science would be able to furnish the proper subsurface design information.

A procedure gradually evolved whereby a PD (Preliminary Layout and Design) Sheet was developed for each structure by the bridge designer. The degree of input varied in proportion to the number of divisions reviewing the plans. With the initiation of the Interstate program in the mid-1950s, the Connecticut Highway Department engaged the services of consulting firms to provide support to its engineers. Communication became a necessity for an orderly design process because so many projects were being designed (Figure 1). Later, a structure studies format was developed. Only structures showing promise for the site were to be studied, thereby keeping most studies to only two or three configurations. These structure studies were distributed to all sections concerned within the department as well as to agencies concerned for their review, and an acceptable type was selected, with modifications as required.

This review process has worked well, especially because there have been fewer reasons for delay due to unforeseen complications or omissions. During this process, a strong bond developed between the geotechnical engineers and the bridge engineers. Each serves in a unique sphere of expertise and recognizes his impact on the other.

CONCLUSIONS

Cooperation among the geotechnical engineer, the bridge and highway engineers, and all the interested participants in the design and construction process means that the public obtains the best structure for the location. This usually results in the most economical structure at the beginning, and invariably, to the end of its useful life.

It is recognized that each agency has a different and unique organization, suited to those who deal with it. Yet there is a growing belief in the profession that the geotechnical unit, with its own soils laboratory, test boring crews, and so on, cooperating with the bridge design and construction units located nearby will provide a more effective solution to the problem. Having the geotechnical functions combined into one unit is beneficial because it provides for a unified control and continuation of personnel, equipment, and experience involved with the same basic geotechnical problems. It also improves guidelines established for continuity of communication and project flow between the various engineering groups and the geotechnical group that serves them.

Many states have sizable areas where conditions are similar, where enormous sums of money can be saved easily merely by the application of current geotechnical analyses and evaluation, and by implementation of these findings by bridge design. As noted earlier, speed of design is not justifable on the basis of design, construction, and cost. However, the logistics of time for travel to construction sites and design offices must be acknowledged, as well as other factors in organizational implementation. These problems are real, but they can be accommodated. There is no one best answer, but there is an acceptable one.

REFERENCES

1. R. D. Goughnour. Soil Management Studies in the State Highway Departments. FHWA, *Highway Focus*, Vol. 8, No. 4, Dec. 1976, pp. 1–10.
2. *Foundation Engineering Management Reviews, Final Report and Executive Summary.* FHWA, U.S. Department of Transportation, 1983.
3. *Foundation Engineering Improvement Program FY 1983–1987.* FHWA, U.S. Department of Transportation, 1983.
4. R. S. Cheney and R. G. Chassier. *Soils and Foundations Workshop Manual.* FHWA, U.S. Department of Transportation, Nov. 1982.
5. P. Keene. Tolerable Movements of Bridge Foundations. In *Transportation Research Record 678,* TRB, National Research Council, Washington, D.C., 1978, pp. 1–6.
6. H. E. Wahls. *NCHRP Project 20–5, Topic 12–06, Shallow Foundations for Highway Structures,* TRB, National Research Council, Washington, D.C., Aug. 1982.
7. O. J. Porter. Discussion of The Use of Soil Mechanics in the Design and Construction of Bridge Foundations. *Proc., Annual Convention of the Association of Highway Officials of North Atlantic States,* Trenton, N.J., 1953.
8. *Standard Specifications for Highway Bridges,* 13th ed., American Association of State Highway and Transportation Officials, Washington, D.C., 1983.
9. P. Keene. The Use of Soil Mechanics in the Design and Construction of Bridge Foundations. *Proc., 48th Annual Meeting American Association of State Highway Officials,* Washington, D.C., 1962.
10. P. Keene. *Proc., 9th Pan American Highway Congress, Organization of American States,* Washington, D.C., 1963.
11. P. Keene. *Design Manual.* Soil Mechanics Bureau, New York State Department of Transportation, Albany, 1978.
12. *Manual on Foundation Investigations,* 2nd ed., American Association of State Highway and Transportation Officials, Washington, D.C., 1978.

Publication of this paper sponsored by Committee on Foundations of Bridges and Other Structures.